Study on Sensitized Luminescence from Lanthanide(III) Ion Hybridized with Nanospherical Systems

by

Nikita Madhukar
Student ID Number: 1256014

A dissertation submitted to the
Engineering Course, Department of Engineering,
Graduate School of Engineering,
Kochi University of Technology,
Kochi, Japan

in partial fulfillment of the requirements for the degree of
Doctor of Philosophy

Assessment Committee:
Supervisor: Akitaka Ito
Co-Supervisor: Kazuya Kobiro
Co-Supervisor: Nagatoshi Nishiwaki
Shotaro Hayashi
Toshiyuki Kawaharamura

March 2025

Declaration

I hereby declare that the work presented in this dissertation, “Study on Sensitized Luminescence from Lanthanide(III) Ion Hybridized with Nanospherical Systems,” was conducted by the regulations of Kochi University of Technology. The dissertation does not contain any material previously published or written by another person, except where proper references have been provided. Some passages have been quoted verbatim from my prior publications.

Nikita Madhukar

Kochi University of Technology

Abstract

Study On Sensitized Luminescence from Lanthanide(III) Ion Hybridized with Nanospherical Systems

This thesis deals with the sensitization of lanthanide(III) ion (Ln^{3+}) luminescence, specifically with a focus on terbium(III) and europium(III) ions. The research investigates strategies to enhance luminescence efficiency by hybridizing these ions in various nanospherical systems. The aim of this research is to develop a cost-effective lanthanide-based material that can potentially be applied in different real-life scenarios, such as sensing, imaging, optical material, etc. Key approaches include utilizing the polymeric material as cation exchange media and employing inorganic host material to simplify the sensitization process. By optimizing these hybrid systems, the study demonstrates significant improvement in the luminescence properties of lanthanide(III) ions and contributes to the multifunctional host materials that can optimize energy transfer and improve the stability of luminescence material.

Lanthanide(III) ions are renowned for their distinctive photophysical properties, such as high color luminescence purity, narrow line-like emission bands, long-lived excited states, etc. These properties make lanthanide(III) ions invaluable for a wide range of applications, including optoelectronic, imaging, sensing, display technologies, etc. However, the direct excitation of the lanthanide(III) ions remains challenging due to their forbidden 4f→4f transitions transition as they are shielded by the outer electron shells. As a result, efficient sensitization processes are essential to enhance the lanthanide(III) ions luminescence. Various approaches have been developed by researchers for sensitizing the lanthanide(III) ions, such as metal complexes, polymer systems, and nanomaterials etc. Though these methods have quite effective results in the sensitization process for lanthanide(III) ions, they are associated with some drawbacks, including high cost, laborious synthesis process, huge preparation time, photobleaching, etc. For example, metal leaching from complexes can lead to environmental contamination and toxic effects on various organisms, raising concerns about their applicability. Therefore, sensitization of lanthanide(III) ions using environmentally friendly material is still challenging.

This work addresses the above limitation by exploring environmentally friendly host materials for lanthanide(III) ions by hybridizing them with nanospherical systems. The nanospherical morphology plays a crucial role in minimizing the light scattering, allowing for more efficient excitation of lanthanide(III) ions and thereby enhancing the luminescence. In this work the lanthanide(III) ions were hybridized in an ionic nanosphere, a dispersible cation exchange media, and an inorganic host material called CaF_2. Lanthanide(III) ions were

incorporated into the ionic nanosphere through a simple mixing process. The integration in inorganic CaF_2 matrices was achieved by the one-step synthesis method. These approaches offer a cost-effective and environmentally friendly alternative to traditional protocols, demonstrating simplicity and risibility in preparing advanced lanthanide-based luminescent materials.

Chapter 2 explores the study of the sensitization of terbium(III) ion using an ionic nanosphere. The study focuses on the synthesis, characterization and photophysical analysis of ionic nanosphere hybridized with terbium(III) ion. The ionic nanosphere is a spherical ion-exchange resin with a poly(*p*-styrenesulfonate-*co*-divinylbenzene) structure with a diameter of less than 300 nm, and hence, it can accommodate cationic species such as terbium(III) ion. Since the ionic nanosphere exhibits the π–π^* absorption/fluorescence of its poly(*p*-SS-*co*-DVB) structure, the nanosphere acts as a photosensitizer for doped terbium(III) ion through the energy transfer as well as a host/medium. The average size of the ionic nanosphere was 166 ± 65 nm by dynamic light distribution. The absorption spectra showed the ionic nanosphere has multiple absorption band <300 nm region. The mass absorption coefficients at 223 nm and 258 nm were determined to be 30.9 L g^{-1} cm^{-1} and 8.7 L g^{-1} cm^{-1}, respectively. Since the values are sufficiently large, the absorption bands can be assigned to the π–π^* transition of the poly(*p*-SS-*co*-DVB) structure. The ionic nanosphere has broad fluorescence in the range of 300 to 400 nm, which matches with the 4f–4f excitation bands of terbium(III) ion. Therefore, the ionic nanosphere plays a novel sensitizer for the terbium(III) ion. The terbium(III) ion were doped in the ionic nanosphere from (5.04 to 299 nmol mg^{-1}) by mixing at room temperature. Upon the photoexcitation at 260 nm, which is the absorption maximum of the nanosphere, new luminescence peaks at 488 nm, 543 nm, and 583 nm appeared, along with the fluorescence from the ionic nanosphere at around 330 nm. The new luminescence bands resembles the 4f–4f luminescence from terbium(III) ion originating from the $^5D_4 \rightarrow {}^7F_J$ (J = 3–6) transitions. The $^5D_4 \rightarrow {}^7F_5$ green emission at 543 nm was observed as the most prominent band, irrespective of the content. The enhanced luminescence of terbium(III) ion was achieved by ionic nanosphere as its excited-state energy of poly(*p*-SS-*co*-DVB) transfer to the terbium(III) ion, and enhanced luminescence from terbium(III) ion was observed from (5.04 to 299 nmol mg^{-1}). The stability of the luminescent properties in aqueous dispersions (H_2O and D_2O) was also analyzed, demonstrating minimal quenching and degradation over time, which is essential for practical applications. Therefore, the ionic nanosphere serves as both a rigid medium and a photosensitizer for terbium(III) ion. The ability to create stable dispersions in water without the need for toxic solvents opens new avenues for the safe application of terbium(III) ion

luminescent materials in various sectors, including biomedical research and environmental sensing. The primary advantage of this system lies in its simplicity and versatility, as the hybrid material can be synthesized using straightforward and facile methodologies. Additionally, the conditions, such as the content within the nanosphere, can be easily varied without the need for complex or rigorous synthesis processes.

Chapter 3 focuses on the sensitization of lanthanide(III) ions by ionic nanosphere copolymerized with 5-(4-vinylphenyl)-1,10-phenanthroline (pPhen) as a ligating moiety. The innovative design of the ionic nanosphere aims to enhance the luminescence of terbium(III) and europium(III) ions through improved energy transfer efficiency. The ligating ability of pPhen to lanthanide(III) ions enables efficient energy transfer. Upon photoexcitation, the excited state energy of the ionic nanosphere accumulates in the pPhen moiety, and the efficient energy transfer happens to the terbium(III) and europium(III) ions. The chapter outlines the synthesis process of 5-(4-vinylphenyl)-1,10-phenanthroline by using cross coupling reaction using the reagent vinyl 4-phenyl boronic acid and 5-bromo-1,10-phenanthroline and its purification and characterization using ^{1}H NMR techniques to ensure the successful synthesis of 5-(4-vinylphenyl)-1,10-phenanthroline. The successful synthesis of pPhen moiety led to the synthesis of copolymerized ionic nanosphere with pPhen ligating moiety. The average size of the new nanosphere was determined to be 65±10 nm by dynamic light scattering measurement, confirming the successful synthesis of ionic nanosphere with pPhen ligating moiety. The ionic nanosphere with ligating moiety is smaller than the conventional one (166±65 nm). The size reduction can be explained by the introduction of a more hydrophobic unit pPhen ligating moiety. The absorption band of the new ionic nanosphere with the pPhen ligating unit shows multiple absorption bands <350 nm region. The broad absorption band around 260 nm arise due to the π–π* excited state of the poly(*p*-SS-*co*-DVB) backbone, and a new absorption band around 280–310 nm came from the π–π* transition of pPhen lighting moiety. The calculated mass absorption coefficients at 231 nm, 256 nm, and 300 nm were determined to be 8.6 L g^{-1} cm^{-1}, 6.3 L g^{-1} cm^{-1} and 0.94 L g^{-1} cm^{-1}, respectively. The large extinction coefficient indicates that the copolymerized ionic nanosphere can be an efficient light absorber toward subsequent energy transfer to lanthanide(III) ions. The fluorescence spectra of the copolymerized ionic nanosphere were observed around the 400–550 nm range, which is attributed mainly to the pPhen. The fluorescence mostly emits light in the blue-green region. Moreover, the fluorescence spectra of copolymerized ionic nanosphere, cover the 4f–4f direct excitation of europium(III) (360 nm, 480 nm, 420 nm, 480 nm) and terbium(III) (440 nm, 540 nm, 490 nm) ions. Hence, the ionic nanosphere with pPhen ligating moiety acts as an energy harvester for

the pPhen moiety, and then the energy is transferred to the lanthanide(III) ions.

The europium(III) and terbium(III) ions doped nanosphere were prepared simply by mixing them with copolymerized ionic nanosphere. When excited at 300 nm, the fluorescence and luminescence were observed both from the ionic nanosphere with pPhen moiety and europium(III) and terbium(III) ions. It was also observed that the fluorescence from the ligating moiety shifted to a lower wavelength from 480 nm to 420 nm when europium(III) and terbium(III) doped inside, mainly the binding of these ions to the ligating moiety. The new luminescence was observed from the europium(III) doped nanosphere, which is at 580 nm, 613 nm, and 690 nm, which corresponds to the $^5D_0 \rightarrow {}^7F_J$ (J = 1 to 3) transitions of europium(III) ion. For the terbium(III) doped nanosphere as well, the new luminescence peaks were at 543 nm, which corresponds to the $^5D_4 \rightarrow {}^7F_5$ transition. This green emission at 543 nm is consistently the most intense luminescent feature across all terbium(III)-doped samples, with other possible terbium transitions such as 488 nm and 583 nm not observed in this system. The luminescence performance of europium(III) and terbium(III) differs significantly. While the europium(III) ion exhibits stronger luminance and multiple transitions when doped in the nanosphere, the terbium(III), doped nanosphere samples are only dominated by the 543 nm transition. The difference is due to the better energy match between the nanosphere with pPhen moiety and the europium(III) ion compared to the terbium(III) ion. Overall, the observed luminescence intensities for both europium and terbium ions confirm that the ionic nanosphere with pPhen ligating moiety serves as an effective sensitizer and energy harvester, enabling efficient energy transfer to both europium(III) and terbium(III) ions.

Chapter 4 focuses on the sensitized luminescence of the terbium (III) ion when hybridized with the CaF_2 inorganic material, in which the gallic acid molecule is used as both a capping agent and a sensitizer for the terbium(III) ion. The gallic acid-capped terbium(III) doped CaF_2 nanocrystals were further used for the selective sensing of chromate and permanganate ions. In this system, the CaF_2 inorganic material was chosen for the host of terbium(III) ion, as it has low phonon energies (<400 cm^{-1}), is widely known in synthesis methods, and controls over size. CaF_2 is also known to form small-sized particles with high biocompatibility and thermal stability. Furthermore, gallic acid has been chosen as the capping ligand and the sensitizer for terbium(III) ion due to its multifunctional properties. First of all, it has strong absorption and fluorescence in the UV region, which can transfer its excited state energy to the terbium(III) ion as the fluorescence of gallic acid greatly matches with the direct excitation of terbium(III) ion. In addition, gallic acid has a –COOH group, which can strongly bind with the surface of CaF_2 nanocrystals, and multiple –OH groups, which render water dispersibility of the

nanocrystals. Gallic acid thus plays a dual role in this system, serving as a capping agent for the nanocrystals and acting as a sensitizer for the terbium(III) ion.

The gallic acid-capped terbium(III)-doped CaF_2 was prepared by microwave synthesis process. Different characterization processes, such as PXRD, TEM, and FTIR, were performed to determine the successful synthesis of gallic acid-capped terbium(III)-doped CaF_2 nanocrystals. The luminescence studies were performed in aqueous colloidal dispersion. Upon photoexcitation at 310 nm, strong luminescence was observed at 488 nm, 543 nm, 583 nm and 620 nm. These luminescence peaks are ascribed to the $^5D_4 \rightarrow {}^7F_J$ (J = 3 to 6) transitions of terbium(III) ion. The luminescence observed mainly occurs via gallic acid ligand excitation. This was confirmed when the excitation spectra of gallic acid-capped terbium(III) doped CaF_2 nanocrystals were apprehended around 310 nm when monitored at 543 nm, which is the highest luminescence peak of the terbium(III) ion. The luminescence intensity of terbium(III) ion was nearly increased around 45 times when sensitized via gallic acid sensitization in CaF_2 nanocrystals compared to the direct excitation of terbium(III) ion. The direct excitation was achieved by exciting the citric acid-capped terbium(III)-doped CaF_2 nanocrystals. The observed enhanced luminescence from terbium(III) ion was further used for sensing application for the selective detection of chromate and permanganate ions. Aqueous solution of chromate and permanganate ions was prepared in the concentration range between 1 nM to 3000 nM (3 μM). The chromate and permanganate ions were added to the gallic acid-capped terbium(III) doped CaF_2 nanocrystals, and a significant decrease in the intensity of its luminescence was observed. An almost 90 % decrease in luminescence intensity decreased when around 3000 nM concentration of chromate and permanganate ions were added into the nanocrystals. The reduction of the luminescence intensity occurred because the excitation and emission spectra of gallic acid largely overlap with the absorption spectra of $Cr_2O_7^{2-}$ and as well as with MnO_4^- ions The selectivity of gallic acid caped terbium(III) doped CaF_2 nanocrystals, was determined when different analytes such ClO_4^-, MnO_4^-, SCN^-, CH_3COO^-, S^{2-}, F^-, Br^-, I^-, SO_4^{2-}, IO_3^- etc. were added in the nanocrystals. The results indicated that there were hardly any effects in intensity observed even though the concentration of the other analytes was two times (6 μM) than the chromate and permanganate concentration (3 μM). Therefore, the gallic acid-sensitized terbium(III) doped CaF_2 nanocrystals have shown real-life application and can be further explored for other toxic analytes detection studies.

Overall, this dissertation simplifies the development of lanthanide(III)-doped materials by addressing important issues like synthesis complexity, cost reduction, and the practical application of the materials in real-world situations. The incorporation of nanospherical systems

not only provides a stable and environmental friendly host for lanthanide(III) ions but also plays a crucial role in minimizing light scattering. This ensures uniform light propagation, allowing for more efficient excitation of lanthanide(III) ions and significantly enhancing their luminescence efficiency. Additionally, the well-dispersed nature of the nanospherical system in aqueous media prevents aggregation, ensuring consistent optical performance and broadening potential applications in fields such as optical sensing, bioimaging, and photonic devices.

Acknowledgements

The completion of this thesis marks the end of a significant chapter in my life, and I would like to take this opportunity to express my deepest gratitude to all those who have supported me throughout this journey.

First and foremost, I would like to express my heartfelt gratitude to my supervisor, Prof. Akitaka Ito, for his invaluable guidance, insightful feedback, and constant encouragement. His expertise and mentorship have played a pivotal role in shaping both my research and personal growth. The challenges I faced under his guidance instilled in me a deep sense of perseverance and a passion for scientific inquiry. I am deeply thankful for the opportunities he provided throughout my PhD journey, which have greatly contributed to my academic and professional development.

I also sincerely appreciate the contributions of my co-supervisors, Prof. Kazuya Kobiro and Prof. Nagatoshi Nishiwaki, for their timely feedback and guidance at the end of each semester. Their valuable insights helped shape the direction of my work, and I am grateful for their support. I also thank Prof. Shotaro Hayashi, Prof. Masataka Ohtani, and Prof. Toshiyuki Kawaharamura for their valuable feedback on my research.

I sincerely thank all my lab mates from the Laboratory of Photofunctional Chemistry for their collaboration, support, and friendship. Special thanks to my fellow doctoral students, Mr. Taizo Misato and Ms. Marino Miwa, for their insightful discussions and technical assistance during my experiments. Also, to all my fellow master's and bachelor's students, thank you for your kind support.

My heartfelt appreciation extends to Kochi University of Technology for providing the resources, facilities, and a conducive environment for my research. I would also like to acknowledge the administrative staff, particularly the members of the International Relations Committee (IRC), who ensured the smooth running of day-to-day operations.

I sincerely thank my friends at the International House for the fun moments we shared throughout the three years of my PhD. Special thanks to my close friends, Dr. Akash Gupta and Ms. Shruti JS, for their unwavering support, encouragement, and uplifting conversations that brought me strength and positivity.

I want to give a special mention to my family, whose love and support have been my constant source of strength throughout this journey. To my parents, thank you for your unwavering belief in me and for always encouraging me to pursue my dreams. To my siblings,

Ms. Shweta Madhukar and Mr. Vivek Kumar, thank you for your constant love, encouragement, and belief in me, which gave me the strength to persevere.

Lastly, I would like to thank the Special Scholarship Program provided by Kochi University of Technology, which supported my research and living in Japan.

To everyone who contributed to this endeavour, both personally and professionally, I am deeply grateful.

Thank you.

Table of contents

Chapter 1 Introduction

1.1. Lanthanides

The lanthanide series consists of 15 elements, from lanthanum (atomic number Z = 57) to lutetium (Z = 71), and belongs to the *f*-block in the periodic table (Figure 1-1). This classification is due to the gradual fills of their 4f orbitals, located two shells below the outermost valence shell.[1] Lanthanides possess similar chemical properties, which include a tendency to form stable trivalent ions (Ln^{3+}) and a consistent reactivity across the series. They are classified into "rare earth elements" together with scandium (Z = 21) and yttrium (Z = 39) owing to their similar chemical behaviors, such as comparable ionic sizes and reactivity patterns

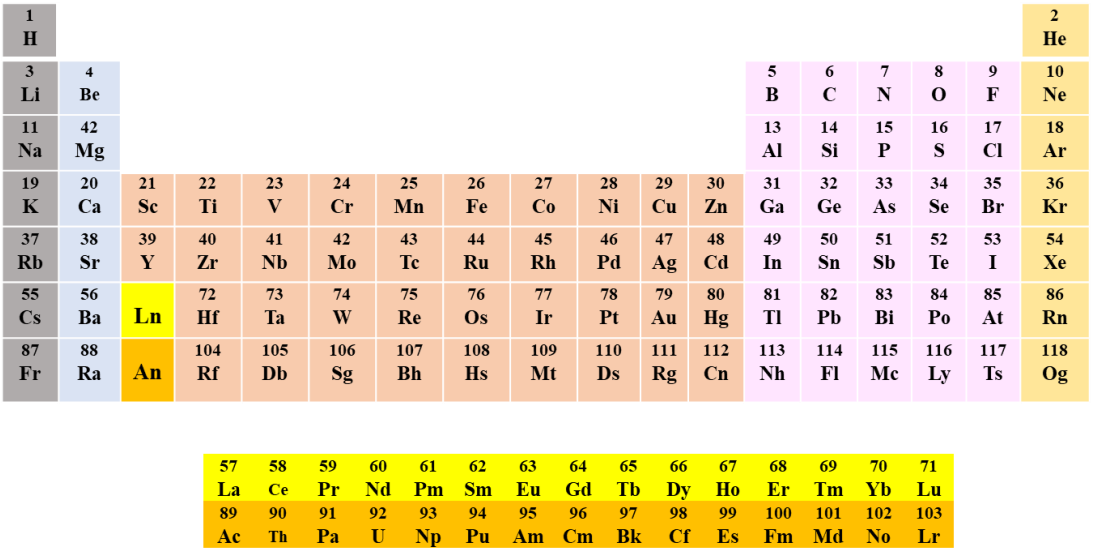

Figure 1-1. The modern periodic table of elements. The lanthanides are displayed at the bottom of the periodic table (yellow color).

The journey to find and isolate lanthanides began in 1752 when the Swedish mineralogist Cronstedt identified a heavy mineral, initially mistaken as a calcium-iron silicate. Later on, Finnish chemist Gadolin, in 1794, successfully extracted an oxide from a mineral in Ytterby, Sweden, and named it "ytterbia." In 1842, Mosander further divided "ytterbia" into fractions, which he called "yttria," "erbia" and "terbia," although these were complex mixtures. Full isolation of the lanthanides was achieved only in 1908–1909 because of the challenges posed by their similar chemical properties.

This challenge in separation arises because lanthanides commonly exhibit a +3 oxidation state, with minor variations in how they dissolve and form complexes, an effect known as the "lanthanide contraction."[2] In 1913, X-ray spectroscopy verified that only 14 elements exist between La and Hf, a result later explained by Bohr's theory on the gradual filling of the 4f

orbital. In the years before World War II, McCoy developed separation techniques, which isolated europium (Eu) by reducing it and then precipitated it as a sulfate. Large-scale separation of lanthanides advanced amid the Manhattan Project, which utilized ion-exchange chromatography based on small differences in stability among chelates. This technique, along with liquid-liquid extraction developed in the 1950s, remains in use today for commercial lanthanide separation.[3]

1.2. Characteristics and electronic transitions of lanthanides

Valence electron configurations of lanthanides are similar due to the subsequent fill of the 4f orbital by electrons. As a result, they exhibit similar coordination tendencies and chemical reactivity. Electron configurations of the elements range from $[Xe](6s)^2(5d)^1$ for lanthanum (La) to $[Xe](6s)^2(4f)^{14}(5d)^1$ for lutetium (Lu), and those of their trivalent cations follow the pattern $[Xe](4f)^n$, where *n* varies from 1 for cerium (Ce^{3+}) to 14 for lutetium (Lu^{3+}) (see Table 1-1).

Table 1-1. Electronic configuration of lanthanide elements.

Atomic Number	Element	Symbol	Electronic Configuration	
			Atom	Ln^{3+} Ion
57	lanthanum	La	$[Xe](6s)^2(4f)^0(5d)^1$	$[Xe](4f)^0$
58	cerium	Ce	$[Xe](6s)^2(4f)^1(5d)^1$	$[Xe](4f)^1$
59	praseodymium	Pr	$[Xe](6s)^2(4f)^3(5d)^0$	$[Xe](4f)^2$
60	neodymium	Nd	$[Xe](6s)^2(4f)^4(5d)^0$	$[Xe](4f)^3$
61	promethium	Pm	$[Xe](6s)^2(4f)^5(5d)^0$	$[Xe](4f)^4$
62	samarium	Sm	$[Xe](6s)^2(4f)^6(5d)^0$	$[Xe](4f)^5$
63	europium	Eu	$[Xe](6s)^2(4f)^7(5d)^0$	$[Xe](4f)^6$
64	gadolinium	Gd	$[Xe](6s)^2(4f)^7(5d)^1$	$[Xe](4f)^7$
65	terbium	Tb	$[Xe](6s)^2(4f)^9(5d)^0$	$[Xe](4f)^8$
66	dysprosium	Dy	$[Xe](6s)^2(4f)^{10}(5d)^0$	$[Xe](4f)^9$
67	holmium	Ho	$[Xe](6s)^2(4f)^{11}(5d)^0$	$[Xe](4f)^{10}$
68	erbium	Er	$[Xe](6s)^2(4f)^{12}(5d)^0$	$[Xe](4f)^{11}$
69	thulium	Tm	$[Xe](6s)^2(4f)^{13}(5d)^0$	$[Xe](4f)^{12}$
70	ytterbium	Yb	$[Xe](6s)^2(4f)^{14}(5d)^0$	$[Xe](4f)^{13}$
71	lutetium	Lu	$[Xe](6s)^2(4f)^{14}(5d)^1$	$[Xe](4f)^{14}$

In 1906, during the study of the mineral xenotime (YPO_4), which included amounts of

erbium, cerium, and thorium, Becquerel made the first observation of the distinctive, narrow absorption lines of lanthanides.[4] At that time, the origin of these different and distinct lines was not well understood. Further research by Bethe, Kramer, and Becquerel attributed these lines to intra-configurational 4f→4f transitions.[5] The 4f electrons are effectively shielded by the filled 5s and 5p orbitals, which reduces the influence of the crystal field on the 4f electrons. Although parity-forbidden under the Laporte selection rule, weak emission peaks are observed, which initially posed a challenge to researchers. van Vleck explained this phenomenon in 1937 that in a non-centrosymmetric environment, the Laporte rule is weakened, which partially permits lanthanide ions to undergo certain transitions.[6]

These emission lines arise from various transitions and, therefore, include electric, magnetic, and quadrupole dipole moments. For lanthanide(III) ions, magnetic dipole transitions are inherently allowed, while electric dipole transitions are forbidden due to the possible interaction of 4f and 5d orbitals. In non-centrosymmetric systems, electric dipole transitions can occur through the admixture of opposite-parity configurations, such as $(4f)^n \rightarrow (4f)^{n-1}(5d)^1$. Central ions may be moved from their equilibrium positions due to vibrational action inside the crystal lattice, which momentarily disrupts symmetry and generates mixed orbitals.

In lanthanide(III) ions, magnetic dipole transitions are generally weak but remain largely unaffected by the surrounding matrix and are easily calculated. A well-known example of a magnetic dipole transition is the $^5D_0 \rightarrow {}^7F_1$ emission line of europium(III) ion.[7] Electric dipole transitions in lanthanides are induced by the ligand field and are highly sensitive to the coordination environment. Some of these transitions, known as hypersensitive transitions, can exhibit significant enhancement in emission intensity, which relies on the ligand field, with the $^5D_0 \rightarrow {}^7F_2$ emission line of europium(III) as a prominent example. The selection rules govern $4f^n \rightarrow 4f^n$ transitions in lanthanides are influenced by total spin angular momentum (S), total orbital angular momentum (L), and total angular momentum (J). Due to the forbidden nature of these transitions, both electric and magnetic dipole transitions in lanthanides are generally weak, which gives rise to narrow emission lines and long luminescence lifetimes, often in the millisecond range. A partial energy level diagram, with crystal field splitting, is provided in Figure 1-2, and a summary of the selection rules for these transitions is available in Table 1-2.

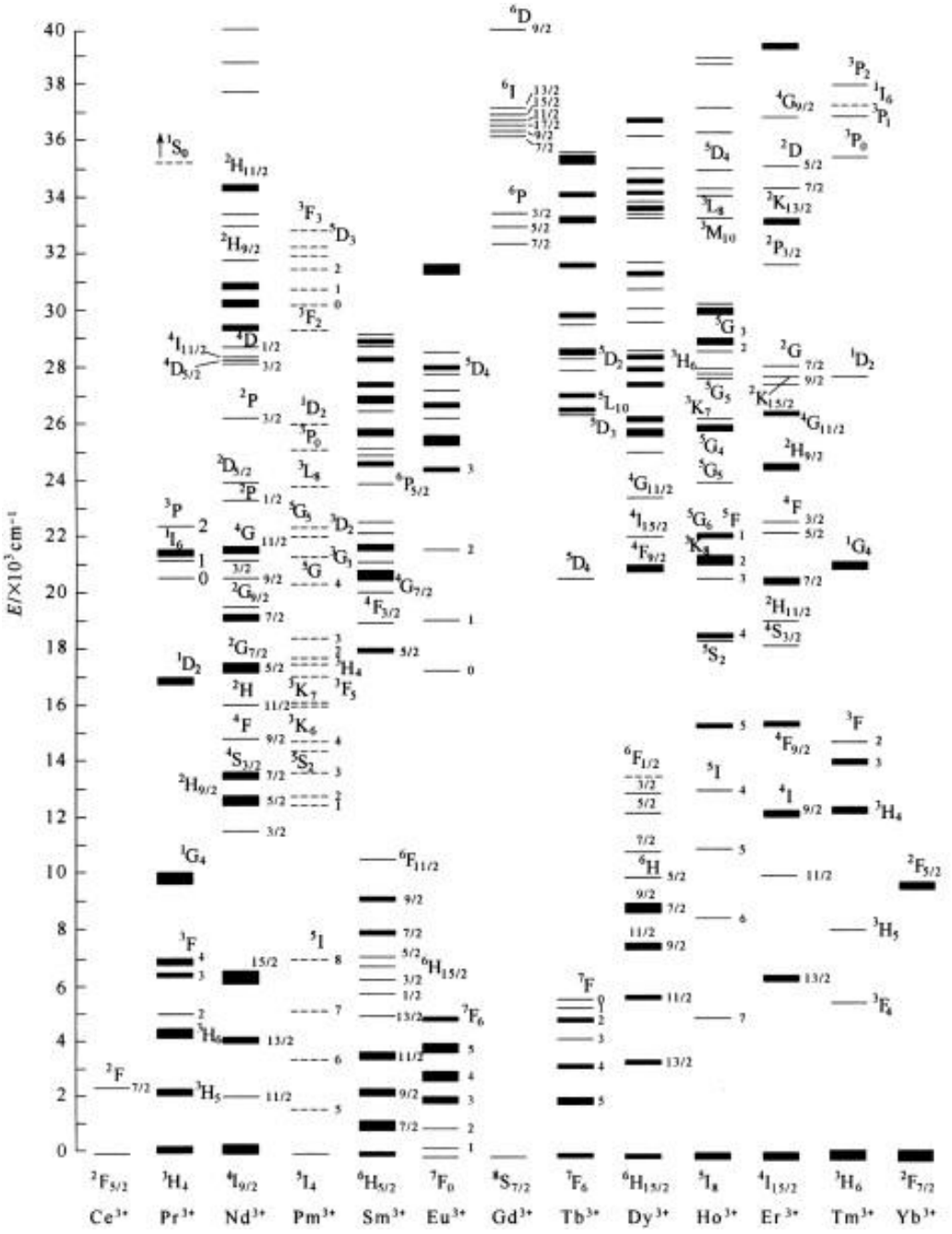

Figure 1-2. Partial energy level diagram of lanthanide(III) ions.[8] Reproduced with permission from ScienceDirect (License Number: 5912500331505).

Table 1-2. Selection rules for 4f→4f transitions of lanthanide(III) ions.

Magnetic Dipolar Transition	Electric Dipolar Transition
$\Delta S = 0$	$\Delta S = 0$
$\Delta L = 0$	$\Delta L \leq 6$
$\Delta J = 0, \pm 1$; $0 \leftrightarrow 0$ = forbidden	$\Delta J \leq 6$; $\Delta J = 2, 4, 6$

1.3. Lanthanide(III) ions luminescence

The majority of lanthanide(III) ions are luminescent, although their emission intensity varies. The distinct emissive colors of each lanthanide(III) ions with their applications are illustrated in Figure 1-3. The specific color emitted by a lanthanide(III) ions depends on the energy gap between its ground state and stable excited state energy levels.[9] Luminescence from lanthanide(III) ions spans a broad spectral range, from the ultraviolet (UV) to the near-infrared (NIR), and in some cases extends into the mid-infrared (MIR) region when excited by UV to NIR light. For example, gadolinium(III) exhibits near-UV emission around 311 nm, while thulium(III) and dysprosium(III) emit blue light at 450 nm and 478 nm, respectively. Terbium(III) ion is known for its green emission at 542 nm, samarium(III) displays orange emission near 575 nm and 590 nm, and europium(III) and praseodymium(III) are characterized by red emission at approximately 615 nm. Additionally, ions such as ytterbium(III), erbium(III), neodymium(III), samarium(III), praseodymium(III), holmium(III), and thulium(III) show luminescence in the IR region, with wavelengths ranges from 0.8 μm to about 3 μm. This wide spectral coverage makes lanthanide(III) ions versatile for various applications, such as lighting, bioimaging, telecommunications, and sensing.[10]

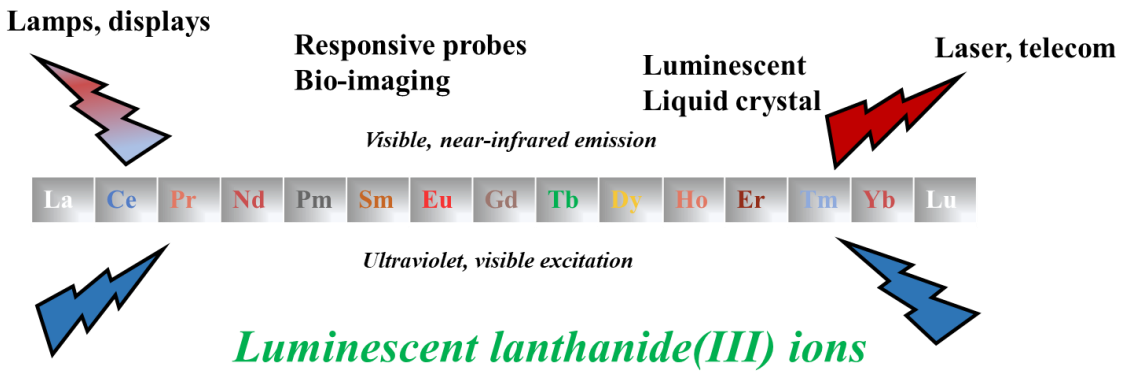

Figure 1-3. Lanthanide(III)-ion luminescence and their applications.

Narrow emission spectra are characteristics of lanthanide(III) ions luminescence that are typically observed when the ions are excited by high-energy photons. The emissive properties of lanthanide(III) ions depend on how readily their excited states can be populated and how much non-radiative deactivation is minimized.[11] The lanthanide(III) ions exhibit luminescence when they are excited by a specific wavelength of light or electromagnetic radiation. When the

high energy photon was given, the 4f electron got excited from the ground state to the higher-lying electronic excited state. Then, it comes back to the ground state by emitting the characteristic emission of lanthanide(III) ions. Therefore, the luminescence occurs at a longer wavelength than the excitation wavelength. This large Stokes-shifted luminescence is quite characteristics of the lanthanide(III) ions and is generally known as downshifted luminescence. The radiative lifetimes of lanthanide(III) ions vary from microseconds to milliseconds.[12] Different lanthanide(III) ions have different color emissions based on the energy gap between the ground and lowest-energy excited states.

Although lanthanide(III) ions show exceptional optical qualities, several obstacles prevent their use in practice, most notably vibrational quenching from interactions with ligand and solvent molecules. This quenching limits the luminescence efficiency and brightness of lanthanide(III) ions in real-world applications. Embedded lanthanide(III) ions in a carefully selected host matrix provide a viable way to overcome these restrictions. For various applications, this matrix protects the ions from vibrational interactions, maintains their luminescence qualities, and, therefore, enhances their stability and efficiency.

1.4. Principles of lanthanide(III) ion luminescence

The exclusive forbidden 4f–4f luminescence of lanthanide(III) ions is primarily due to its low absorption coefficient. It is essential to consider the chemical environment surrounding the emissive ion to identify the parameters that need to be optimized. The luminescence sensitization can be enhanced through various approaches based on whether the emissive ion is embedded in an inorganic or organic system.[13–17] The energy transfer process by direct and indirect sensitization can be illustrated in Figure 1-5.

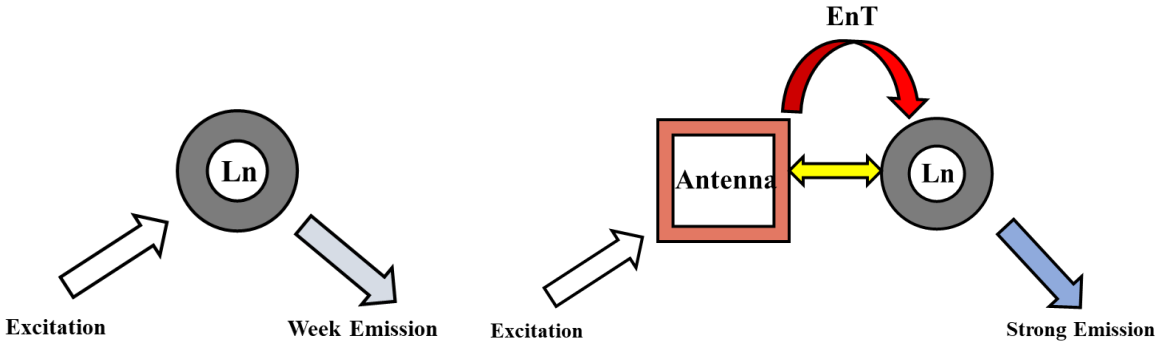

Figure 1-5. Simplified schemes depicting the energy transfer processes.

In the first step, the surrounding ligand(s) absorb light and reach an excited state, typically a singlet excited state in compounds with organic ligands. In the second composite step, the energy is funnelled onto a donor state (such as a triplet state) with an ideally long lifetime and then transferred to one or several excited states of the lanthanide(III) ion. Finally, metal-centred luminescence is emitted after suitable internal conversion to an emissive state. As a result, a new quantum yield must be defined, which is different from the intrinsic lanthanide quantum yield ($_{Ln}Q^{Ln}$). This new quantum yield is the overall quantum yield, $^{L}Q_{Ln}$:

$$^{L}Q_{Ln} = I_{Ln}(E) / I_{L}(A),$$

where $I_{Ln}(E)$ represents the number of photons emitted by the metal ion and $I_{L}(A)$ represents the number of photons absorbed by the ligand. The maximum value of this quantum yield can be equal to the intrinsic lanthanide quantum yield, $^{Ln}Q_{Ln}$, which is expressed as:

$$\eta_{sens} = {}^{L}Q_{Ln} / {}^{Ln}Q_{Ln}.$$

From a conceptual perspective, to maximize the luminosity of lanthanide-doped materials is relatively straightforward: (i) the surrounding metal-ion environment must have strong absorption with large molar absorption coefficients, (ii) energy transfer losses must be minimized, and (iii) radiationless deactivation of the excited metal ion should be reduced.

1.4.1. Mechanism to enhance Lanthanide(III) luminescence

Crosby and Whan proposed the widely accepted energy transfer mechanism from organic ligands to lanthanide(III) ions.[18] When exposed to UV light, organic ligands of the lanthanide complexes are excited to the first excited singlet state ($S_0 \rightarrow S_1$). For example, when the molecule interacts with solvent molecules, it quickly internalizes to lower vibrational levels of the S_1 state. The excited singlet state may undergo nonradiative intersystem transfer from the singlet state S_1 to the triplet state T_1, or it may deactivate radiatively to the ground state (molecular fluorescence, $S_1 \rightarrow S_0$). The spin-forbidden transition $T_1 \rightarrow S_0$ can deactivate the triplet state T_1 radiatively to the ground state, S_0. This result corresponds to molecular phosphorescence. Alternatively, the complex may also undergo a nonradiative transition from the triplet state to an excited state of the lanthanide(III) ions. Following this indirect energy transfer excitation, the lanthanide(III) ions may be deactivated by a nonradiative mechanism or undergo a radiative transition to a lower 4f state by exhibiting distinctive line-like photoluminescence. A typical energy transfer process mechanism can be seen in Figure 1-6.

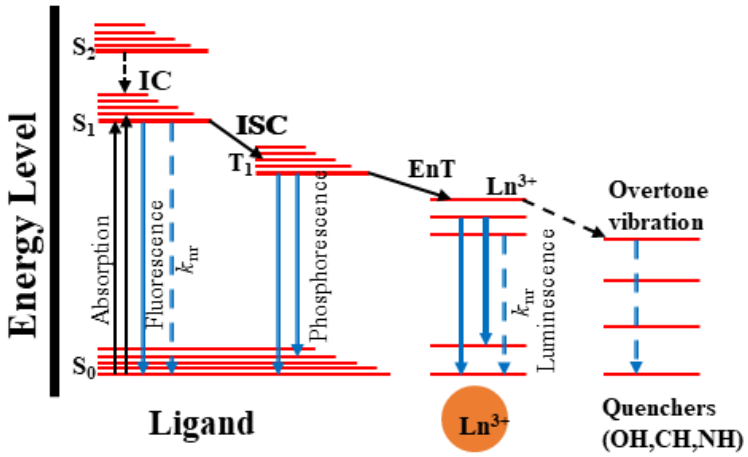

Figure 1-6. Systematic energy transfer process from ligand to lanthanide(III) ion.

According to Whan and Crosby, the main cause of the nonradiative deactivation of lanthanide(III) ions is vibronic coupling with ligand and solvent molecules.[19] Although Kleinerman proposed a mechanism of direct transfer of energy from the excited singlet state S_1 to the energy levels of the lanthanide(III) ions, this mechanism is now considered not to be of great importance.[20] Indeed, this process is often not efficient due to the short lifetime of the singlet excited state. Direct light in the triplet level followed by energy transfer to the lanthanide(III) ions is a less observed and less studied phenomenon. Luminescence by the lanthanide(III) ions is only possible from certain levels, which are termed resonance levels.[21] The main resonance levels are $^4G_{5/2}$ for samarium(III) (17 800 cm^{-1}), $^5D_0$ for europium(III) (17 250 cm^{-1}), $^5D_4$ for terbium(III) (20 430 cm^{-1}), and $^4F_{9/2}$ for dysprosium(III) (20 960 cm^{-1}). If the lanthanide(III) ions is excited to a non-emitting level, either directly by excitation in the 4*f* levels or indirectly by energy transfer, the excitation energy is dissipated via nonradiative processes until a resonance level is reached. Radiative transitions become competitive with nonradiative processes, and metal-centered emission can be observed. Line emission by a lanthanide(III) ions is only possible if nonradiative deactivation, molecular fluorescence, and phosphorescence can be minimized.[22] To populate a resonance level of a lanthanide(III) ions, the lowest triplet state of the complex must be located at an energy nearly equal to or above the resonance level of the lanthanide(III) ions, not below. When the energy levels of the organic ligands are below that of the resonance level of the lanthanide(III) ions, molecular fluorescence or phosphorescence of the ligand is observed, or no light emission at all is observed. The luminescence observed for a specific lanthanide complex is, therefore, a sensitive function of the lowest triplet level of the complex relative to a resonance level of the lanthanide(III) ions. Because the position of the triplet level depends on the type of ligand, it is, therefore, possible to control the luminescence intensity observed for a given lanthanide(III) ions by variation of

the ligand.

1.4.2 Role of triplet state

Triplet states play a central role in the energy migration between organic ligands and lanthanide(III) ions and vice versa. This occurs either by participation in the sensitization process, when the lowest energy triplet state, ^3T, is located above the emitting state; early studies by Sato and Wada reported on the quantum yield and lifetime of europium(III) and terbium(III) tris- and tetrakis-β-diketones, along with time-resolved experiments demonstrates the mechanism of energy transfer and the role of triplet states.[23] They observed that the quantum yield was maximized when the triplet state (T_1) was about 3500 cm^{-1} above the $^5D_0$ level of europium(III) ions. Back energy transfer occurred when the triplet state (^3T) was nearly resonant with the $^5D_0$ level, which reduced the quantum yield. Furthermore, when the triplet state was lower than the $^5D_0$ level, no energy transfer occurred. Similarly, for terbium(III) chelates, the optimal energy gap between the triplet state of the ligand and the $^5D_4$ level is about 2400 cm^{-1}.[24] Therefore, to develop lanthanide luminescent materials, the most important consideration is to ensure that the triplet state of the donor group is effectively aligned for energy transfer to the lanthanide(III) ions.

In addition to the triplet states of the donor organic ligand, other processes must be considered to develop highly luminescent lanthanide materials, whether through inorganic or organic synthesis processes. For instance, to minimize vibrational deactivation processes is crucial.

1.5. Lanthanide(III)-based luminescent hybrid material

The emission color of a lanthanide(III) ions is mainly determined by the specific ion itself and is largely independent of its surrounding environment. Traditionally, research on luminescent lanthanide compounds has focused on inorganic materials like lanthanide phosphors,[25–27] molecular lanthanide complexes such as *β*-diketonate complexes,[28–30] and lanthanide-based polymer systems.[31–34] However, the development of organic-inorganic hybrid materials based on lanthanides has attracted much attention in recent years.

These hybrids incorporate a molecular lanthanide complex into an inorganic host matrix, such as sol-gel-derived materials,[35–38] or embed an inorganic lanthanide compound like polyoxometalate complexes or lanthanide-doped nanoparticles into organic polymer matrices.[39–41] Lanthanide-based polymeric systems also play a significant role, as they offer versatility in structure and functionality.

The classification of these hybrid materials is sometimes indistinct, as seen in systems like organically modified xerogels. The study of luminescent lanthanide compounds within these hybrids is of considerable scientific interest, as these materials show potential for several uses, such as optical amplifiers, optical waveguides, and OLEDs. Generally, hybrid materials exhibit enhanced mechanical properties, improved thermal stability, and greater processability than pure molecular lanthanide complexes. Furthermore, lanthanide complexes can be embedded in a polymeric system or hybrid matrix to improve luminescence output and provide a stable and efficient platform for photonic applications.

1.5.1. Lanthanide(III) complexes

Lanthanide(III) complexes are coordination complexes formed between lanthanide(III) ions and *β*-diketone (1,3-diketones) ligands.[42–45] They are among the most popular and widely studied luminescent lanthanide coordination compounds. The wide range of *β*-diketone ligands that are commercially available and the relatively simple process of synthesis associated with the lanthanide complexes are the factors for their popularity. Some of the famous *β*-diketone ligands are shown in Figure 1-7. Additionally, these complexes are extremely beneficial in optical applications because of their remarkable luminescence properties. However, a notable drawback of lanthanide *β*-diketones is their limited photostability when exposed to UV irradiation, which can lead to degradation over time. The neutral tris complexes or tris(*β*-diketonates) usually have three *β*-diketonate ligands for each lanthanide(III) ions, and they can be represented by the general formula [Ln(*β*-diketonate)$_3$].[46–47] Because the coordination sphere of the lanthanide(III) ions is unsaturated in these six-coordinate complexes, the lanthanide(III) ions can expand its coordination sphere by oligomer formation (with bridging *β*-diketonate ligands) but also by adduct formation with Lewis bases, such as water, 1,10-phenanthroline (phen),[47–51] 2,2′-bipyridine (bpy),[51–52] or tri-*n*-octylphosphoxide. Some of the Lewis bases used in lanthanide ions are shown in Figure 1-8.

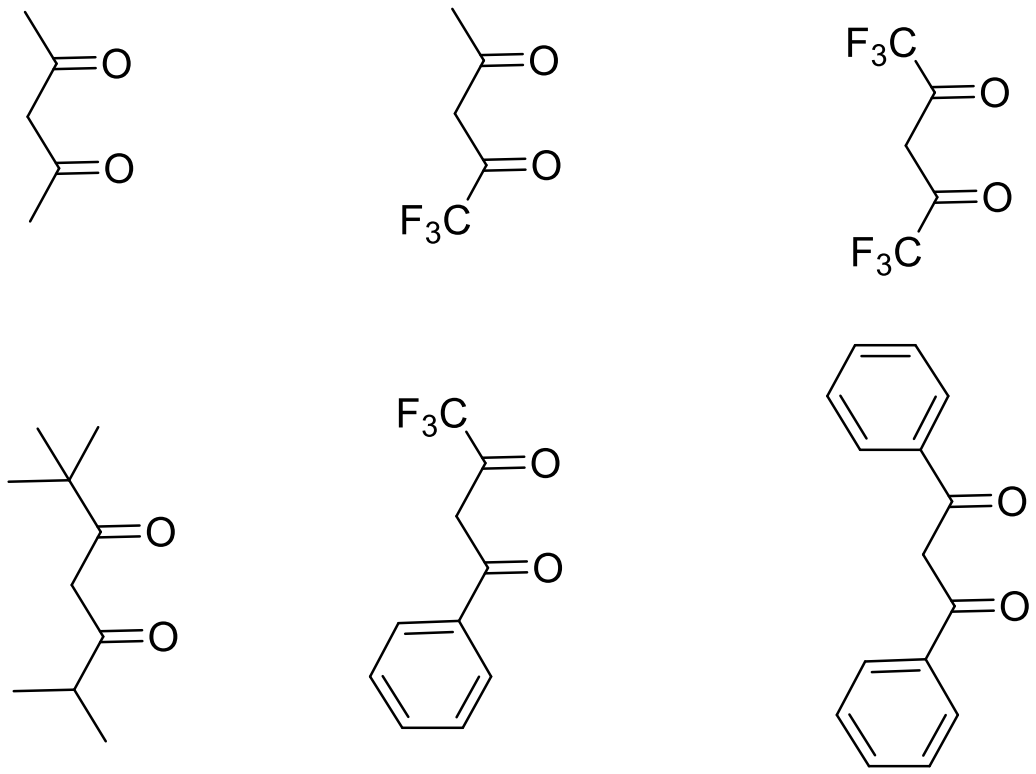

Figure 1-7. Chemical structures of diketones.

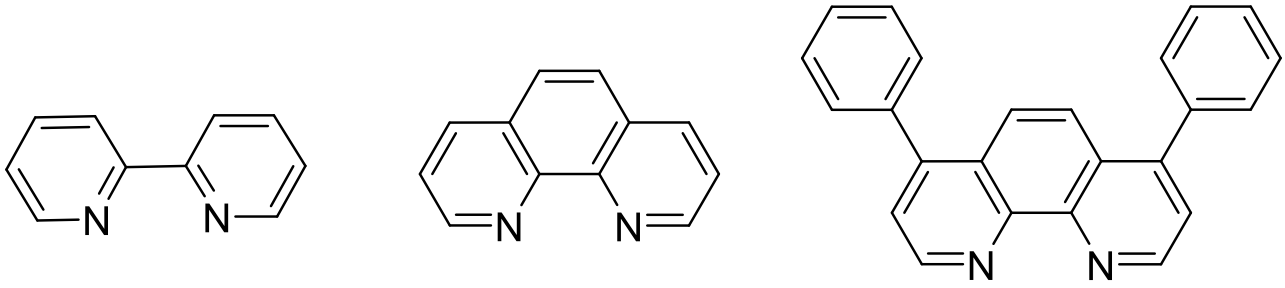

Figure 1-8. Structures of Lewis bases used in lanthanide *β*-diketonate complexes.

The luminescent europium(III) *β*-detonate complex, [Eu(tta)$_3$(phen)],[53] features a central europium(III) ion coordinated by three *β*-detonate ligands (thenoyltrifluoroacetone, tta) and one phenanthroline (phen) molecule as shown in Figure 1-9. In this structure, each tta ligand forms a stable chelate ring around the europium ion by coordinating through its oxygen atoms, while the phenanthroline ligand coordinates via its two nitrogen atoms, therefore enhances the stability of the complex. The overall coordination geometry around the europium(III) ion is eight-coordinate, formed by the three bidentate tta ligands and the bidentate phen ligand. The complex is known for its strong red luminescence, which results from efficient energy transfer from the tta ligands to the europium ion, followed by characteristic red emission from the europium(III) 4f–4f transitions. However, while [Eu(tta)$_3$(phen)] is popular for its bright red

emission, it may require additional stabilization as it can suffer from photodegradation under prolonged UV exposure.

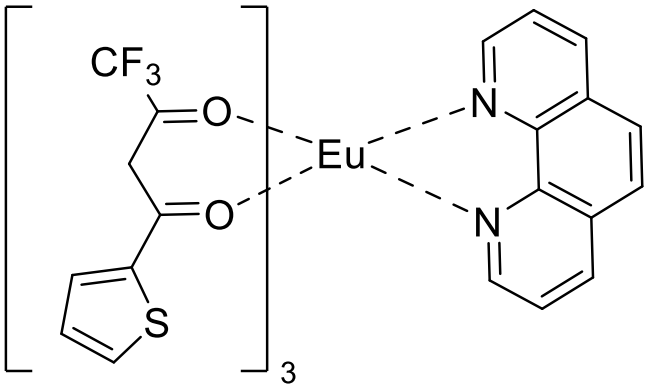

Figure 1-8. Structure of the luminescent europium(III) β-diketonate complex [Eu(tta)$_3$(phen)].

1.5.2. Nanocomposites lanthanide-doped inorganic material

Lanthanide-doped inorganic nanocomposites offer numerous advantages over traditional lanthanide complexes, due to their unique structural and material properties. One primary benefit is the enhanced photostability provided by the inorganic matrix, which protects lanthanide ions from UV radiation and environmental factors that can lead to photodegradation—an issue frequently observed with β-diketonate complexes. Additionally, these nanocomposites exhibit improved thermal stability, which makes them suitable for applications that involve higher temperatures, where β-diketonate complexes would be prone to thermal breakdown. In terms of luminescent performance, nanocomposites often show superior quantum efficiency. The inorganic matrix minimizes vibrational coupling and nonradiative decay processes, which are more prominent in organic β-diketonate complexes. Therefore, the inorganic matrix leads to brighter and more efficient luminescence. The common comparison between lanthanide inorganic hybrid and lanthanide complexes is described in Table. 1.3. Moreover, the inorganic host matrix can broaden the excitation range and allow the material to absorb over a broader UV–visible region. This feature enables lanthanide-doped nanocomposites to be excited by a more extensive range of light sources compared to the narrower absorption profiles of β-diketonate complexes. Lanthanide-doped inorganic nanocomposites are generally more robust against environmental degradation, such as oxidation or hydrolysis, which extends their usability in various applications. These advantages make lanthanide-doped inorganic nanocomposites very attractive for diverse applications in lighting, displays, bioimaging, and sensing technologies, where both durability and efficient luminescence are essential.

Table 1-3. Comparison between inorganic and organic lanthanide luminescent material.

Doped Lanthanide(III)–Inorganic Hybrid	Lanthanide(III) Complexes
Physicochemical properties tuned by surface modification	Physicochemical behaviour tuned at the atomic level through molecular chemistry
Radiative process is more efficient	Nonradiative deactivation makes luminescence weak
Used for lighting, display, telecom technology	Used in medical tests, bioimaging and luminescent doped polymers

1.5.3. Inorganic host matrices for lanthanide(III) ions

The luminescence intensity of lanthanide(III) ions is significantly influenced by concentration quenching, a process where energy transfer between neighboring lanthanide(III) ions facilitates non-radiative relaxation, thereby decreases emission intensity. This occurs due to the close proximity of the ions, which increases the probability of energy migration to non-radiative centers, such as defects or impurities. To minimize concentration quenching, the lanthanide(III) ions are typically diluted within a host matrix and maintain concentrations between 1 and 5 mol% relative to the host cations. This dilution ensures that the lanthanide(III) ions remain sufficiently separated, reduces energy migration and enhances luminescence. In addition to avoid concentration quenching, the choice of the host matrix is crucial to control non-radiative relaxation processes. The matrix provides a protective environment for the lanthanide(III) ions and reduces vibrational coupling with high-energy oscillators such as O–H or N–H bonds. Therefore, in a host matrix with low phonon energy, the non-radiative losses can be minimized, which ultimately improves the luminescence quantum efficiency. Common host matrices include oxides, fluorides, and phosphates, which offer a combination of low phonon energy and chemical stability, which makes them ideal for luminescent applications. Numerous host materials are available for lanthanide(III) ions, categorized by their anion types, includes fluorides (e.g., $NaYF_4$, $LiYF_4$),[54–55] oxides (e.g., Y_2O_3, Gd_2O_3),[51] vanadates, garnets (e.g., $Y_3Al_5O_{12}$, $Lu_3Ga_5O_{12}$),[56] molybdates, and phosphates. Materials which contain alkaline earth ions, such as CaF_2, BaF_2, and SrF_2, are also suitable hosts for lanthanide(III) ions.[57–58] Fluorides and oxides are the most commonly employed among the host matrices used for lanthanide(III)-doped nanocrystals (NCs). Oxides are favored for their excellent chemical

stability, which ensures durability in various applications. However, their relatively high phonon energy (~600 cm^{-1}) facilitates non-radiative relaxation processes and potentially lowers the luminescence efficiency of the embedded lanthanide(III) ions. This characteristic makes them less ideal for applications as they require high quantum yield. Fluorides, on the other hand, offer a significant advantage due to their lower phonon energy (~350 cm^{-1}). This reduction in phonon energy minimizes non-radiative cross-relaxation processes and enhances the luminescence efficiency of lanthanide(III) ions. Additionally, fluorides maintain chemical stability, which makes them a superior choice for lanthanide(III)-doped host matrices.

Among fluoride hosts, calcium fluoride (CaF_2) has proven to be an effective and desirable matrix for lanthanide(III)-doped nanocrystals due to its unique structural and optical properties. The ionic size of Ca^{2+} closely matches that of most lanthanide(III) ions, which minimizes crystal defects and reduces lattice stress. This structural compatibility allows for a high solubility of both sensitizer and activator ions and enables the synthesis of efficient phosphors across a broad concentration range. The simple cubic structure of CaF_2 also facilitates uniform doping and contributes to its widespread use.

As a dielectric material, CaF_2 exhibits an impressive optical window range from 0.13 to 10 μm, making it suitable for diverse optical applications such as infrared and ultraviolet optics, microscopy, astronomical instrumentation, and spectroscopy. Chen et al. reported the development of sub-10 nm cerium(III)/terbium(III)-doped CaF_2 nanoprobes for time-resolved luminescence bio-detection, which underscores the versatility of CaF_2 in biomedical and analytical applications.[57–59] These nanoprobes showcased high sensitivity and specificity in luminescence-based detection, which demonstrates their potential in various bio-analytical fields. The success of these nanoprobes further highlights the functional adaptability of CaF_2 as a host matrix for lanthanide-doped nanocrystals, ultimately favours it as an excellent choice for applications ranging from fundamental research in material science to practical implementations in biomedicine and diagnostics.

1.6. Lanthanide(III)-doped nanocrystals: detection application

Lanthanide(III)-doped nanocrystals are highly advantageous for detection and sensing applications due to their exceptional luminescent properties. They exhibit long luminescence lifetimes, allow time-gated detection and effectively reduce background interference. Additionally, their narrow emission peaks remain unperturbed by the crystal field, therefore establishes precise and reliable signals.[60] These nanocrystals also possess a large Stokes shift, minimize the overlap between excitation and emission spectra and high photobleached

resistance, and enhance their durability under prolonged exposure to light. These features make lanthanide(III)-doped nanocrystals superior to other luminescent markers, such as quantum dots and organic dyes, which often suffer from shorter lifetimes and poor stability. Detection *via* lanthanide(III)-doped nanocrystals typically relies on the resonance energy-transfer mechanism, which requires two conditions: an overlap between the emission spectrum of the nanocrystals and the absorption band of the acceptor and an optimal distance between the donor and acceptor molecules. The versatility of lanthanide(III) ions, which emit across the UV to NIR regions of the electromagnetic spectrum, allows for the design of tailored sensing systems. Through the selection of the appropriate lanthanide(III) ions, effective spectral overlap with target analytes can be achieved, enables highly specific and efficient sensing applications.

1.7. Purpose of the study

The primary purpose of this thesis is to investigate efficient methods for the development of lanthanide-based luminescent materials, focused to achieve cost-effective luminescence from lanthanide(III) ions to enhance their practical applicability in real-life scenarios. This research explores polymeric systems as cation-exchange media and inorganic host media, aims to optimize the sensitization processes, and broadens their potential applications in fields such as sensing, imaging, and optoelectronics.

This work introduces a straightforward and effective strategy to enhance lanthanide(III) ions luminescence by employing ionic nanospheres as cation-exchange media. The hybridized lanthanide(III) ions, through the interaction with these media, have demonstrated significant luminescence enhancement. In the case of ionic nanospheres, luminescence is sensitized through energy transfer mechanisms, where the nanospheres function not only as hosts for lanthanide(III) ions but also as efficient photosensitizers. This innovative approach, which utilizes an aqueous environment, offers numerous advantages over conventional methods, which include reduced costs, simplified preparation, and shorter synthesis times.

Additionally, this work explores the hybridization of lanthanide(III) ions with ligand-sensitized inorganic hosts. These ligand-sensitized materials have shown potential real-life applications, particularly in the detection of chromate and permanganate ions. The methods developed to achieve sensitized luminescence from lanthanide(III) ions through cation-exchange media, as well as other hybridization approaches, represent a novel contribution to the field. This research aims to simplify the development of lanthanide(III) ions luminescent materials by employing the unique photophysical properties of lanthanide(III) ions. The study addresses key challenges, such as synthesis complexity, cost reduction, and practical integration

of these materials into real-world applications. This work seeks to drive advancements in critical fields such as bioimaging, environmental sensing, optoelectronics, which broadens the applicability and impact of lanthanide-based luminescent materials.

1.8. References

1) S. Cotton, *Lanthanide and Actinide Chemistry*, John Wiley & Sons, **2024**.
2) M. Seitz, A. G. Oliver, K. N. Raymond, *J. Am. Chem. Soc.* **2007**, *129*, 11153.
3) M. H. Werts, *Sci. Prog.* **2005**, *88*, 101.
4) J. Becquerel, *Compt. Rend. Hebd. Acad. Sci.* **1906**, *142*, 775–779.
5) J. C. G.Bünzli, & S. V. Eliseeva, *Lanthanide Luminescence: Photophysical, Analytical and Biological Aspects*, 2011, 1–45.
6) H. Bethe, *Z. Phys.* **1930**, *60*, 218.
7) J. H. Van Vleck, *J. Phys. Chem.* **1937**, *41*, 67.
8) Chen, D., Wang, Y., & Hong, M. *Nano Energy* **2012**, *1*(1), 73–90.
9) K. Binnemans, *Coord. Chem. Rev.* **2015**, *295*, 1.
10) W. D. Horrocks Jr., D. R. Sudnick, *Acc. Chem. Res.* **1981**, *14*, 384.
11) A. G. Bispo-Jr., A. J. de Morais, C. M. S. Calado, I. O. Mazali, F. A. Sigoli, *J. Lum.* **2022**, *252*, 119406.
12) N. S. Singh, R. S. Ningthoujam, M. N. Luwang, S. D. Singh, R. K. Vatsa, *Chem. Phys. Lett.* **2009**, *480*, 237.
13) L. D. Carlos, R. A. Ferreira, V. D. Z. Bermudez, S. J. Ribeiro, *Adv. Mater.* **2009**, *21*, 509.
14) K. Binnemans, *Chem. Rev.* **2009**, *109*, 4283.
15) P.Escribano, B. Julián-López, J. Planelles-Aragó, E. Cordoncillo, B. Viana, C. Sanchez, *J. Mater. Chem.* **2008**, *18*, 23.
16) P. Dorenbos, *Chem. Mater.* **2005**, *17*, 6452.
17) J. Feng, H. Zhang, *Chem. Soc. Rev.* **2013**, *42*, 387.
18) R. E. Whan, G. A. Crosby, *J. Mol. Spectrosc.* **1962**, *8*, 315.
19) R. E. Whan, G. A. Crosby, *J. Mol. Spectrosc.* **1962**, *8*, 315.
20) M. Kleinerman, *J. Chem. Phys.* **1969**, *51*, 2370.
21) D. A. Atwood (Ed.), *The Rare Earth Elements: Fundamentals and Applications*, John Wiley & Sons, **2013**.
22) S. V. Eliseeva, J. C. G. Bünzli, *Chem. Soc. Rev.* **2010**, *39*, 189.

23) M. Latva, H. Takalo, V. M. Mukkala, C. Matachescu, J. C. Rodríguez-Ubis, J. Kankare, *J. Lum.* **1997**, *75*, 149.
24) J. Khanagwal, R. Kumar, R. Devi, M. Bala, P. Sehrawat, S. P. Khatkar, V. B. Taxak, *Luminescence* **2021**, *36*, 742.
25) X. Qin, X. Liu, W. Huang, M. Bettinelli, X. Liu, *Chem. Rev.* **2017**, *117*, 4488.
26) S. K. Gupta, R. M. Kadam, P. K. Pujari, *Coord. Chem. Rev.* **2020**, *420*, 213405.
27) J. Shi, Y. Hou, W. Chu, X. Shi, H. Gu, B. Wang, Z. Sun, *Inorg. Chem.* **2013**, *52*, 5013.
28) K. Binnemans, *Handbook on the Physics and Chemistry of Rare Earths*, Elsevier, **2005**, *35*, 107.
29) O. Sun, T. Gao, J. Sun, G. Li, H. Li, H. Xu, ... P. Yan, *CrystEngComm* **2014**, *16*, 10460.
30) O. Guillou, C. Daiguebonne, *Handbook on the Physics and Chemistry of Rare Earths*, **2004**, *34*, 359.
31) A. V. Yakimanskii, M. Y. Goikhman, I. V. Podeshvo, T. D. Anan'Eva, T. N. Nekrasova, R. Y. Smyslov, *Polym. Sci., Ser. A* **2012**, *54*, 921.
32) D. T. De Lill, C. L. Cahill, *Prog. Inorg. Chem.* **2007**, *55*, 143.
33) C. Daiguebonne, N. Kerbellec, Y. Gérault, O. Guillou, *J. Alloys Compd.* **2008**, *451*, 372.
34) R. Su, J. Gao, S. Deng, R. Zhang, Y. Zheng, *J. Sol-Gel Sci. Technol.* **2016**, *78*, 606.
35) H. F. Lu, B. Yan, *J. Photochem. Photobiol., A: Chem.* **2008**, *194*, 136.
36) T. Jin, S. Inoue, S. Tsutsumi, K. I. Machida, G. Y. Adachi, *J. Non-Cryst. Solids* **1998**, *223*, 123.
37) H. Li, X. Wang, T. Y. Ohulchanskyy, G. Chen, *Adv. Mater.* **2021**, *33*, 2000678.
38) L. Prodi, E. Rampazzo, F. Rastrelli, A. Speghini, N. Zaccheroni, *Chem. Soc. Rev.* **2015**, *44*, 4922.
39) S. B. Meshkova, V. E. Kuz'Min, Y. E. Shapiro, Z. M. Topilova, I. V. Yudanova, D. V. Bol'shoi, V. P. Antonovich, *J. Anal. Chem.* **2000**, *55*, 102.
40) A. I. Petrov, M. A. Lutoshkin, I. V. Taydakov, *Eur. J. Inorg. Chem.* **2015**, *2015*, 1074.
41) M. A. Lutoshkin, A. I. Petrov, Y. N. Malyar, A. S. Kazachenko, *Inorg. Chem.* **2021**, *60*, 3291.
42) A. Hooda, K. Nehra, A. Dalal, S. Singh, R. K. Saini, S. Kumar, D. Singh, *Inorg. Chim. Acta* **2022**, *536*, 120881.
43) K. Nehra, A. Dalal, A. Hooda, S. Bhagwan, R. K. Saini, B. Mari, D. Singh, *J. Mol. Struct.* **2022**, *1249*, 131531.
44) P. A. Vigato, V. Peruzzo, S. Tamburini, *Coord. Chem. Rev.* **2009**, *253*, 1099.

45) R. van Staveren, G. A. van Albada, J. G. Haasnoot, H. Kooijman, A. M. M. Lanfredi, P. J. Nieuwenhuizen, A. L. Spek, F. Ugozzoli, T. Weyhermuller, J. Reedijk, *Inorg. Chim. Acta* **2001**, *315*, 163.

46) A. Bellusci, G. Barberio, A. Crispini, M. Ghedini, M. La Deda, D. Pucci, *Inorg. Chem.* **2005**, *44*, 1818.

47) I. V. Taydakov, V. M. Korshunov, Y. A. Belousov, Y. V. Nelyubina, F. Marchetti, R. Pettinari, C. Pettinari, *Inorg. Chim. Acta* **2020**, *513*, 119922.

48) G. Brito-Santos, B. Gil-Hernández, I. R. Martín, R. Guerrero-Lemus, J. Sanchiz, *RSC Adv.* **2020**, *10*, 27815.

49) L. F. Marques, H. P. Santos, K. A. D'Oliveira, N. P. Botezine, M. C. R. Freitas, R. O. Freire, ... F. C. Machado, *Inorg. Chim. Acta* **2017**, *458*, 28.

50) I. J. Al-Busaidi, R. Ilmi, D. Zhang, J. D. Dutra, W. F. Oliveira, N. K. Al Rasbi, ... M. S. Khan, *Dyes Pigm.* **2022**, *197*, 109879.

51) G. Blasse, *Spectra and Chemical Interactions*, **1976**.

52) D. Tu, Y. Liu, H. Zhu, R. Li, L. Liu, X. Chen, *Angew. Chem.* **2013**, *125*, 4.

53) X. Xue, S. Uechi, R. N. Tiwari, Z. Duan, M. Liao, M. Yoshimura, Y. Ohishi, *Opt. Mater. Express* **2013**, *3*, 989.

54) V. Buissette, D. Giaume, T. Gacoin, J. P. Boilot, *J. Mater. Chem.* **2006**, *16*, 529.

55) X. Zhou, K. Zhou, Y. Li, Z. Wang, Q. Feng, *J. Lum.* **2012**, *132*, 3004.

56) N. Dubey, S. Gupta, S. B. Shelar, K. C. Barick, S. Chandra, *Molecules* **2024**, *29*, 4177.

57) B. Jiang, L. Zheng, D. Jiang, H. Yin, J. Zheng, Q. Yang, G.Cheng, L. Su, *J. Rare Earths* **2021**, *39*, 390.

58) R. K. Sharma, S. Nigam, Y. N. Chouryal, S. Nema, S. P. Bera, Y. Bhargava, P. Ghosh, *ACS Appl. Nano Mater.* **2019**, *2*, 927.

59) W. Zheng, S. Zhou, Z. Chen, P. Hu, Y. Liu, D. Tu, X. Chen, *Angew. Chem. Int. Ed.* **2013**, *52*, 26.

60) X. Ling, R. Shi, J. Zhang, D. Liu, M. Weng, C. Zhang, W. Huang, *ACS Sensors* **2018**, *3*, 1683.

Chapter 2 Sensitized luminescence from terbium(III) ion doped in ionic nanosphere

2.1. Summary

In this chapter, ionic nanospheres was employed as a novel sensitizer for terbium(III) ion through a straightforward ion-exchange process. This work focuses on the development of a highly luminescent hybrid material, where terbium(III) ion is doped into the ionic nanosphere framework. The ionic nanospheres serve as an efficient host and photosensitizer, providing an optimized environment that enhances the luminescence properties of terbium(III) ion. The study highlights the simplicity of the ion-exchange process, which ensures uniform doping while preserving the structural integrity of the nanospheres. This approach effectively facilitates energy transfer, reduces nonradiative relaxation, and significantly improves the photophysical performance of terbium(III) ion. The results demonstrate the potential of these hybrid materials for applications in bioimaging, sensing, and optoelectronic devices and offer a practical and scalable solution to develop advanced luminescent systems.

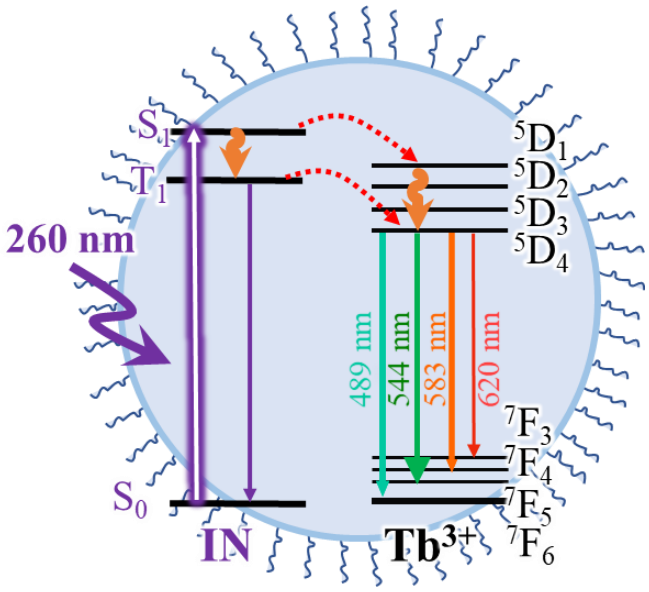

Figure 2-1. Systematic energy transfer from ionic nanosphere to terbium(III) ion

2.2. Introduction

Terbium(III) ion which belongs to the lanthanide group of rare-earth elements is distinguished by its distinctive green luminescence which is caused by its unique 4f–4f transition.[1–4] The electrons and 4f orbitals of terbium(III) ion are insensitive to the surrounding environment because they are situated in the inner orbitals and therefore terbium(III) has narrow

luminescence bands. The long-lived excited states and luminescence color purity of terbium(III) ion have enabled the utilization various photochemical applications (e.g., sensing, photovoltaics, phosphor, photocatalysis, bioimaging).[5–9] Despite the aforementioned benefits, the absorption coefficient hardly reaches unity. Thus a range of highly luminescent terbium(III) ion system have been developed by in terms of light absorption, accelerated radiative processes, and decelerated nonradiative processes. These systems includes discrete metal complexes,[10–14] coordination polymers,[15–18] nanomaterial[19–22] and many more. Although these techniques have demonstrated remarkable efficacy in enhancing the luminescence of terbium(III) ion, they require a rigorous synthesis procedure and are typically laborious and time consuming. As a result, it is still challenging to get luminescence from terbium(III) ion using an easy and straightforward procedure.

In this study, sensitization of luminescence from terbium(III) ion was succeeded by doping in the ionic nanosphere. This method has a huge advantage over these methods as the terbium luminescence was achieved by a simple mixing process, which is a novel process and a time-saving method. The ionic nanosphere is a water dispersion medium of copolymer sodium styrene sulphonate and divinylbenzene (DVB), which can act as a cation exchange resin with an average diameter of <300 nm.[23] The typical chemical structure of the ionic nanosphere is shown in Scheme 2-1. It can also accommodate various cations in its nanometer-scale space by a facile procedure. Since the ionic nanosphere possesses a poly(*p*-styrenesulfonate-*co*-divinylbenzene) backbone, it acts as a photosensitizer for doped terbium(III) ions through the energy transfer in an aqueous medium.

One of the key functions of the ionic nanosphere is to create a hydrophobic environment around terbium(III) ions, which helps to protect terbium(III) ions from being quenched by -OH vibration in an aqueous medium. This is important as terbium(III) ions are highly susceptible to such a quenching effect, which can reduce their luminescence. Another role of the ionic nanosphere is facilitating energy transfer processes between the terbium ions and other species in the system. When the nanosphere is excited by light, it can transfer its excited energy to the terbium ions leading to the luminescence of terbium ions in their characteristic emission peak in the visible region. Therefore, the ionic nanosphere will emerge as a new type of photosensitizer for the lanthanide ion and can be used not only for terbium ions but also for other lanthanide ions for the down-conversion and up-conversion process. Hence, I have succeeded in developing a water-dispersion luminescent lanthanide polymeric system.

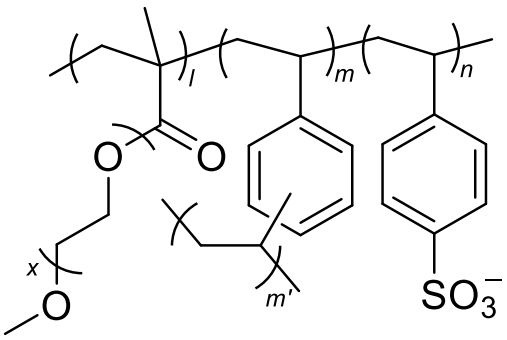

Scheme 2-1. Chemical structure of ionic nanosphere.

2.3. Experimental

2.3.1. Materials and analysis

Chemicals were supplied from FUJIFILM Wako Pure Chemical Corporation, Tokyo Chemical Industry Co., Ltd. or Sigma–Aldrich Co., LLC and used without purification unless otherwise noted. Deionized water for the synthesis and sample preparations were supplied from a WL220 ion-exchange water purifier (Yamato Scientific Co., Ltd.). Column chromatography was performed using silica gel PSQ60B (Fuji Silysia Chemical Ltd.). A ^{1}H-NMR spectrum of purified DVB in $CDCl_3$ was recorded by a JEOL JMN-ECZ400S spectrometer (400 MHz), and the chemical shift was determined using tetramethylsilane as an internal standard. Dialyses of the nanosphere samples were performed using a regenerated cellulose dialysis tube Spectra/Pro 6 (Spectrum Laboratories Inc., cut-off molecular weight (COMW): 50 kDa) or a cellulose dialysis tube (ASONE, COMW: 12–14 kDa). Particle-size distributions of the nanosphere samples were evaluated using a Malvern Panalytical Zetasizer Nano ZSP dynamic light scattering instrument. Elemental analyses by the inductively-coupled plasma optical emission spectroscopy (ICP-OES) for samples decomposed by additions of concentrated nitric acid followed by microwave irradiation were performed by an Agilent 5800 VDV ICP-OES in the Kochi Prefectural Industrial Technology Center.

2.3.2. Synthesis of ionic nanosphere

DVB was purified according to a reported procedure[24] with slight modifications. Copper(I) chloride (34 g, 340 mmol) was added in small quantities to commercial 55% DVB (100 g, ~420 mmol), which was stirred at 4°C in an ice bath. To a resulting yellow viscous suspension was added toluene (35 mL) and then stirred at 4°C for a further 30 min. The collected yellow solids were poured into toluene (100 mL) at 4°C. The solid was collected by filtration. The obtained copper(I)–DVB complex was suspended in toluene (60 mL) and heated at 80°C for 1 h. After

removing grey insolubles by a hot filtration, the filtrate was concentrated under reduced pressure. A trace amount of copper(I) complex was removed by silica-gel column chromatography (eluent: *n*-hexane), affording DVB as a meta/para mixture (1/2, mol/mol by ^{1}H-NMR). A solution of sodium *p*-styrenesulfonate (*p*-SS, 0.49 g, 2.4 mmol), purified DVB (0.31 g, 2.4 mmol), poly(ethylene glycol)methacrylate methyl ether (M_n: 2000, 50wt% in water, 1.06 g), and ammonium persulfate (0.0228 g, 0.010 mmol) in DMF/water (7.5 mL/4.5 mL) was deaerated by argon-gas bubbling at 0°C for 30 min. The solution was stirred at 72°C for 6 h under an argon-gas atmosphere. The resulting suspension was dialyzed (COMW: 50 kDa) for 3 d with a gradual change of dialysate from DMF/water (3/2, *v*/*v*) to pure water, affording an aqueous dispersion of the ionic nanosphere (17.72 ± 0.26 mg/mL from freeze drying experiments).

2.3.3. Preparation of terbium(III)- and gadolinium(III)-doped ionic nanospheres

Terbium(III)-doped nanospheres (5.04, 10.1, 20.2, 30.2, 40.3, 49.9, 99.8, 200, and 299 nmol mg^{-1}) were prepared by soaking and stirring the ionic nanosphere (2.13 mg/mL, 3 mL) in aqueous solutions of terbium(III) chloride [(4.59–273) × 10^{-6} mol dm^{-3}, 7 mL] at room temperature for 3 d. Undoped species were removed by dialysis (COMW: 12–14 kDa, dialysate: water, 1 d × 3). An aqueous dispersion of gadolinium(III)-doped nanosphere (213 nmol mg^{-1}) was prepared similarly. Terbium(III)-doped nanospheres in D_2O and H_2O were obtained by repeated dialyses using D_2O and H_2O, respectively, after soaking the neat nanosphere in an aqueous terbium(III) chloride solution (300 nmol mg^{-1}).

2.3.4. Spectroscopic and photophysical measurements

All the spectroscopic measurements were performed for the aqueous dispersions of the nanospheres. Absorption spectra were recorded by a Hitachi High-Tech U-3900 spectrophotometer equipped with a ϕ60 integrating sphere. Steady-state luminescence and excitation spectra were measured using a Hitachi High-Tech F-4500 fluorescence spectrophotometer equipped with a red-sensitive R928 photomultiplier tube and long-pass filters (295 and 305 nm). For luminescence decay measurements, a third harmonics of a Continuum Surelite™ II-10 nanosecond Q-switched Nd:YAG laser (355 nm, repetition rate: 10 Hz, 12 mJ/pulse) was used as an excitation light. Luminescence from a sample was monochromated by an Acton SpectraPro® 2300i and monitored by an IWATSU ViewGo-II DS-5532A digital oscilloscope (frequency bandwidth: 350 MHz, peak detect resolution: 1 ns) through a Hamamatsu R928 photomultiplier tube amplified by a Hamamatsu C9663 wide

bandwidth amplifier unit. Due to weak luminescence arising from small absorbances at 355 nm, wave-form baselines were reduced using a sine function. For the phosphorescence measurement, 254-nm light from a UVP compact UV lamp was irradiated to a frozen aqueous dispersion of gadolinium(III)-doped nanosphere, whose temperature was controlled at 77 K by an Oxford Instruments optistatDN cryostat, and the luminescence after a disappearance of fluorescence upon turning off the UV lamp was recorded by a Princeton Instruments PI-MAX ICCD camera with an Acton SpectraPro 2300i imaging spectrograph/ monochromator. Samples for the luminescence measurements were diluted with HPLC-grade distilled water (FUJIFILM Wako Pure Chemical Corporation) to avoid the inner-filter effect and then deaerated by argon-gas bubbling to remove molecular oxygen. Vertical axes of all the luminescence spectra are given in a photon-number scale.

2.4. Characterization of ionic nanosphere

The average particle size of the ionic nanosphere was determined by dynamic light scattering measurement as shown in Figure 2-2. The mean diameter size was determined to be 166±65 nm, suggesting that the ionic nanosphere was successfully synthesized. The single peak observed in the DLS measurement suggest a spherical shape of ionic nanosphere, as no additional peaks were detected even after repeated measurements. In contrast, non-spherical particles, such as fibers, rectangles, or cubic etc. would produce multiples peaks due to variations in light scattering at different angles. The absence of such peaks further supports the spherical morphology of the ionic nanosphere. Other morphology analysis such as TEM or SEM, could not performed as the synthesized ionic nanosphere exist in an aqueous dispersion. These techniques are not suitable for accurately assessing the morphology of aqueous dispersion samples.

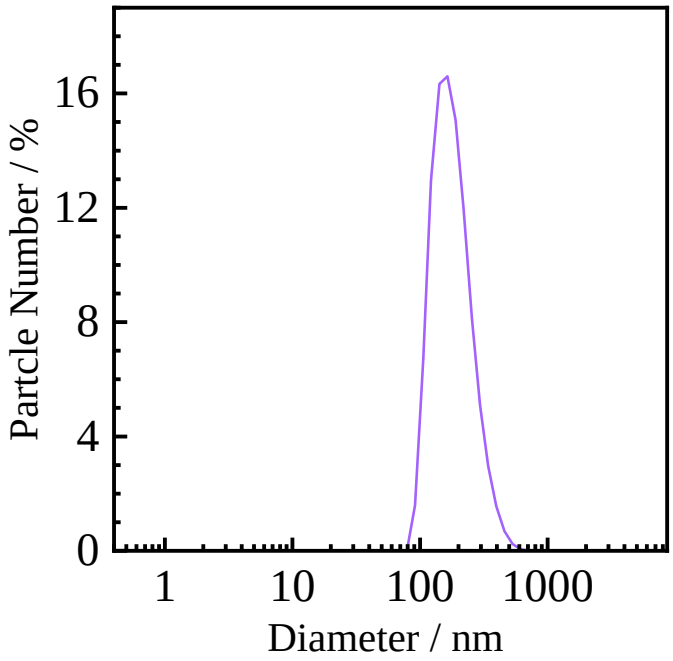

Figure 2-2. Particle-size distribution of the aqueous dispersion of the ionic nanosphere.

Absorption and fluorescence spectra of the ionic nanosphere is shown in Figure 2-3. The ionic nanosphere has several bands of absorption in the <320 nm range. The mass absorption coefficients at 223 and 258 nm were found to be 30.9 L g^{-1} cm^{-1} and 8.7 L g^{-1} cm^{-1}, respectively, and the absorbances of the bands rose proportionately with an increase in the nanosphere concentration, as stated by the Beer law. The absorption bands can be attributed to the π–π* transition of the poly(*p*-SS-*co*-DVB) structure since the values are suitably large. The fluorescence spectrum of ionic nanosphere falls between 300 nm and 400 nm. The fluorescence from the ionic nanosphere was ascribed to the π–π* excited state of the poly(*p*-SS-*co*-DVB) system in the nanosphere because of the band-shape resemblance to the absorption band. The broad fluorescence band of the ionic nanospheres corresponds to the direct 4f–4f excitation bands of terbium(III) ion, which are visible at 318 nm, 342 nm, 352 nm, 370 nm, 377 nm, and so on (see Figure 2-4). Thus, in addition to its strong absorption of UV light, the ionic nanosphere should also function as a good photosensitizer for terbium(III) ions.

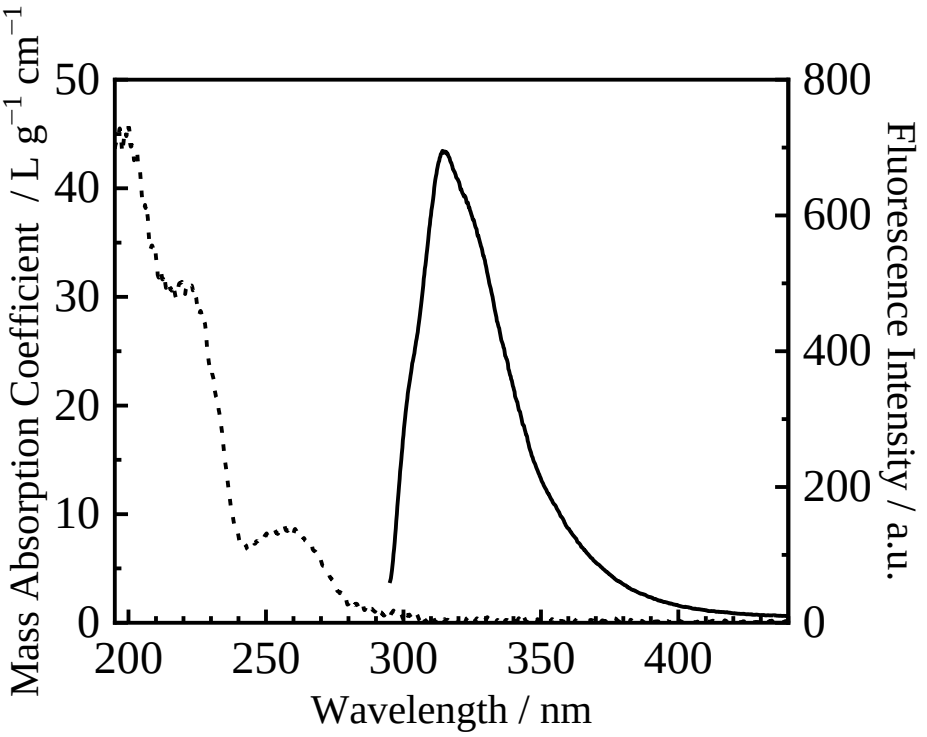

Figure 2-3. Absorption (broken curve) and fluorescence spectra (solid curve, λ_{ex} = 260 nm) of the ionic nanosphere.

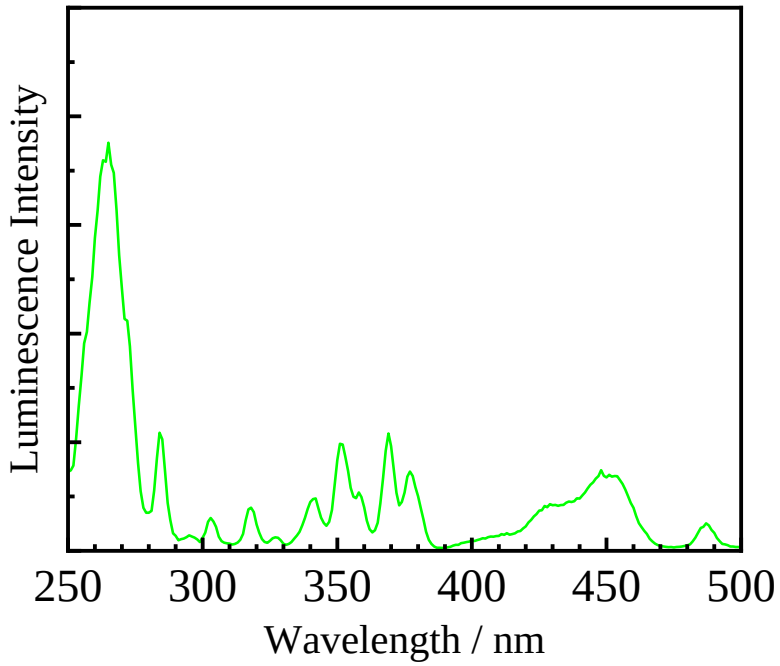

Figure 2-4. Excitation spectrum of $TbCl_3$ in water (λ_{em} = 543 nm).

2.5. Doping of terbium(III) ion in ionic nanosphere

Terbium(III)-doped ionic nanospheres were straightforwardly made by mixing an aqueous

solution of terbium(III) chloride with an aqueous dispersion of the ionic nanosphere. By adjusting the concentration of terbium(III) chloride, the amount of terbium(III) ion could be controlled. Dialysis was performed to eliminate undoped species, such as sodium chloride, produced by the ion-exchange reaction. It can be assumed that the terbium(III) ion was quantitatively doped in the nanosphere because no luminescence from terbium(III) species was seen for the dialysate, even under concentrated conditions. The contents of the terbium(III) ion in the nanosphere were found to be 5.04 to 299 nmol mg^{-1}. For further characterization, elemental analyses by ICP-OES were performed for the nanospheres in the absence and presence of terbium(III) ion (299 nmol mg^{-1}). The Tb/S and Na/S molar ratios of the terbium(III)-doped samples were 0.196±0.005 and 0.167±0.007, respectively, whereas the Na/S value of the neat nanosphere was 0.768±0.006 (terbium was not detected). Since a variation in the Na/S ratio upon terbium(III) doping is equivalent with the three Tb/S value of the terbium(III)-doped sample, the results clearly indicate that the terbium(III) ion is introduced into the sample by replacing three sodium ions. The dynamic light scattering approach was used to assess the sample particle-size distributions to comprehend the effect of terbium(III)-ion doping on the ionic nanospheres. As seen in Figure 2-5, mean diameters of the terbium(III)-doped nanospheres (<100 nm) were smaller than that of the neat nanosphere. The ion exchange process, in which three sodium ions are discharged on behalf of one terbium (III) ion, explains this size drop. It is anticipated that the terbium(III) ion will form electrostatic bonds with three or more sulfonate groups, causing the ionic nanospheres to contract due to the many ionic bonds. Unlike the sharp drop in the nanosphere's diameter that occurs when terbium(III) is doped, there was no discernible relationship between the samples of terbium(III) content and diameter. It is presumably due to homogeneous distribution of terbium(III) ion in the nanosphere. The diameter of the nanosphere corresponds to the size of the secondary particle, and terbium(III) ion may decrease the distance between primary poly(*p*-SS-*co*-DVB) macromolecules. Although the ion-exchange reactions by the ionic nanospheres are quite fast (<1 min), the suspension was usually soaked and stirred for over 3 d to obtain homogeneously-doped samples. Such homogeneous distribution of terbium(III) ion as a counterion lets the nanosphere shrink effectively even at the small content being 5.04 nmol mg^{-1}. The spherical shape of ionic nanosphere would also help in minimizing the light scattering and enhancing the terbium(III) ion luminescence compared to the non-spherical particles. In non-spherical particles such as rectangles, fibres or cubic shapes the excitation light encounters multiple surfaces at different angles, leading to the unwanted scattering and loss of energy. However, in ionic nanosphere, the light can pass through uniformly without significant scattering, ensuring that the maximum

amount of excitation energy reaches the terbium(III) ion, which leads to a stronger luminescence.

Figure 2-6 shows the absorption spectra of terbium(III)-doped nanospheres (5.04–299 nmol mg^{-1}). The spectra were nearly identical, and the absorption bands at around 220 nm and 260 nm were attributed to the π–π* transitions in the poly(*p*-SS-*co*-DVB) structure. The findings verify that the ionic nanosphere is primarily responsible for the light absorption of the terbium(III)-doped nanospheres and that direct excitation of the terbium(III) ion does not significantly contribute.

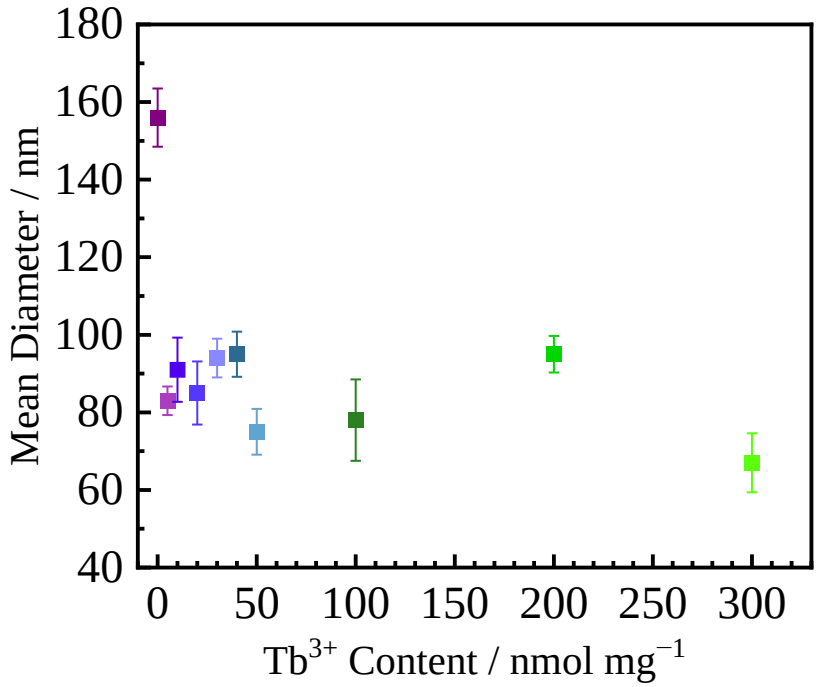

Figure 2-5. Terbium(III)-content dependence on mean diameter (squares and error bars represent averages and standard errors of mean diameters obtained by multiple measurements, respectively).

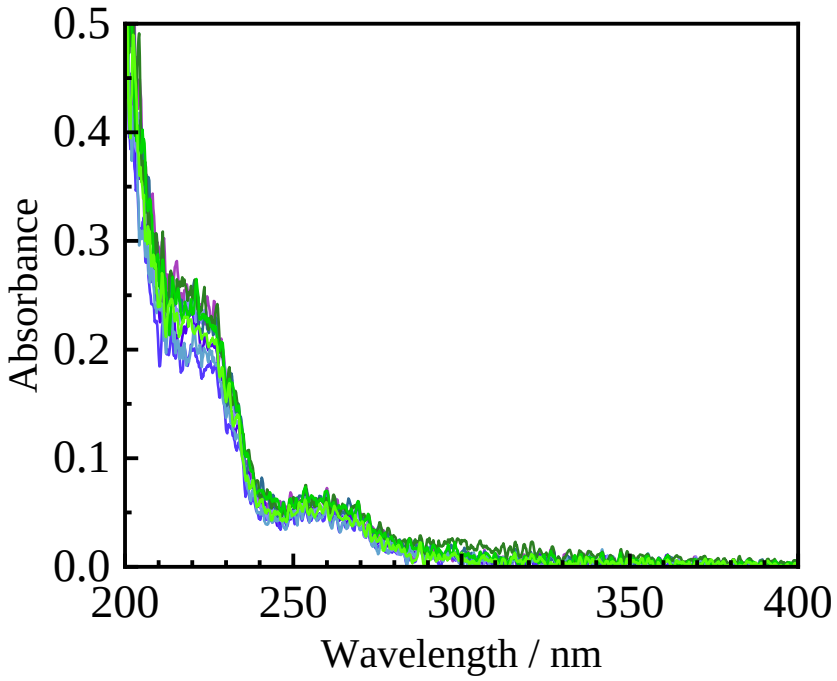

Figure 2-6. Absorption spectra of terbium(III)-doped ionic nanospheres (5.04–299 nmol mg^{-1}, purple → green)

2.6. Luminescence from terbium(III)-doped nanosphere

The luminescence spectra of terbium(III)-doped ionic nanospheres are presented in Figure 2-7. The number of excited species was used to normalize the luminescence. Together with the fluorescence from the ionic nanosphere at about 330 nm, additional luminescence peaks at 488 nm, 543 nm, and 583 nm emerged upon photoexcitation at 260 nm, which is the nanosphere's absorption maximum. The 4f–4f luminescence from terbium(III) species originating from the $^5D_4 \rightarrow {}^7F_J$ (J = 3–6) transitions is similar to the new luminescence bands. Regardless of the composition, the most noticeable band was the $^5D_4 \rightarrow {}^7F_5$ green emission at 543 nm. The luminescence intensity of the $^5D_4 \rightarrow {}^7F_6$ transition at 490 nm is sensitive to a ligand environment and symmetry of a coordination sphere in contrast to the insensitive $^5D_4 \rightarrow {}^7F_5$ transition with a magnetic dipole nature at 543 nm.[25–27] As a result, the coordination environment may be measured using the luminescence intensity ratio of the bands I_{543}/I_{490}. The terbium(III) ion in the nanosphere has local site symmetry with a coordination number of eight, as indicated by the terbium(III)-doped nanospheres' I_{543}/I_{490} value of 2/1. It is important to note that in the absence of the ionic nanosphere, no light is seen for the terbium(III) ion.

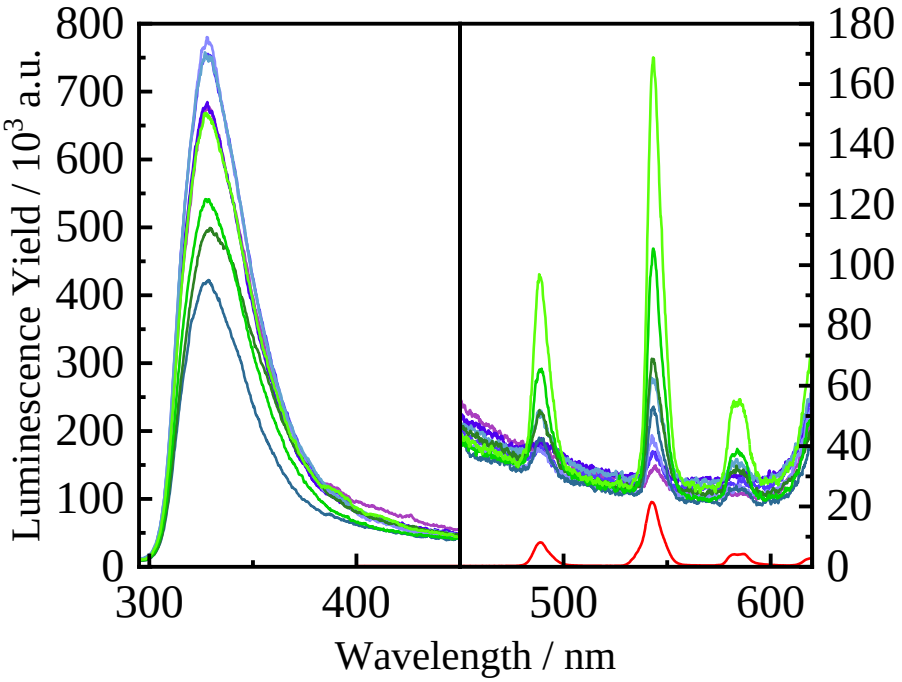

Figure 2-7. Luminescence spectra of terbium(III)-doped ionic nanospheres (5.04–299 nmol mg^{-1}, purple → green, λ_{ex} = 260 nm). Red spectrum represents that of the aqueous $TbCl_3$ solution (λ_{ex} = 365 nm).

The luminescence spectra of an aqueous solution of terbium(III) chloride and a terbium(III)-doped ionic nanosphere (49.9 nmol mg^{-1}) can be seen in Figure 2-8. In order to achieve the same terbium(III) ion concentrations in the aqueous phases (3.2×10^{-10} mol dm^{-3}), the samples were diluted. While the aqueous solution showed no luminescence band, the terbium(III)-doped nanosphere showed faint but noticeable luminescence bands. Even at very low terbium(III) ion concentrations, the data clearly demonstrate the increased luminescence from terbium(III)–nanosphere hybrids, whereas green luminescence from doped terbium(III) ion is not visible under ~260 nm light owing to the presence of intense blue fluorescence from the ionic nanosphere, blue-green luminescence is observable by 365-nm UV irradiation since the light absorption of the nanosphere is quite weak and there is a direct excitation band of terbium(III) ion.

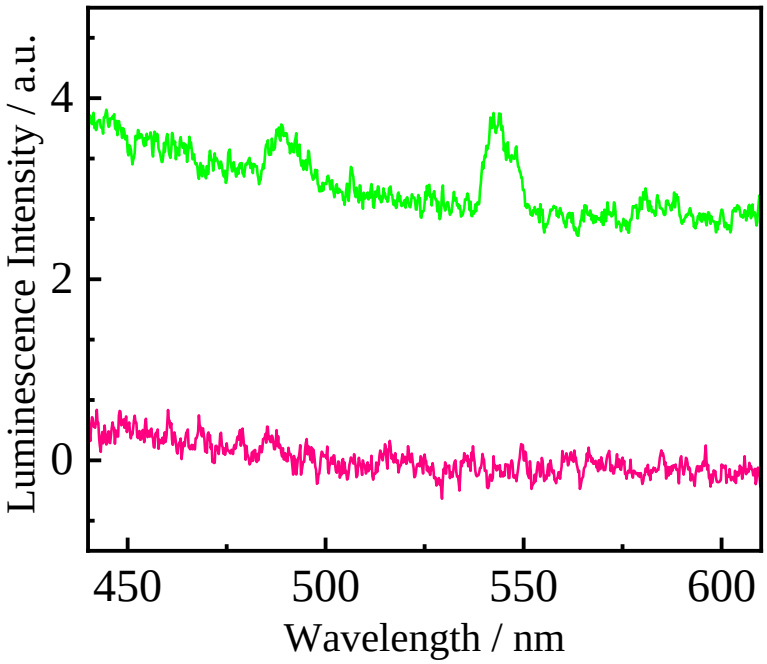

Figure 2-8. Luminescence spectra (λ_{ex} = 260 nm) of terbium(III) ion in the absence (pink, aqueous solution) and presence of the ionic nanosphere (green, 49.9 nmol mg^{-1}) under identical concentrations (3.2 × 10^{-10} mol dm^{-3}).

Excitation spectra of terbium(III)-doped nanospheres (5.04–299 nmol mg^{-1}) measured at 543 nm are shown in Figure 2-9. The excitation bands of all the terbium(III)-doped nanospheres were quite similar to those of the neat ionic nanosphere. There is, furthermore, neither evidence for direct 4f–4f excitation bands observable at >300 nm region nor spin-forbidden and spin-allowed 4f–5d bands at around 265 nm and 230 nm, respectively.[28] These results clarify that the photoexcitation of the nanospheres is the cause of the luminescence at 543 nm. As previously mentioned, terbium(III) luminescence has been successfully found at 543 nm. Consequently, energy transfer from the excited state of the ionic nanosphere is the source of terbium(III) luminescence from the terbium(III)-doped nanospheres. To gain an understanding of the energy transfer processes in the ionic nanosphere, a luminescence measurement for gadolinium(III)-doped ionic nanosphere (213 nmol mg^{-1}) was performed at 77 K. Owing to inaccessibility of the significantly high-energy 4f–4f excited state ascribed to a $^{8}S_{7/2}\rightarrow{}^{6}P_{7/2}$ transition (~32,200 cm^{-1}) and similar spin–orbit coupling constant to other lanthanide(III) ions, gadolinium(III) species are often used to obtain phosphorescence from organic photosensitizers.[29,30] The gadolinium(III)-doped nanosphere at 77 K exhibited long-lived luminescence which was detectable by the naked eye. The long-lived luminescence exhibited a

broad and structureless band with a maximum of 450 nm as shown in Figure 2-10. Such broad spectral and long-lived features assign the luminescence to the phosphorescence from the nanosphere. The triplet-state energy of the nanosphere (~22,000 cm^{-1} from the phosphorescence maximum) greatly matches the excitation bands of terbium(III) ion observed at ~450 nm (see Figure 2-4) and, therefore, the triplet excited state of the ionic nanosphere can act as an energy donor for terbium(III) ion as well as the singlet excited state.

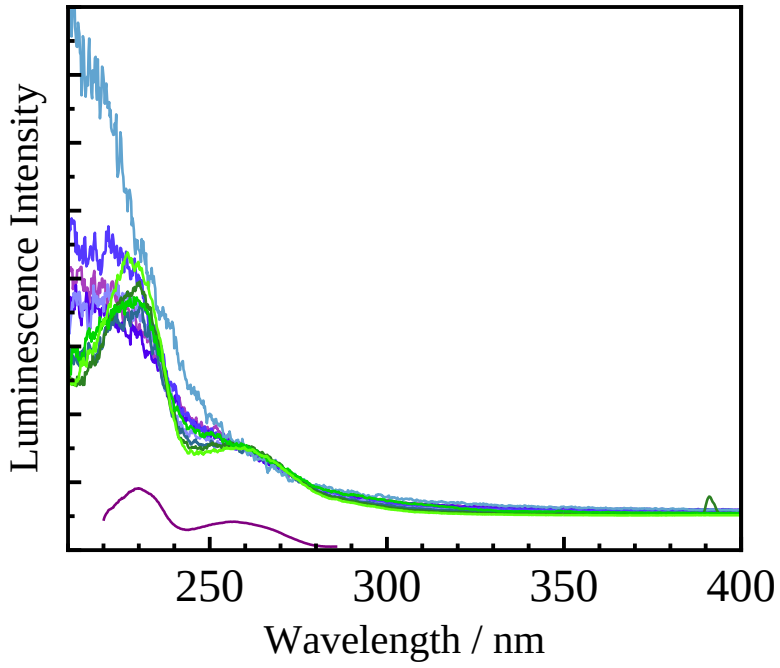

Figure 2-9. Excitation spectra of terbium(III)-doped ionic nanospheres (5.04–299 nmol mg^{-1}, purple → green, λ_{em} = 543 nm). Pink spectrum represent those of the neat ionic nanosphere (λ_{em} = 330 nm).

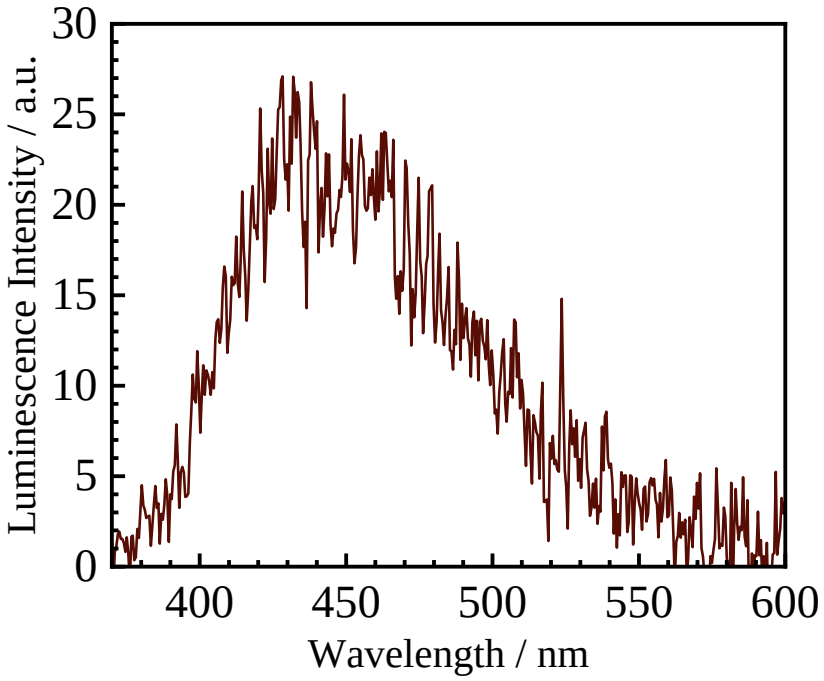

Figure 2-10. Luminescence spectrum of gadolinium(III)-doped ionic nanosphere (300 nmol mg^{-1}, λ_{ex} = 254 nm) at 77 K.

Figure 2-11 shows the luminescence yields at 525 and 543 nm as a function of terbium(III) concentration. In order to assess the former luminescence, the luminescence yield at 525 nm was subtracted as a background, since the luminescence yield at 543 nm is a sum of those of the terbium(III) ion and ionic nanosphere. The terbium(III) luminescence increased nearly linearly as the terbium(III) ion content increased. The linear dependence is explained as follows. The luminescence yield of a terbium(III)–photosensitizer system is determined by multiplying the photosensitizer's energy-transfer efficiency to the terbium(III) ion by the internal luminescence efficiency terbium(III) ion. Although the former efficiency increased with increasing content of terbium(III) ion, under the relatively low content region in the present study, sites for terbium(III) ion in the nanosphere still remain and, therefore, a fraction of the excited-state terbium(III) ion does not largely change. In practice, fluorescence from the nanosphere has been observed even for the sample with 299 nmol mg^{-1} terbium(III) ion. Furthermore, the internal luminescence quantum yield of terbium(III) ion in the nanosphere is expected to be independent of the content since our system simply traps terbium(III) ion inside the nanosphere by the electrostatic interactions and no change in a coordination system is applied. Thus, luminescence from terbium(III) ion doped in the ionic nanosphere was obtained by the photoexcitation of the nanosphere followed by the energy transfer to terbium(III) ion.

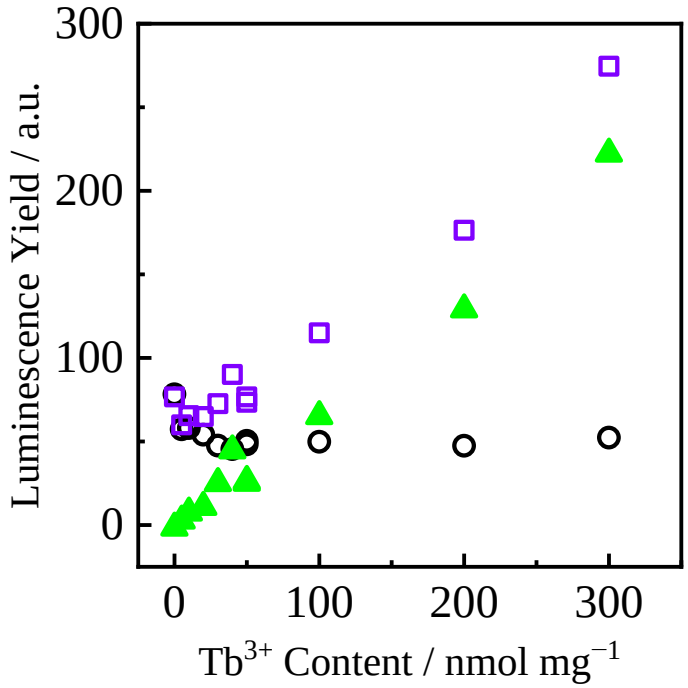

Figure 2-11. Terbium(III)-content dependences of luminescence yields at 525 (black open circles) and 543 nm (purple open squares). Green triangles represent the difference between 543 and 525 nm.

It is important to note that the poly(*p*-SS-*co*-DVB) structure of the nanosphere creates a hydrophobic environment that may increase the internal luminescence quantum yield of the terbium(III) ion by slowing down thermal deactivation through nearby water molecules. The spectroscopic/photophysical data of terbium(III)-doped nanospheres (300 nmol mg^{-1}) in D_2O and H_2O dispersions are compared in Figure 2-12. Because the lower-frequency mode is lower than the O–H stretching, switching the medium to D_2O brings light on how water and/or aqua ligands affect a nonradiative decay process or processes of the terbium(III) ion.[31–34] Surprisingly, the absorption and luminescence spectra of the D_2O dispersion resemble those in H_2O. In addition, there was no significant difference between the luminescence decay profiles, in which terbium(III) ion was mainly excited by a 355-nm light, in D_2O and H_2O (luminescence lifetimes were determined to be 140 and 110 μs, respectively). Because of the hydrophobic environment created by the poly(*p*-SS-*co*-DVB) structure, the photophysical characteristics of the terbium(III)–nanosphere hybrids in D_2O and H_2O media are similar, which makes it evident that the O–H vibration has little effect on the nonradiative decay process or processes of terbium(III) ion doped in the ionic nanosphere. As a result, in the current system, the ionic nanosphere serves as a hydrophobic medium and photosensitizer for terbium(III) ions.

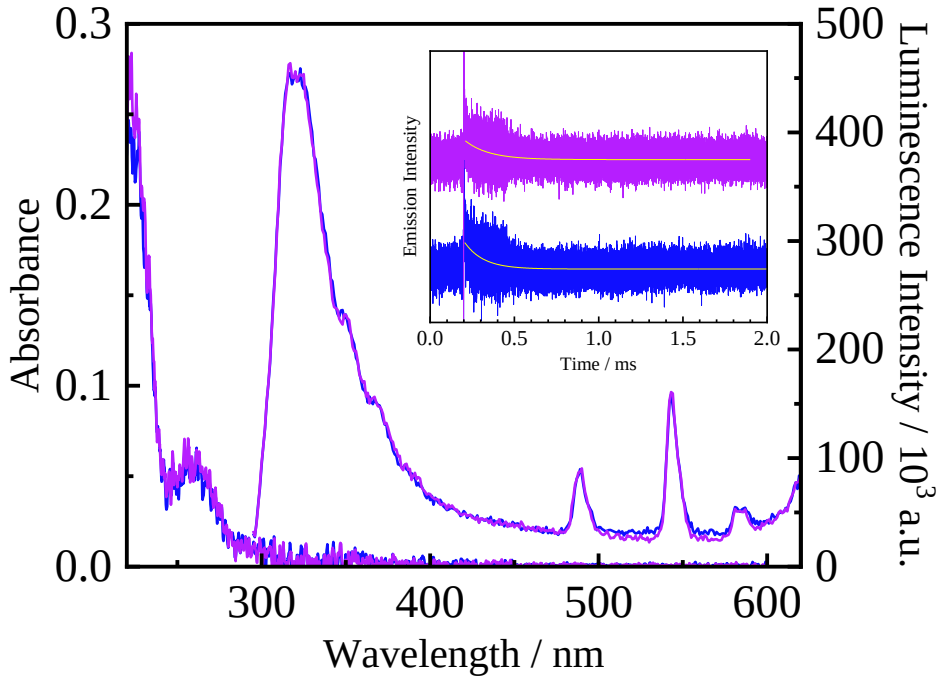

Figure 2-12. Absorption and luminescence spectra of terbium(III)-doped ionic nanospheres (300 nmol mg^{-1}, λ_{ex} = 260 nm) in H_2O (blue) and D_2O (purple). Inset: luminescence decay profiles (λ_{ex} = 355 nm, λ_{em} = 543 nm).

2.7. Conclusion

The ionic nanosphere successfully hybridized with the terbium(III) ion to sensitize its luminescence. The excited-state energy transferred to the terbium(III) ion doped within the nanosphere upon photoexcitation. Consequently, the ionic nanosphere is a photosensitizer and a rigid media for the terbium(III) ion. The primary benefits of this system are that the hybrid can be generated using a very easy and straightforward technology and that the condition (i.e., the content in the nanosphere) can be changed without requiring laborious synthesis procedures. As a result, the ionic nanosphere will become a novel kind of photosensitizer for terbium(III) ions as well as other lanthanide(III) ions. Its enhanced luminescence will be useful for biomedical, bioimaging, and sensing applications.

2.8. References

1) H. Mizuno, M. Masuda, *Bull. Chem. Soc. Jpn.* **1964**, *37*, 1239.
2) J. Zhang, L. X. Wang, L. Zhang, Y. Chen, Q. T. Zhang, *Rare. Metals.* **2013**, *32*, 599.
3) S. Sato, A. Ishii, C. Yamada, J. Kim, C. H. Song, A. Fujiwara, M. Takata, M. Hasegawa, *Polymer J.* **2015**, *47*, 195.

4) A. Dehelean, S. Rada, M. Zagrai, R. Suciu, C. Molnar, *Anal. Lett.* **2021**, *54*, 88.
5) K. Miyata, Y. Konno, T. Nakanishi, A. Kobayashi, M. Kato, K. Fushimi, Y. Hasegawa, *Angew. Chem. Int. Ed.* **2013**, *52*, 6413.
6) M. Hatanaka, Y. Hirai, Y. Kitagawa, T. Nakanishi, Y. Hasegawa, K. Morokuma, *Chem. Sci.* **2017**, *8*, 423.
7) Y. Kumamoto, T. Matsumoto, H. Tanaka, T. Takamatsu, *Sci. Rep.* **2019**, *9*, 10745.
8) L. Oulmaati, S. Belmokhtar, K. Bouziane, A. Bouajaj, M. Britel, F. Enrichi, C. Armellini, A. Chiappini, M. Ferrari, *Solar Energy Adv.* **2022**, *2*, 100012.
9) R. Kamal, M. Saif, *Spectrochim. Acta A: Mol. Biomol. Spectrosc*. **2020**, *229*, 117928.
10) N. Shiraishi, R. Karashimada, N. Iki, *Bull. Chem. Soc. Jpn*. **2019**, *92*, 1847.
11) J. Manzur, C. Poblete, J. Morales, R. Costa de Santana, L. J. Q. Maia, A. Vega, P. Fuentealba, *E. Spodine, Inorg. Chem*. **2020**, *59*, 5447.
12) Y. Kitagawa, K. Matsuda, P. P. Ferreira da Rosa, K. Fushimi, Y. Hasegawa, *Chem. Commun*. **2021**, *57*, 8047.
13) A. Hooda, A. Dalal, K. Nehra, D. Singh, S. Kumar, R. S. Malik, P. Kumar, Chem. *Phys. Lett*. **2022**, *794*, 139495.
14) Y. Kitagawa, K. Shima, T. Nakai, M. Kumagai, S. Omagari, P. P. Ferreira da Rosa, S. Shoji, K. Fushimi, Y. Hasegawa, *Commun. Chem*. **2023**, *6*, 122.
15) C. Seward, N.-X. Hu, S. Wang, J. *Chem. Soc., Dalton Trans*. **2001**, 134.
16) N. Kerbellec, D. Kustaryono, V. Haquin, M. Etienne, C. Daiguebonne, O. Guillou, *Inorg. Chem*. **2009**, *48*, 2837.
17) X.-Y. Xu, B. Yan, *ACS Appl. Mater. Interfaces.* **2015**, *7*, 721.
18) P.-F. Zhang, G.-P. Yang, G.-P. Li, F. Yang, W.-N. Liu, J.-Y. Li, Y.-Y. Wang, *Inorg. Chem.* **2019**, *58*, 13969.
19) J. Zhao, L. Huang, S. Zhao, S. Xu, *J. Am. Cer. Soc*. **2019**, *102*, 1720.
20) V. N. K. B. Adusumalli, H. V. S. R. M. Koppisetti, N. Madhukar, A. Mondal, V. Mahalingam, *J. Mater. Chem. C*. **2021**, *9*, 4267.
21) X. Chen, H. Lu, Q. Gu, N. Zhang, S. Wang, S. Wu, *CrystEngComm.* **2022**, *24*, 2551.
22) D. R. Lavanya, G. P. Darshan, J. Malleshappa, H. B. Premkumar, S. C. Sharma, S. A. Hariprasad, H. Nagabhushana, *Sci. Rep*. **2022**, *12*, 8898.
23) H. Yamamoto, M. Taomoto, A. Ito, D. Kosumi, *J. Photochem. Photobiol. A: Chem.* **2020**, *401*, 112771.
24) R. H. Wiley, J. I. Jin, Y. Kamath, *J. Pol. Sci. A*. **1968**, *6*, 1065.
25) F. J. Steemers, W. Verboom, D. N. Reinhoudt, E. B. van der Tol, J. W. Verhoeven, *J. Am.*

Chem. Soc. **1995**, *117*, 9408.

26) J.-C. G. Bünzli, *Coord. Chem. Rev*. **2015**, *293*, 19.

27) J. Manzur, C. Poblete, J. Morales, R. C. de Santana, L. J. Q. Maia, A. Vega, P. Fuentealba, E. Spodine, *Inorg. Chem*. **2020**, *59*, 5447.

28) P. Dorenbos, *J. Lumin*. **2000**, *91*, 91.

29) V. Divya, M. L. P. Reddy, *J. Mater. Chem. C.* **2013**, *1*, 160.

30) M. Hasegawa, H. Ohtsu, D. Kodama, T. Kasai, S. Sakurai, A. Ishii, K. Suzuki, *New J. Chem*. **2014**, *38*, 1225.

31) W. D. Horrocks Jr, D. R. Sudnick, *J. Am. Chem. Soc*. **1979**, *101*, 334.

32) A. Beeby, I. M. Clarkson, R. S. Dickins, S. Faulkner, D. Parker, L. Royle, A. S. de Sousa, J. A. G. Williams, M. Woods, *J. Chem. Soc. Perkin Trans*. **1999**, *2*, 493.

33) D. Costa, H. D. Burrows, M. da Graça Miguel, *Langmuir*. **2005**, *21*, 10492.

34) Y. Zama, K. Yanai, J. Takeshita, A. Ishii, M. Yamanaka, M. Hasegawa, *RSC. Adv*. **2019**, *9*, 1949.

Chapter 3 Light-harvested luminescence from lanthanide(III) ion doped in ionic nanosphere with ligating moiety

3.1. Summary

In this chapter, luminescence from lanthanide(III) ion has been sensitized by doping in the ionic nanosphere in which 5-phenyl-1,10-phenanthroline (pPhen) ligating moiety is copolymerized. The ligating ability of the pPhen moiety to lanthanide(III) ions enables efficient sensitization of lanthanide(III) luminescence. The low-energy nature of the pPhen excited state, furthermore, accumulates the excited-state energy following the photoexcitation of the poly(*p*-SS-*co*-DVB) moiety. Such synergistic energy transfer phenomena underscore the role of poly(*p*-SS-*co*-DVB) as a versatile energy-harvesting scaffold and the pPhen moiety as a sensitizing ligand.

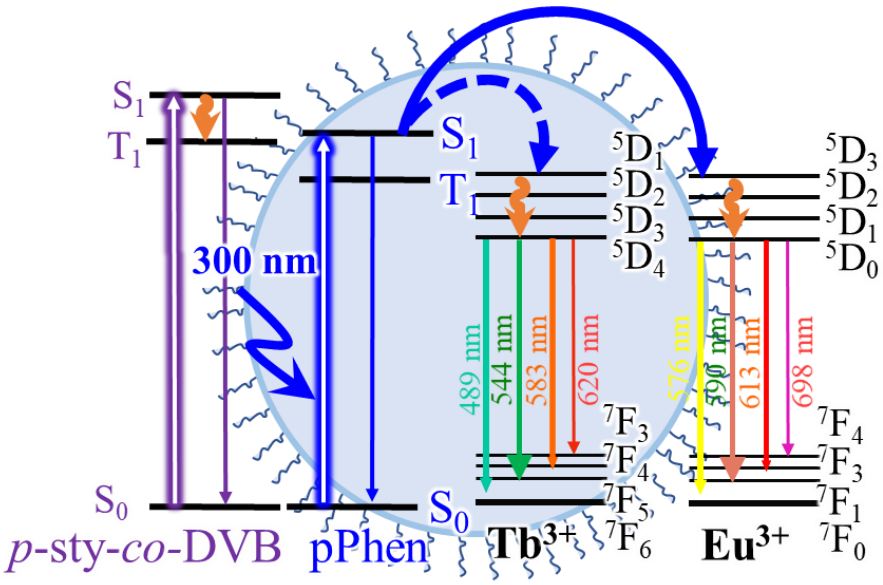

Figure 3-1. Schematic energy transfer process from poly(*p*-SS-*co*-DVB)-pPhen to terbium(III) and europium(III) ions

3.2. Introduction

Luminescent materials based on rare-earth ions such as terbium(III) and europium(III) have been recognized for their exceptional optical properties, including narrow emission bands in visible region, high color purity, and long luminescence lifetimes.[1–4] These characteristics make lanthanide(III)-based materials ideal for applications requiring precise control over emission properties, such as in light-emitting diodes (LEDs),[5–6] display devices,[7–8] and biological

imaging probes.[9–13] Despite these advantages, the practical application of terbium(III) and europium(III) ions are hindered by their weak light absorption, a direct consequence of the forbidden nature of their 4f–4f electronic transitions.[14–16] This limitation results in low quantum efficiency when terbium(III) and europium(III) ions are directly excited, necessitating alternative approaches to enhance their luminescence. The antenna effect is one practical strategy to increase the luminescence efficiency. This strategy involves using an organic fluorophore with a relatively high absorption coefficient as a sensitizer for lanthanide(III) ions. As a results of the organic effective light absorption, the luminescence from lanthanide(III) ions is significantly increased.

However, lanthanide complexes have been the focus of the majority of research on the annetna effects.[17–18] Additionally, organic compounds are difficult to use as sensitizers since they are susceptible to photobleaching and show comparatively poor stability when exposed to light for extended periods of time. One such approach is the sensitization of terbium(III) and europium(III) ions through the use of a light-harvesting system in an aqueous medium. Light harvesting is a key process in natural photosynthesis, where plants efficiently capture and convert the sunlight into chemical energy.[19–21] Natural light-harvesting systems (LHSs) are complex supramolecular assemblies in which large numbers of chromophores need to be densely stacked for high photosynthetic efficiency.[22–23] Inspired by the above concept, a lot of suitable and environmentally friendly light harvesting materials have been developed by mimicking photosynthesis have been fabricated for different applications, such as fluorescent probes, luminescent materials, bio-imaging, and photocatalysis.[24–26] Recent advances in nanotechnology have opened new avenues for enhancing the performance of light-harvesting systems, particularly through the use of nanostructured materials. Among these, ionic nanospheres have gained attention as a versatile platform for assembling light-harvesting systems. Ionic nanospheres[27–28] are polymeric ionic frameworks which offer several key advantages for luminescent applications as provide a high surface area for ligand attachment, and they can also enhance the solubility and dispersibility of terbium(III) and europium(III) ions in aqueous medium ensuring optical clarity and stability of the luminescent material. Keeping all these in mind, I have constructed a light-harvesting system based on the ionic nanosphere by copolymerizing the ligating unit called 5-(4-vinylphenyl)-1,10 phenanthroline ligand. Incorporating phenanthroline ligands into ionic nanospheres is a powerful strategy for creating highly efficient light-harvesting systems. 1,10-Phenanthroline, a nitrogen-containing heterocyclic compound, has emerged as a leading candidate for the sensitization of europium(III) and terbium(III) ions.[29–31] Its strong chelating ability, coupled with its favorable

photophysical properties, makes phenanthroline particularly well-suited for this role. Phenanthroline absorbs light in the UV-visible region and can form stable complexes with terbium(III) and europium(III) ions, providing a robust framework for energy transfer. In this configuration, the ionic nanospheres serve as a scaffold that organizes the phenanthroline ligands around the terbium(III) and europium(III) ions, maximizing the overlap between the ligand's absorption and the lanthanide ion's emission. This spatial organization is crucial for efficient energy transfer, as it ensures that the energy absorbed by the ligand is effectively channeled to the terbium(III) and europium(III) ions rather than being lost through non-radiative pathways. Additionally, the ionic nature of the nanospheres can influence the local environment around the terbium(III) and europium(III) ions, potentially enhancing their luminescence through effects such as local field enhancement, ionic screening, or changes in the coordination geometry. Combining phenanthroline ligands and ionic nanospheres offers several potential benefits over traditional terbium(III) and europium(III) complexes. First, the high surface area of the nanospheres allows for a greater density of ligands, leading to more efficient light harvesting and energy transfer. The findings of this study provide new insights into the design and optimization of light-harvesting systems based on rare-earth ions. Moreover, the versatility of the ionic nanosphere platform opens up new possibilities for further functionalization and tailoring of the material properties, paving the way for the development of next-generation luminescent materials with enhanced performance and broad applicability. In this work ionic nanospheres containing a ligating moiety, 5-(4-vinylphenyl)-1,10-phenanthroline was synthesized to study a stable light-harvesting system for the sensitization of terbium(III) and europium(III) ions. The typical structure of the ionic nanosphere with copolymerized pPhen ligating unit is shown in Scheme 3-1. The nanosphere, composed of poly(*p*-SS-*co*-DVB), serves as a hydrophobic support for the terbium(III) and europium(III) ions, while the phenanthroline ligand acts both as a sensitizer and a ligating moiety.

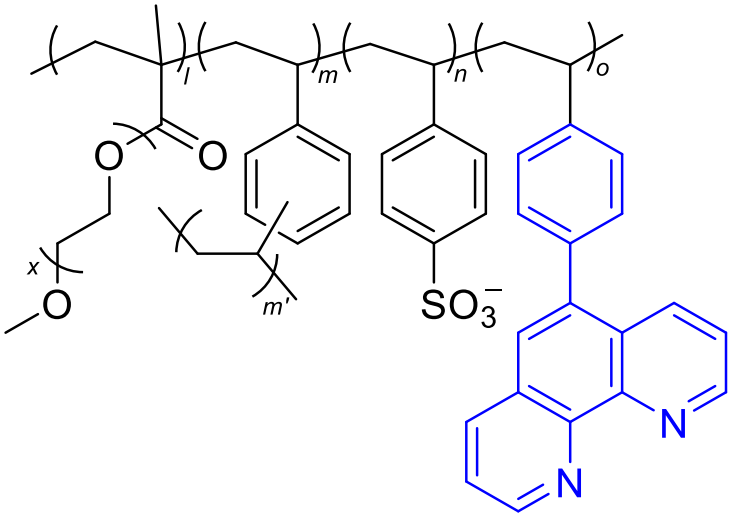

Scheme 3-1. Chemical structure of ionic nanosphere with the pPhen moiety.

3.3. Experimental

3.3.1. Materials, characterization, and spectroscopic/photophysical measurements

All chemicals were purchased from FUJIFILM Wako Pure Chemical Corporation, Tokyo Chemical Industry Co., Ltd., or Sigma–Aldrich Co., LLC, and used as received without further purification, unless otherwise specified. All the other experimental details were identical to those described in Chapter 2.

3.3.2. Synthesis of 5-(4-vinylphenyl)-1,10-phenanthroline

5-(4-Vinylphenyl)-1,10-phenanthroline was prepared by using a Suzuki–Miyaura coupling reaction. 4-Vinylphenylboronic acid (0.103g, 0.70 mmol), 5-bromo-1,10-phenanthroline (0.150g, 0.58 mmol), and potassium carbonate (0.766g, 5.425 mmol) were mixed with toluene (22.5 mL) and ethanol (7.5 mL) in a 100-mL eggplant flask. The resulting biphase mixture was deaerated by argon-gas bubbling at room temperature for 15 min. Tetrakis(triphenylphosphine)palladium(0) (0.0138 g, 0.012 mmol) was then added to the mixture, and the reaction mixture was stirred at 75ºC for 48 h. The reaction mixture was extracted with dichloromethane (100 mL × 3) and washed with water (50 mL). The organic phase was dried over anhydrous magnesium sulfate and filtrated, and then the solvent was evaporated to dryness. The resulting oil product was dissolved in chloroform and precipitated with hexane three times to yield the target product as a light-brown solid (100 mg, 63 %). ^{1}H NMR (400 MHz, $CDCl_3$). 9.21 (dd, 2H, J = 1.4 Hz, 4.2 Hz, 2- and 2′-Ar-H of phen), 8.31 (dd, 1H, J = 1.4 Hz, 8.2 Hz, 4- or 4′-Ar-H of phen), 8.26 (dd, 1H, J = 1.6 Hz, 8.0 Hz, 4- or 4′-Ar-H of phen), 7.75 (s, 1H, 6-Ar-H of phen), 7.67 (dd, 1H, J = 4.4 Hz, 8.0 Hz, 3- or 3′-Ar-H of phen),

7.60 (d, 2H, *J* = 7.6 Hz, Ar-H of ph), 7.76–7.57 (m, 1H, 3- or 3′-Ar-H of phen), 7.51 (d, 2H, *J* = 7.6 Hz, Ar-H of ph), 6.84 (dd, 1H, *J* = 11 and 17 Hz, CH of vinyl), 5.88 (d, 1H, *J* = 18 Hz, CH of vinyl), 5.37 (d, 1 H, *J* = 11 Hz, CH of vinyl).

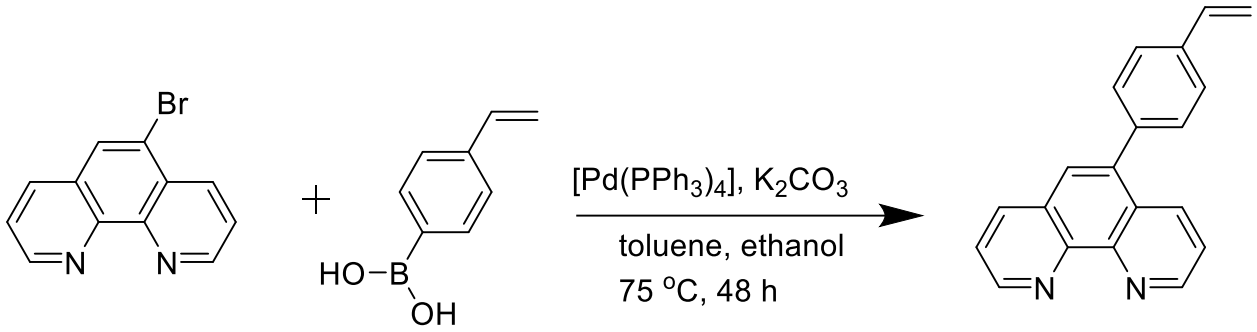

Scheme 3-1. Synthetic route for 5-(4-vinylphenyl)-1,10-phenanthroline

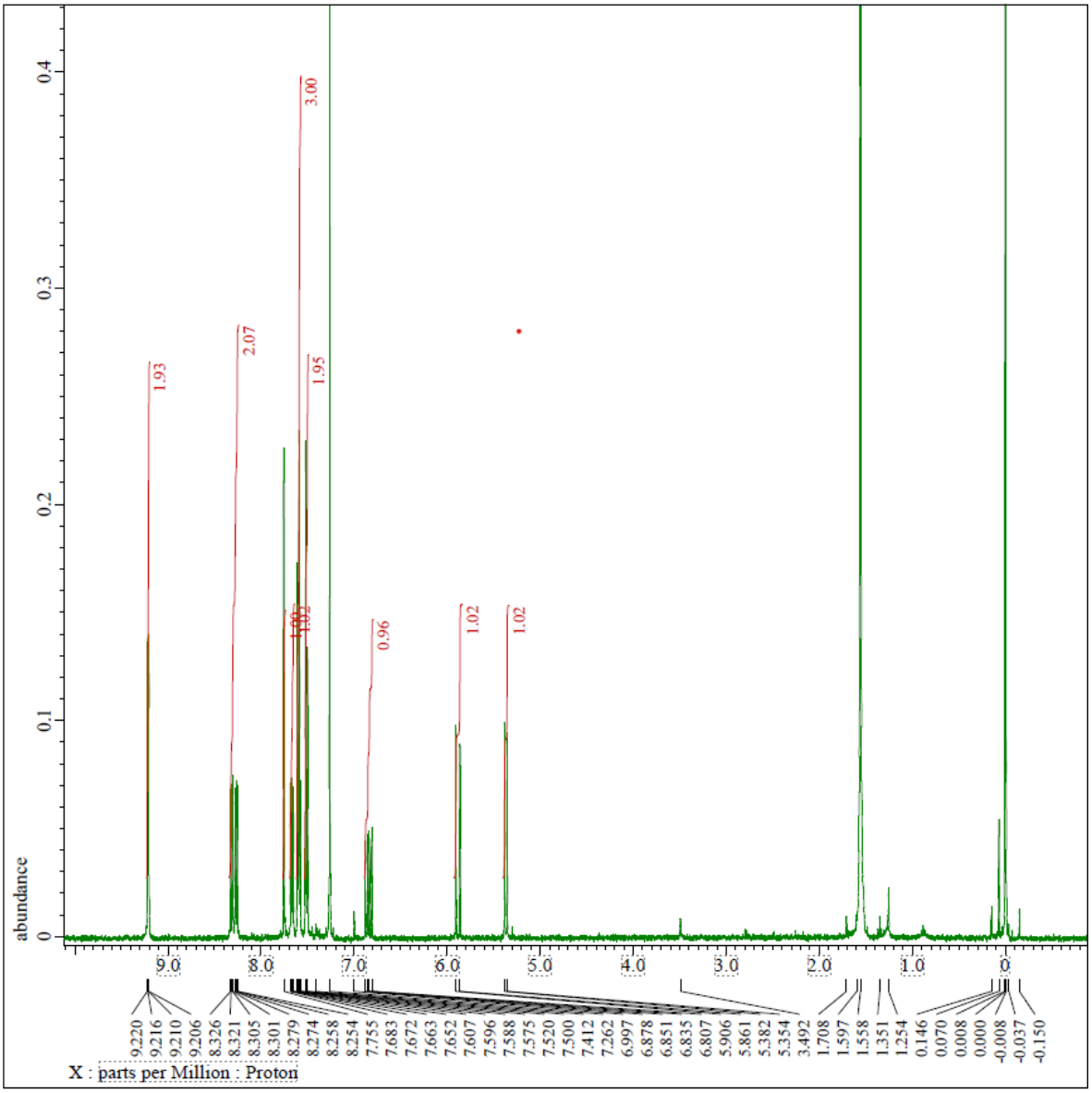

Figure 3-2. ^{1}H-NMR spectrum of 5-(4-vinylphenyl)-1,10-phenanthroline in $CDCl_3$.

3.3.3. Synthesis of ionic nanosphere

A solution of sodium *p*-styrenesulfonate (0.46 g, 2.254 mmol), 5-(4-vinylphenyl)-1,10-phenanthroline (0.013 g, 0.046 mmol), DVB purified in Chapter 2 (0.31 g, 2.30 mmol), poly(ethylene glycol)methacrylate methyl ether (M_n: 2000, 50wt% in water, 0.98 g) and ammonium persulfate (0.0232 g, 0.0833 mmol) in DMF/water (7.5 mL/4.5 mL) was deaerated by argon-gas bubbling at 0°C for 30 min. The solution was stirred at 72°C for 4 h under an argon-gas atmosphere. The resulting suspension was dialyzed (COMW: 50 kDa) for 3 d with a gradual change of dialysate from DMF/water (3/2, v/v) to pure water, affording an aqueous dispersion of the ionic nanosphere (16.55 ± 0.08 mg/mL from freeze drying experiments).

3.3.4. Preparation of lanthanide(III)-doped ionic nanospheres

Europium(III)- (5.1, 10.2, 20.5, 30.7, 40.9, 50.2, 102, 205 and 307 nmol mg^{-1}) or terbium(III)-doped nanospheres (5.1, 10.2, 20.4, 30.5, 40.7, 50.9, 101, 204 and 305 nmol mg^{-1}) were prepared by soaking and stirring the ionic nanosphere (2.11 mg/mL, 3 mL) in aqueous solutions of $EuCl_3$ [(3.25 to 195) × 10^{-6} mol dm^{-3}, 7 mL] or $TbCl_3$ [(3.23 to 194) × 10^{-6} mol dm^{-3}, 7 mL], respectively, at room temperature for 3 d. Undoped species were removed by dialysis (COMW: 12 to 14 kDa, dialysate: water, 1 d × 3). An aqueous dispersion of Gd^{3+}-doped nanosphere (300 nmol mg^{-1}) was prepared similarly. terbium(III) and europium(III)-doped nanospheres in D_2O and H_2O were obtained by repeated dialyses using D_2O and H_2O, respectively, after soaking the neat nanosphere in aqueous $EuCl_3$ and $TbCl_3$ solutions (300 nmol mg^{-1}).

3.4. Characterization of ionic nanosphere with pPhen moiety

The particle size distribution of the aqueous dispersion of the ionic nanosphere copolymerized with the pPhen moiety is shown in Figure 3-3. The mean diameter of the nanosphere is determined to be 69±10 nm, suggesting that the ionic nanosphere has been successfully prepared. In this case as well the morphology of ionic nanosphere considered to be spherical in shape as no additional peaks were observed even after repeated measurements. The nanosphere with the pPhen moiety was smaller than that of the conventional ionic nanosphere prepared under identical conditions (166±65 nm). The size reduction can be explained by the enhanced hydrophobicity introduced by the phenanthroline moiety: an increase in hydrophobicity likely causes tighter packing within the nanosphere structure.

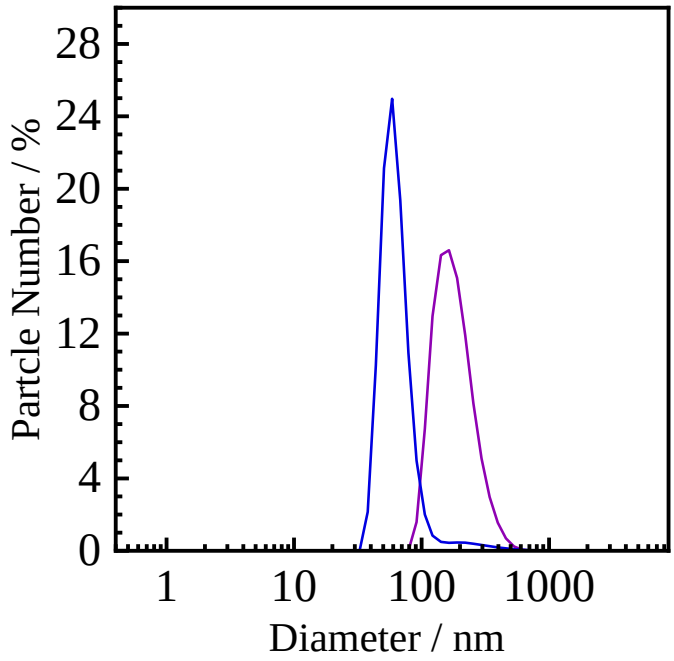

Figure 3-3. The particle size distribution of ionic nanospheres with (blue) and without the pPhen moiety (purple, compiled from Figure 2-2).

The absorption and fluorescence spectra of the ionic nanosphere with the pPhen ligating moiety are shown in Figure 3-4. The copolymerized nanosphere exhibited multiple absorption bands in the <350 nm region. The broad absorption band of the ionic nanosphere with a maximum of 260 nm corresponds to the π–π* excited state of the poly(*p*-SS-*co*-DVB) backbone as described in Chapter 2, and the absorption shoulder observed at 280–310 nm is attributed to the π–π* transition in the pPhen moiety. The absorbances of the bands proportionally increased with an increase in the concentration of the nanosphere, and the mass absorption coefficients at 231 nm, 256 nm and 300 nm were determined to be 8.6 L g^{-1} cm^{-1}, 6.3 L g^{-1} cm^{-1} and 0.94 L g^{-1} cm^{-1}, respectively. The large extinction coefficient indicates that the copolymerized ionic nanosphere can act as an efficient light absorber toward subsequent energy transfer to lanthanide(III) ions.

The fluorescence from the copolymerized nanosphere upon the excitation at 300 nm is observed in the 400–550 nm range, indicating that the nanosphere emits light primarily in the blue-green region. This emission can be attributed to the π–π* transition of the pPhen moiety. This characteristic blue-green emission under UV light is an important feature, indicating the efficient energy harvesting within the nanosphere to pPhen ligating moiety (*vide infra*). The broad fluorescence band of the copolymerized ionic nanosphere covers the 4f–4f direct

excitation of europium(III) ion observable at 360 nm, 380 nm, 420 nm, 480 nm and so forth (Figure 3-5) and terbium(III) at 440 nm, 450 nm, 490 nm (see Figure 2-4). Although there is limited overlap between the fluorescence of the ionic nanosphere and the excitation bands of terbium(III) ion (see Figure 2-4), energy transfer to the terbium(III) ion is still possible. Hence, the ionic nanosphere is expected to act as an energy harvester of the pPhen ligand and as the sensitizer for terbium(III) and europium(III) ions.

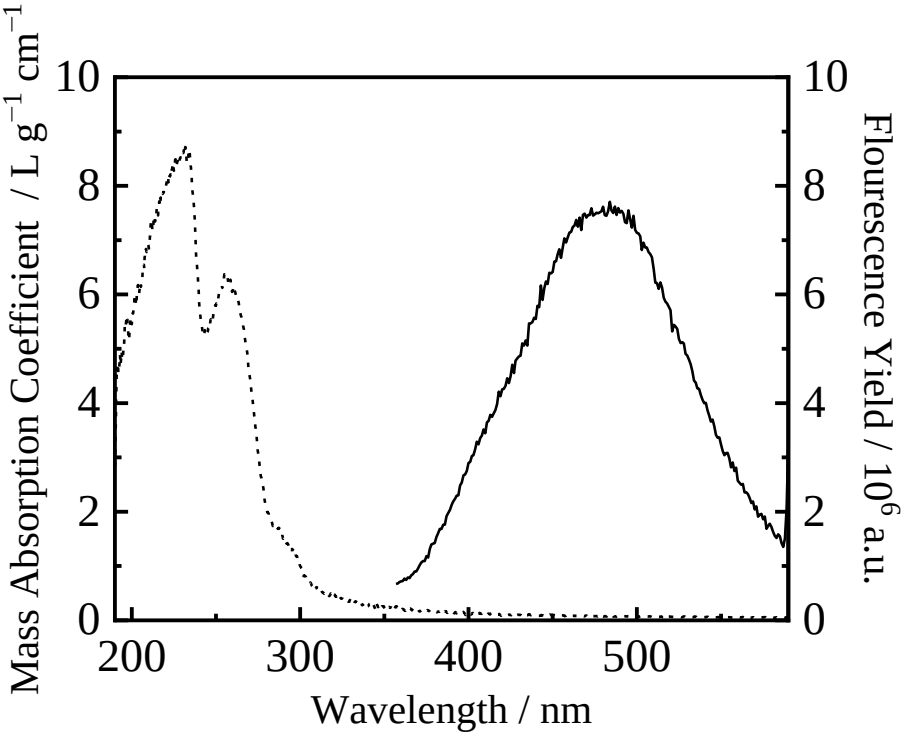

Figure 3-4. Absorption (broken curve) and fluorescence spectra (solid curve, λ_{ex} = 300 nm) of the ionic nanosphere with the pPhen moiety

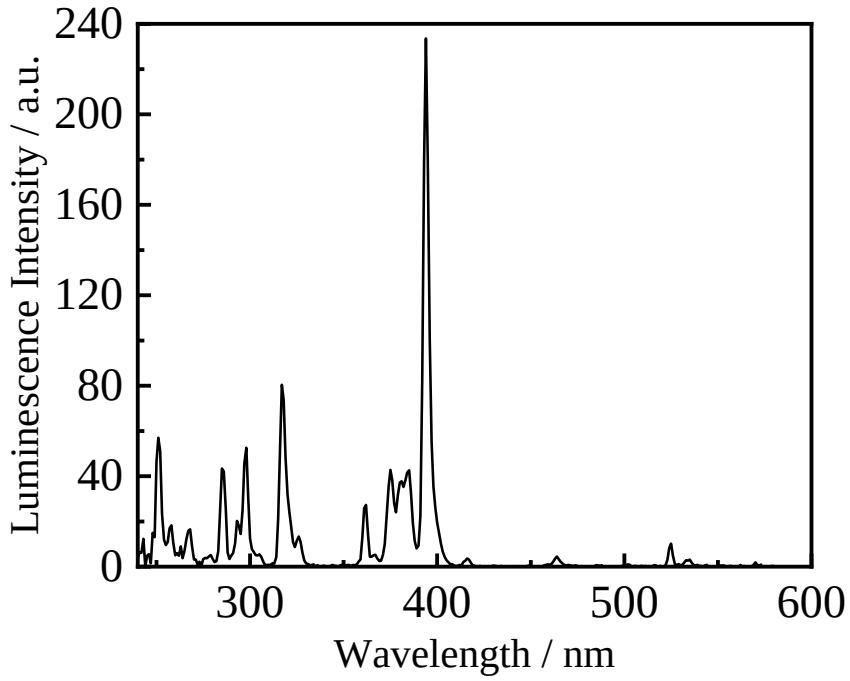

Figure 3-5. Excitation spectrum of $EuCl_3$ in water (λ_{em} = 613 nm).

3.5. Energy harvesting in ionic nanosphere with pPhen moiety

To study the role of ionic nanosphere as an energy harvester for the pPhen ligating moiety, the fluorescence properties of the copolymerized ionic nanosphere were investigated as shown in Figure 3-6. Upon an excitation at 260 nm which corresponds to the absorption band of the poly(*p*-SS-*co*-DVB) moiety, the ionic nanosphere functionalized with the pPhen ligating unit exhibited two fluorescence bands at 330 nm and 480 nm. The former is attributed to the as shown in Figure 2-3. The spectral similarity to the fluorescence spectrum excited at 300 nm (Figure 3-4) assigns the latter fluorescence band to the π–π* excited state of the pPhen moiety. The most interesting observation from this data is the intensity ratio between the two fluorescence bands. Despite the mole fraction of the pPhen moiety being estimated to be around 1%, the fluorescence intensity ratio of 480 nm to 330 nm is greater than 0.6. The large fluorescence from the pPhen moiety strongly suggests that the excited-state energy absorbed by the poly(*p*-SS-*co*-DVB) moiety is effectively funneled towards the pPhen ligating unit. Such energy concentration toward the pPhen moiety indicates efficient energy transfer from the ionic nanosphere, which acts as an energy harvesting platform for the ligating unit. The energy transfer from the poly(*p*-SS-*co*-DVB) moiety to the pPhen moiety was supported by the excitation spectra (Figure 3-7). The spectrum monitored at 480 nm was identical to that monitored at 320 nm and that of the conventional ionic nanosphere. The results suggest that the

excited-state energy in the copolymerized nanosphere is efficiently harvested into the pPhen moiety. Thus, these findings demonstrate that the ionic nanosphere plays a crucial role in capturing and channeling the absorbed excited-state energy into the pPhen ligating unit. The energy transfer process highlights the potential of this system for applications in energy harvesting, where the selective functionalization of nanospheres could be used to target and optimize energy transfer to specific ligating units for enhanced performance.

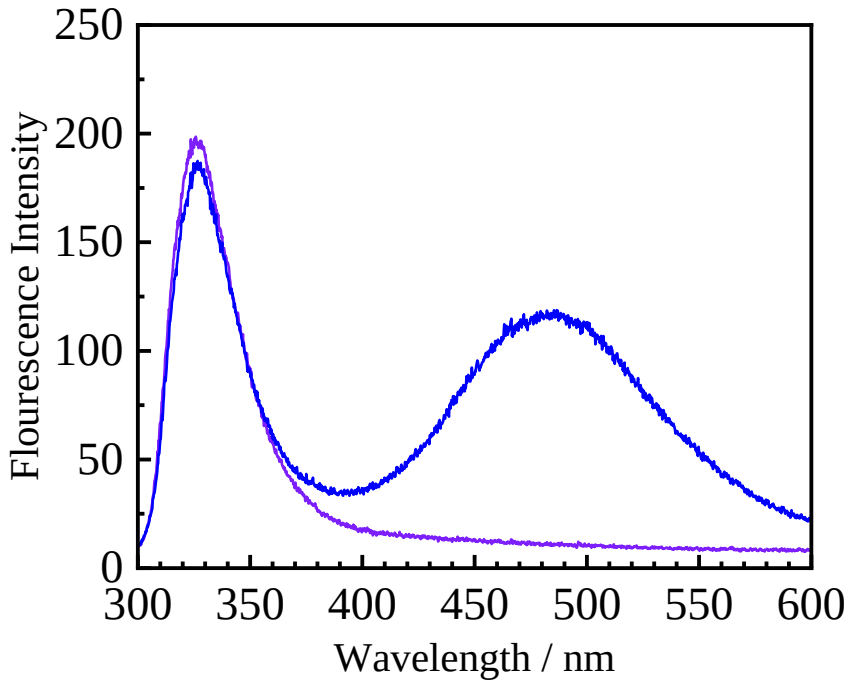

Figure 3-6. Fluorescence spectra (λ_{ex} = 260 nm) of the ionic nanospheres with (blue) and without the pPhen moiety (purple).

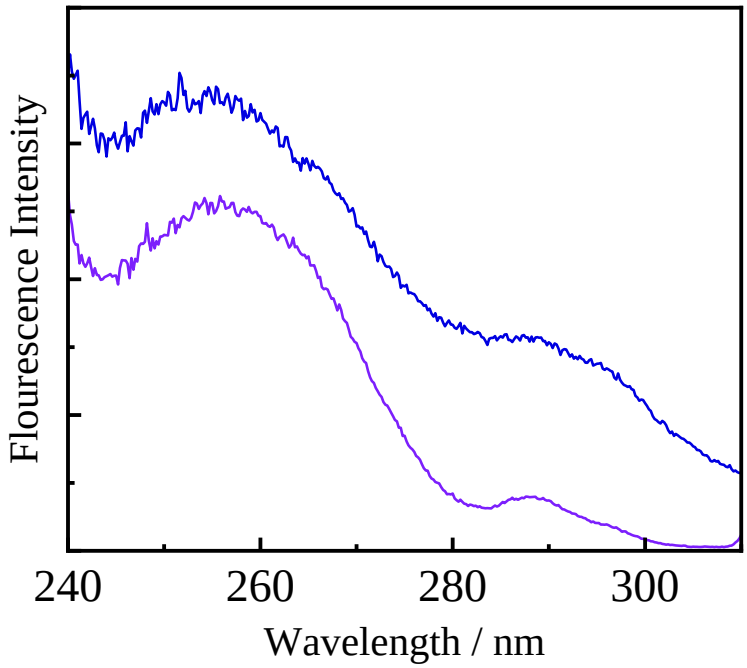

Figure 3-7. Excitation spectra of the ionic nanosphere with the pPhen moiety (λ_{em} = 320 (purple) and 480 nm (blue)).

3.6. Doping of europium(III)/terbium(III) ion in ionic nanosphere

terbium(III) and europium(III)-doped ionic nanospheres were prepared by mixing an aqueous solution of $EuCl_3$ and $TbCl_3$ with an aqueous dispersion of the copolymerized ionic nanosphere. The concentration of terbium(III) and europium(III) ions is adjusted by varying the concentration of the $EuCl_3$ and $TbCl_3$ solution. Dialysis was performed to remove the undoped species and the sodium chloride generated by the ion exchange reaction. No luminescence from terbium(III) and europium(III) species was observed for the dialysate samples, even at the higher concentration, indicating that terbium(III) and europium(III) ions were quantitatively doped into the nanosphere. The terbium(III) and europium(III) contents in the nanospheres were determined to be (0–307.1 nmol mg^{-1}) and (0–305.4 nmol mg^{-1}) respectively. Figure 3-8 shows particle size distributions of europium(III) and terbium(III)-doped samples. The mean diameters of terbium(III) and europium(III)-doped nanospheres are <50 nm, smaller than that of the neat ionic nanosphere. Thus, europium(III) and terbium(III) ions are doped within the ionic nanospheres through both electrostatic interactions with sulfonate groups (replacing sodium ions) and coordination with phenanthroline groups. In addition, the chelation of europium(III) and terbium(III) ions may promote cross-linking between phenanthroline groups, further contributing to the contraction of the nanosphere structure.

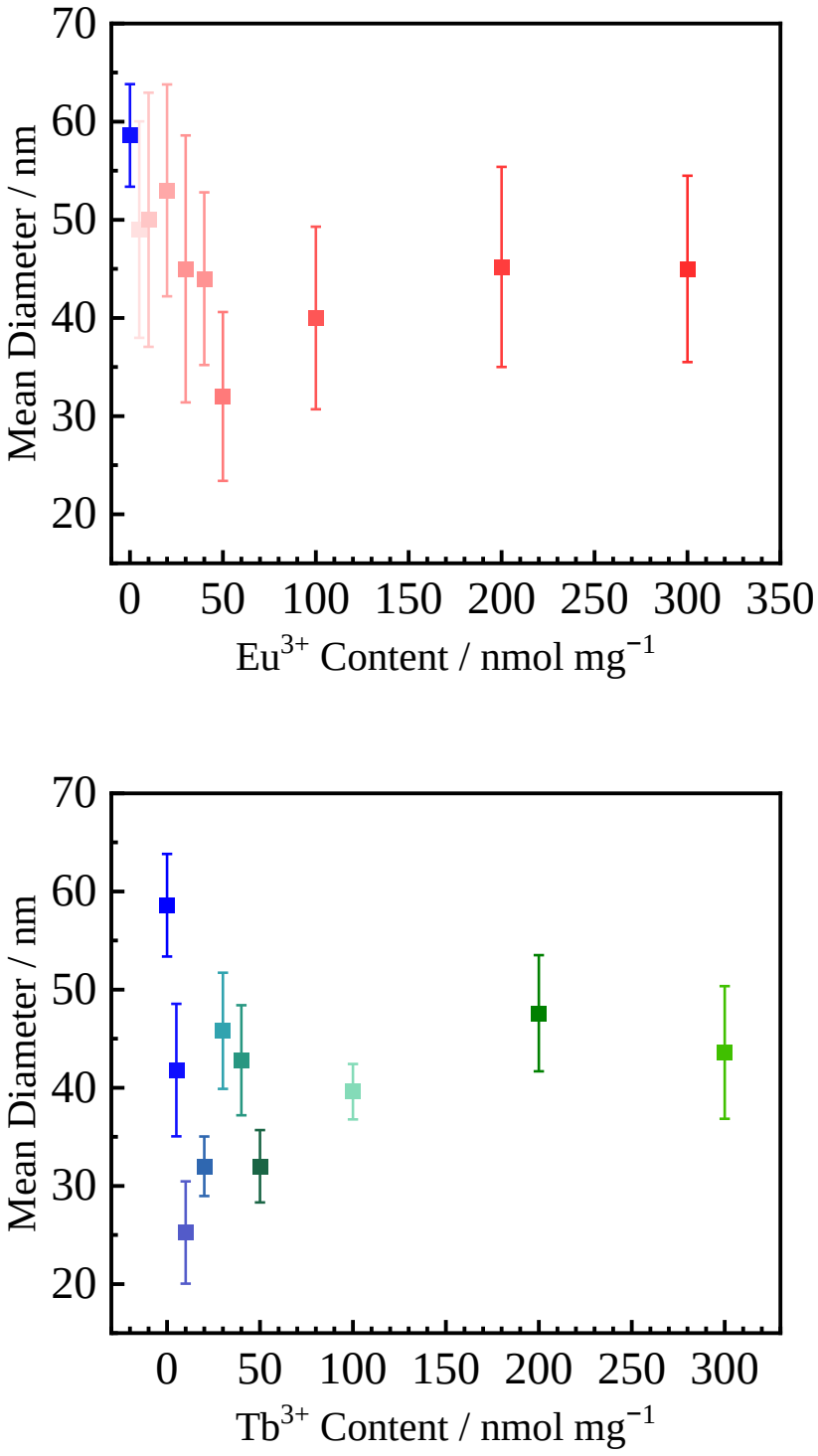

Figure 3-8. Particle size distributions of europium(III)- (upper panel) and terbium(III)-doped ionic nanospheres with the pPhen moiety (lower panel).

Although the size of ionic nanospheres decreases with europium and terbium doping, no clear dependence on ion concentration was observed, but a slight increase in size occurred from 50.2 to 307 nmol mg^{-1} for europium(III) ion, and similar results were obtained for terbium(III) ion as well. This is likely due to the uniform distribution of europium(III) and terbium(III) ions within the ionic nanospheres. The doped ions may also reduce the spacing between the primary structures of the poly(*p*-SS-*co*-DVB) and the phenyl phenanthroline-ligating moiety macromolecules.

The absorption spectra of europium(III)- and terbium(III)-doped nanospheres are shown in Figure 3-9. Both spectra display absorption bands around 220 nm and 260 nm, which are attributed to the π-π^* within the poly(*p*-SS-*co*-DVB) structure. Also, absorption bands near 300 nm, arising from the pPhen ligating moiety, were observed. The spectra of the europium(III) and terbium(III)-doped nanospheres are nearly identical, indicating a similar light absorption behavior for both systems. These results confirm that in the europium(III) and terbium(III)-doped nanospheres, the majority of light absorption occurs through the ionic nanosphere, specifically via the π-π^* of the poly(*p*-SS-*co*-DVB) and the ligating moiety. Importantly, this suggests that the direct excitation of the europium(III) and terbium(III) ions does not significantly contribute to the overall absorption process. Instead, the energy is likely transferred from the nanosphere to the europium(III) and terbium(III) ions via indirect sensitization rather than direct excitation.

The luminescence spectra of the europium(III)- and terbium(III)-doped nanospheres are shown in Figure 3-10, with luminescence intensity normalized by the number of excited species. For europium(III)-doped nanospheres, when excited at 300 nm, the spectra reveal both fluorescence and luminescence contributions from the ionic nanosphere and europium(III) ions, with doping concentrations ranging from 0 to 307 nmol mg^{-1}. The fluorescence from the ligating moiety in the doped samples (5.1–307 nmol mg^{-1}) shifts to a shorter wavelength range (from 480 nm to 420 nm) compared to the undoped samples (0 nmol mg^{-1}), likely due to the binding of europium(III) ions to the ligating moiety. Alongside nanosphere fluorescence, new luminescence peaks appear at 580 nm, 613 nm, and 690 nm, corresponding to the $^5D_0 \rightarrow {}^7F_J$ (J = 1 to 3) transitions. The $^5D_0 \rightarrow {}^7F_2$ (613 nm) red emission is the most prominent feature in europium(III)-doped samples, regardless of concentration. Similarly, in the terbium(III)-doped nanospheres, excitation at 300 nm shows both fluorescence and luminescence contributions from the ionic nanosphere and terbium(III) ions across the 0–305 nmol mg^{-1} doping range. The fluorescence of the ligating moiety in terbium(III)-doped samples (5.1–305 nmol mg^{-1}) also shifts to a shorter wavelength (from 480 nm to 420 nm) compared to undoped samples, likely

due to terbium(III) ion binding. Along with the nanosphere fluorescence, a new luminescence peak appears solely at 543 nm, attributed to the $^5D_4 \rightarrow {}^7F_5$ transition. This green emission at 543 nm is consistently the most intense luminescent feature across all terbium-doped samples, with other possible terbium(III) transitions–such as 488 nm and 583 nm not observed in this system.

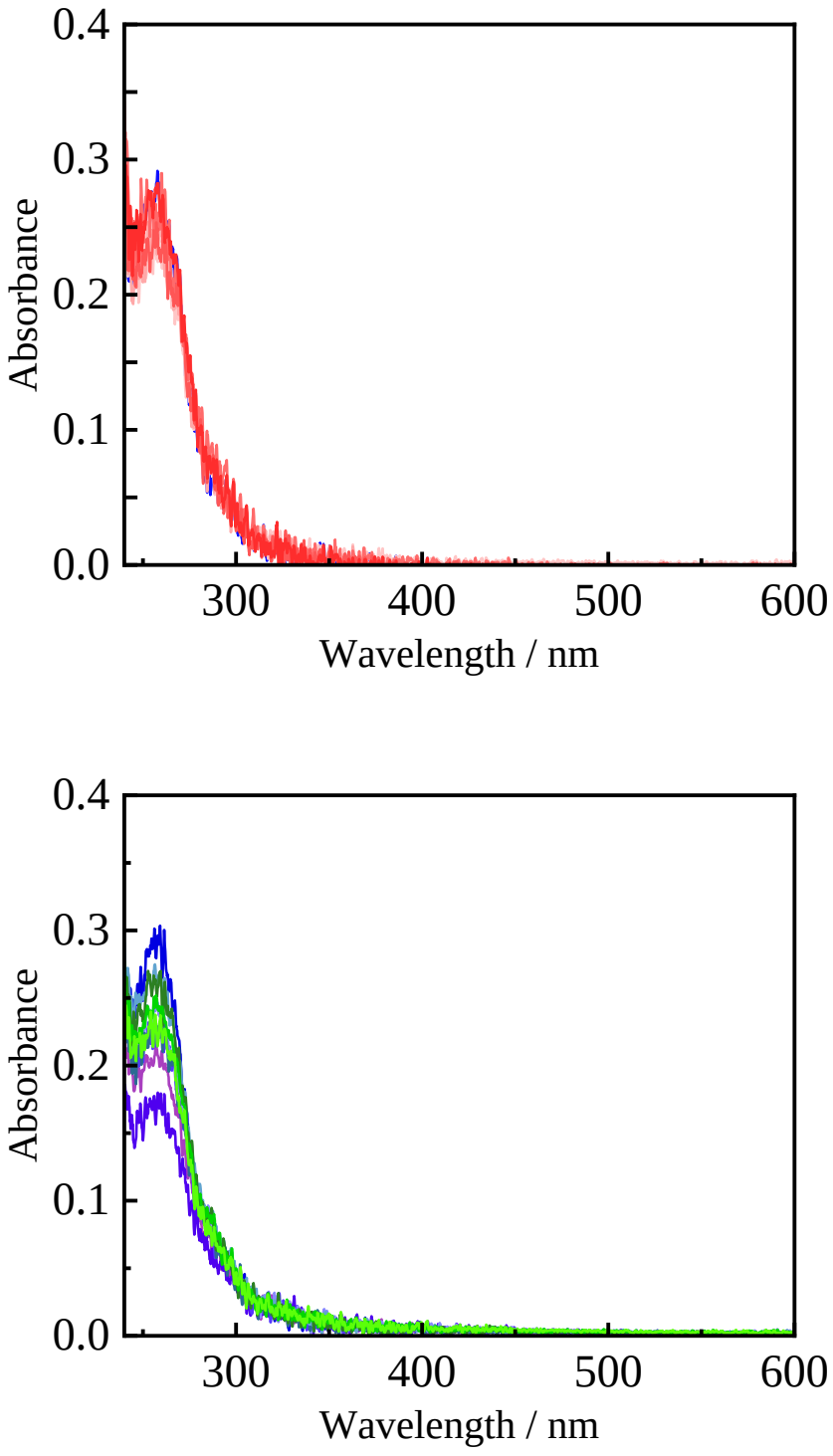

Figure 3-9. Absorption spectra of a europium(III)- (upper panel) and terbium(III)-doped ionic nanosphere with pPhen ligating moiety (lower panel) (0–300) nmol mg^{-1}.

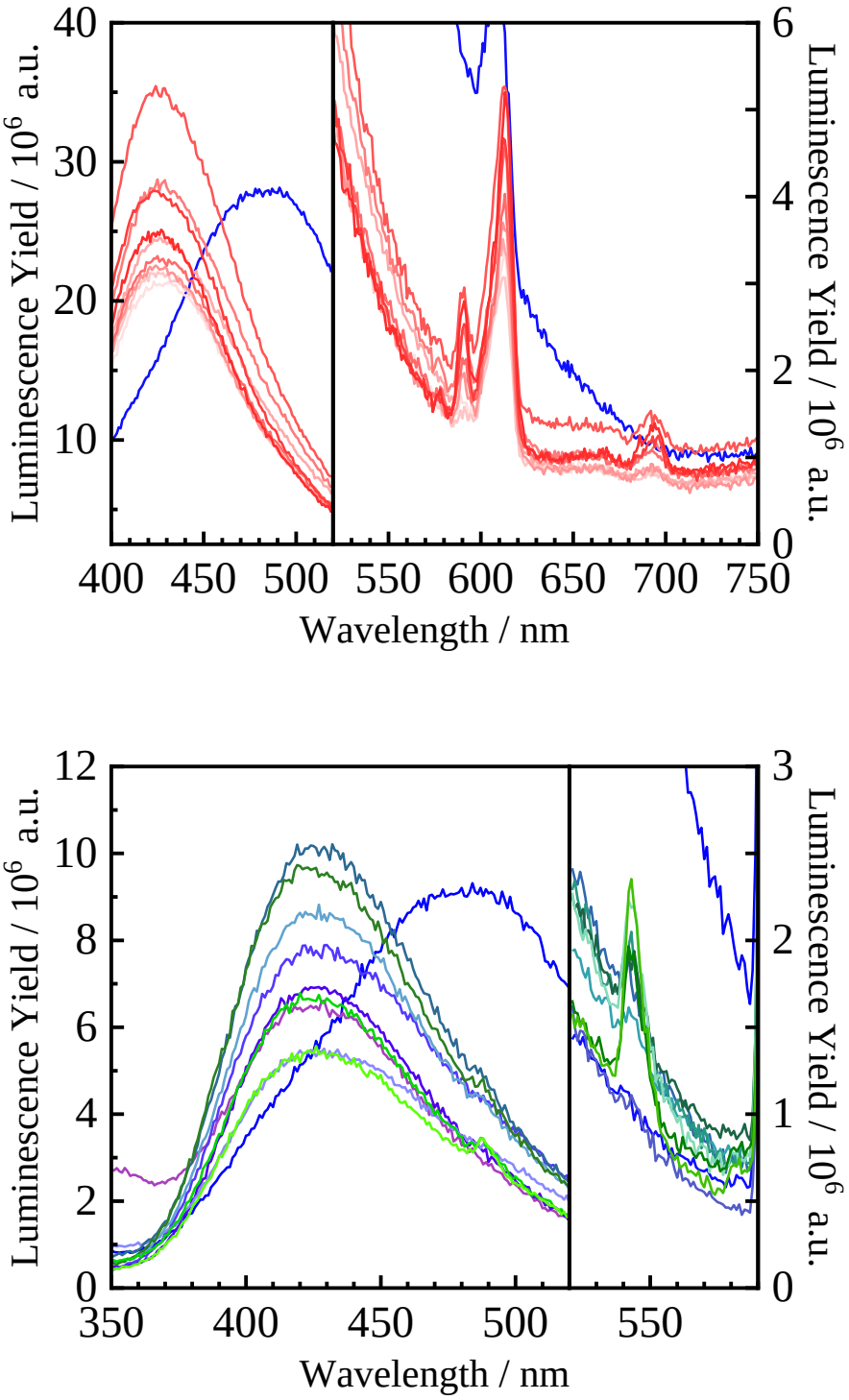

Figure 3-10. Luminescence spectra (λ_{ex} = 300 nm) of europium(III)- (upper panel, 0–307 nmol mg^{-1}) and terbium(III)-doped ionic nanospheres with the pPhen moiety (lower panel, 0–305 nmol mg^{-1}).

Comparing the luminescence performance of europium(III) and terbium(III)-doped samples reveals a distinct difference: europium-doped nanospheres exhibit stronger overall luminescence intensity and feature multiple emission transitions ($^5D_0 \rightarrow 7F_J$, J = 1 to 3) compared to terbium(III)-doped samples, which show a more limited luminescent profile dominated solely by the 543 nm transition. This difference in emission profiles likely arises from a better energy match between the nanosphere matrix and europium ions, enabling more efficient energy transfer and enhanced luminescence in europium-doped samples, as discussed in Figure 3-10. The terbium(III) ion, by contrast, demonstrates a limited range of observed transitions due to a less optimal energy transfer match with the nanosphere matrix. Overall, the observed luminescence intensities for both europium(III) and terbium(III) ions confirm that the ionic nanosphere serves as an effective sensitizer and energy harvester, enabling efficient energy transfer to both europium(III) and terbium(III) ions.

The excitation spectra of europium(III) and terbium(III)-doped nanospheres were measured to further verify that energy is being transferred from the ionic nanosphere, as shown in Figure 3-11. For europium(III)-doped nanospheres (5.1–307 nmol mg^{-1} samples), monitored at the maximum luminescence intensity of the europium(III) ion at 613 nm, the excitation spectrum exhibited a peak at 260 nm. This peak closely matched the excitation spectrum of the ionic nanosphere with the ligating moiety. Similarly, for terbium(III)-doped nanospheres (5.1-305 nmol mg^{-1}), monitored at 543 nm, the excitation spectrum also showed a maximum at 260 nm, aligning mg^{-1}), monitored at 543 nm, the excitation spectrum also showed a maximum at 260 nm, aligning with the ionic nanosphere's excitation spectrum with ligating moieties. Importantly, no evidence of 4f–4f excitation bands was observed above the 300 nm region for both terbium(III) and europium(III) ions. These results confirm that the red and green luminescence at 613 nm and 543 nm, from europium and terbium(III) ions, respectively, originates due to the photoexcitation of the nanosphere containing the ligating moiety

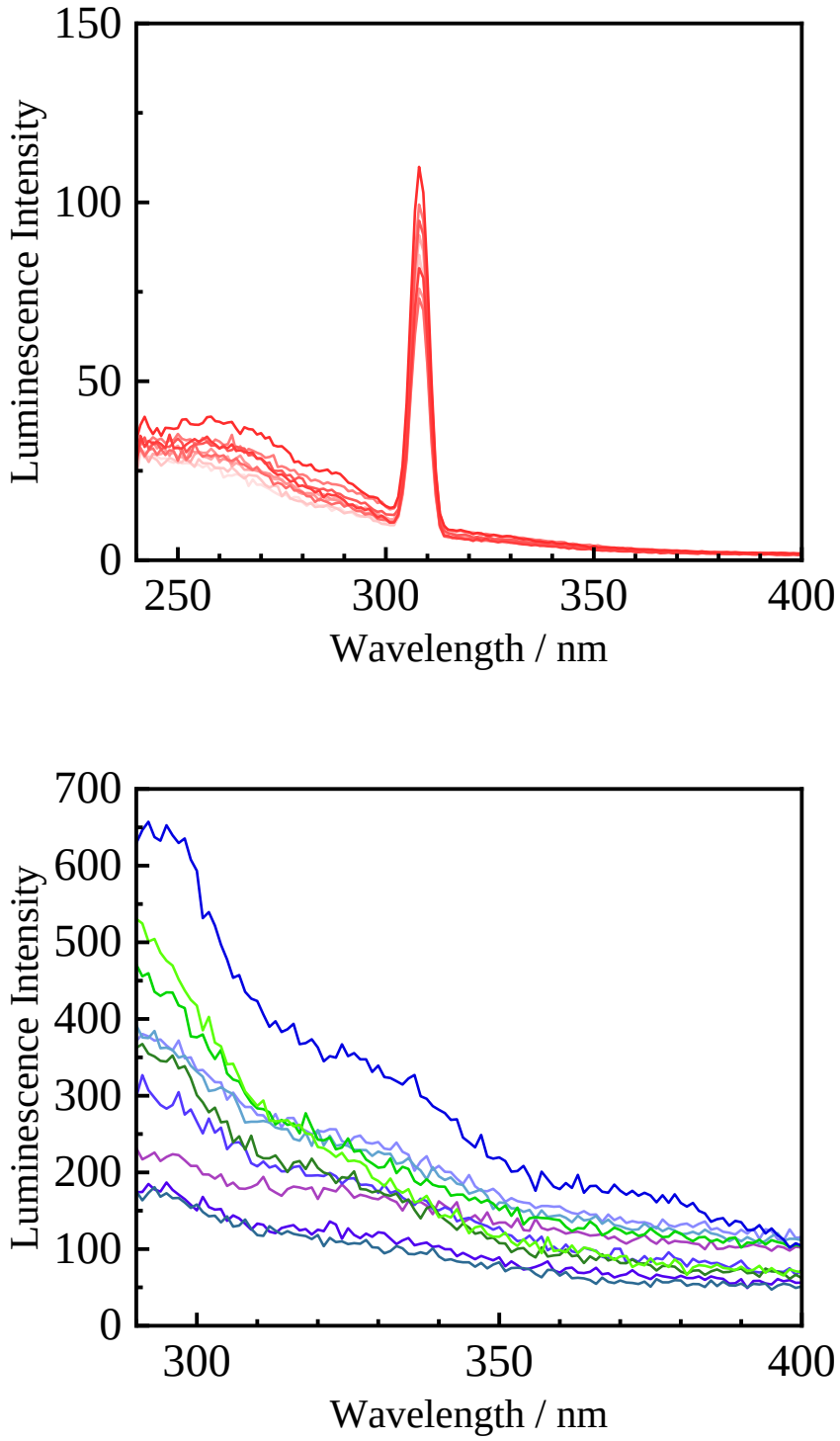

Figure 3-11. Excitation spectrum (λ_{em} = 613 nm) of europium(III)- (upper panel, 0–307 nmol mg^{-1}) and (λ_{em} = 543 nm) terbium(III)-doped ionic nanospheres with the pPhen moiety (lower panel, 0–305 nmol mg^{-1}).

Figure 3-12 shows the europium(III) and terbium(III) content dependences of the luminescence yields at 550 and 613 nm for europium(III) and 530 and 543 nm for terbium(III) ions. The luminescence at 613 nm and 543 nm from europium(III) and terbium(III) ions is the sum of europium(III) and terbium(III) ions and the nanosphere. Therefore, the luminescence yield for both europium(III) and terbium(III) ions was evaluated by subtracting luminescence yield at 550 nm for europium(III) ions and at 530 nm for terbium ions as backgrounds. For the europium(III)-doped nanosphere, the luminescence yield showed a spike in the intensity when the content increased from 0 to 40 nmol/mg around. Then, as the content increased further from (50–300) nmol mg^{-1}, the luminescence yield did not increase significantly. Similarly, for the terbium(III)-doped nanosphere, the luminescence yield content showed almost a similar pattern to europium(III) ions. First, the luminescence yield increased as the content of terbium(III) ion from (0–40) nmol mg^{-1} samples increased, and further increase of content from(50–300) nmol mg^{-1} had very little effect on luminance yield. Therefore, for both europium(III) and terbium(III) ions, luminescence yield has not increased linearly with an increase in their content. This can be explained as follows. The luminescence from the europium(III) and terbium(III) were increased when the concentration increased from (0 to 40) nmol mg^{-1}. However, further increasing the content up to 300 nmol mg^{-1} did not result in a significant increase in luminescence. This plateau is likely due to energy transfer limitations when the lanthanide(III) ions coordinates to the phenanthroline. Given that only 1% phenanthroline was copolymerized with the poly(*p*-SS-*co*-DVB) backbone, only around 40 nmol mg^{-1} of lanthanide(III) ions could bind with the phenanthroline moiety, leaving the remaining lanthanide ions free in the nanosphere surroundings. Additionally, the poly(*p*-SS-*co*-DVB) backbone does not act as a sensitizer for the lanthanide(III) ions in this setup. Instead, all the energy from the poly(*p*-SS-*co*-DVB) backbone migrates and is trapped within the phenanthroline moiety. This sequential energy transfer from the poly(*p*-SS-*co*-DVB) backbone to the phenanthroline moiety and then to the lanthanide(III) ions supports our argument that the ionic nanosphere is an effective energy harvester. As a result, luminescence from the lanthanide(III) ions was successfully achieved, but further increases in concentration did not yield substantial changes.

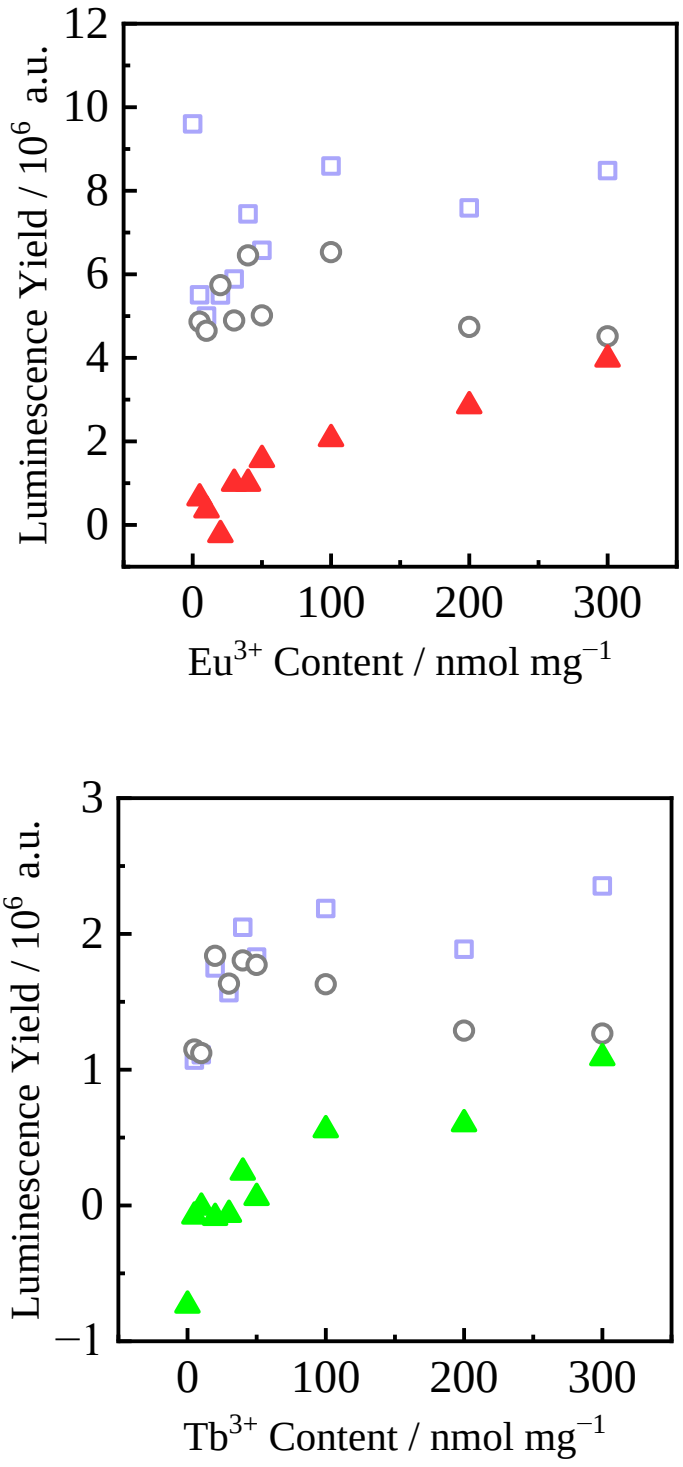

Figure 3-12. Europium(III) (upper panel) and terbium(III)-content (lower panel) dependences of luminescence yields at 550 and 535 (grey open circles), 613 nm and 543 nm (purple open squares). Red and green triangles represent the difference between (613 and 550) nm and (543 and 530) nm for europium(III) and terbium(III) ion content.

3.7. Energy transfer mechanism

A proposed energy transfer mechanism between IN to pPhen to terbium(III) and europium(III) ions is schematically shown in Figure 3-13. Upon 300 nm excitation, pPhen gets excited from S_0 to S_1 levels. A broad fluorescence was observed for pPhen ligating moiety by following the radiative process. Along with the radiative fluorescence, some part of energy was being transferred to its triplet state as well by the non-radiative process. From the excited singlet and triplet states of pPhen, energy transfer happened to the europium(III) ion. Radiative relaxation from $^5D_3$ to $^5D_0$ and from $^5D_0$ energy levels of europium(III) ion lead to the 613 nm visible emissions. Similarly, for terbium(III) ions doped with IN, upon excitation of 300 nm, pPhen gets excited from S_0 to S_1 levels. A broad fluorescence was observed for pPhen ligating moiety by following the radiative process. Along with the radiative fluorescence, some part of energy was being transferred to its triplet state as well by the non-radiative process. From the excited singlet and triplet states of pPhen, energy transfer happened to the terbium(III) ions. Radiative relaxation from $^5D_4$ levels to the $^5D_0$ and from $^5D_0$ energy levels of terbium(III) ions lead to the 544 nm visible emissions.

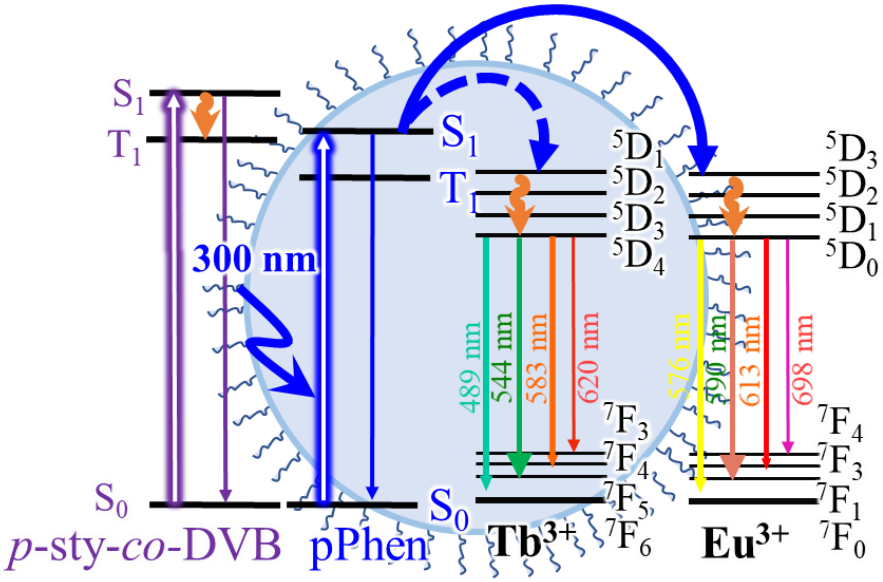

Figure 3-13. Schematic proposed energy transfer mechanism of europium(III) and terbium(III) ion doped in ionic nanosphere with pPhen ligating moiety.

3.8. Conclusion

In this study, an efficient light-harvesting system based on ionic nanospheres copolymerized with a 5-(4-vinylphenyl)-1,10-phenanthroline ligating moiety was successfully

developed in an aqueous medium. This system serves as an effective sensitizer for europium(III) and terbium(III) ions when integrated with nanospheres. The excited state of the phenanthroline ligand coordinates effectively with europium(III) and terbium(III) ions, facilitating efficient energy transfer from the pPhen moiety to these ions. The ionic nanospheres act as robust energy harvesters, capturing energy within the pPhen moiety and transferring it to the europium(III) and terbium(III) ions. Notably, this system offers a straightforward approach, as it requires only mixing without extensive synthesis processes. This novel light-harvesting system shows promise as a potent sensitizer for lanthanide ions, with potential applications in sensing, bioimaging, and biomedical fields.

3.9. References

1) J. C. G. Bünzli, C. Piguet, *Chem. Soc. Rev.* **2005**, *34*, 1048.
2) J. C. G. Bünzli, *Handbook on the Physics and Chemistry of Rare Earths*, Vol. 50, Elsevier, **2016**, *141*.
3) M. H. Werts, *Sci. Prog.* **2005**, *88*, 101.
4) G. Tessitore, G. A. Mandl, S. L. Maurizio, M. Kaur, J. A. Capobianco, *RSC Adv.* **2023**, *13*, 17787.
5) M. Zhang, J. Xue, Y. Zhu, C. Yao, D. Yang, *ACS Appl. Mater. Interfaces* **2020**, *12*, 22191.
6) Y. Wang, S. Bai, H. Liang, C. Li, T. Tan, G. Yang, J. Wang, *J. Alloys Compd.* **2023**, *934*, 167952.
7) L. Ma, O. R. Evans, B. M. Foxman, W. Lin, *Inorg. Chem.* **1999**, *38*, 5837.
8) H. J. Chen, L. Q. Chen, L. R. Lin, L. S. Long, L. S. Zheng, *Inorg. Chem.* **2021**, *60*, 6986.
9) J. Xu, A. Gulzar, P. Yang, H. Bi, D. Yang, S. Gai, F.He, J. Lin, B. Xing, D. Jin, *Coord. Chem. Rev.* **2019**, *381*, 104.
10) S. N. Misra, M. A. Gagnani, R. S. Shukla, *Bioinorg. Chem. Appl.* **2004**, *2*, 155.
11) A. J. Amoroso, S. J. Pope, *Chem. Soc. Rev.* **2015**, *44*, 4723.
12) D. Kim, *Nanomaterials* **2021**, *11*, 723.
13) B. Keller, A. McLean, B. G. Kim, K. Chung, J. Kim, T. Goodson III, *J. Phys. Chem. C* **2016**, *120*, 9088.
14) G. Liu, X. Chen, *Handbook on the Physics and Chemistry of Rare Earths*, **2007**, *37*, 99.
15) K. Nehra, A. Dalal, A. Hooda, S. Bhagwan, R. K. Saini, B. Mari, K.Sumit, D. Singh, *J. Mol. Struct.* **2022**, *1249*, 131531.

16) J. Cybinska, C. Lorbeer, A. V. Mudring, *J. Lum.* **2016**, *170*, 641.
17) M. Hasegawa, H. Ohmagari, *Chem. Lett.* **2020**, *49*, 845.
18) K. Nehra, A. Dalal, A. Hooda, P. Kumar, D. Singh, S. Kumar, R.S. Malik, P. Kumar, *J. Lum.* **2022**, *249*, 119032.
19) H. Lokstein, G. Renger, J. P. Götze, *Molecules* **2021**, *26*, 3378.
20) P. Manna, G. S. Schlau-Cohen, *Biochim. Biophys. Acta (BBA)-Bioenergetics* **2022**, *1863*, 148543.
21) C. B. Winiger, S. Li, G. R. Kumar, S. M. Langenegger, R. Häner, *Angew. Chem. Int. Ed.* **2014**, *53*, 13609.
22) T. Xiao, Y. Shen, C. Bao, K. Diao, D. Ren, H. Qian, L. Zhang, *RSC Adv.* **2021**, *11*, 30041.
23) T. Xiao, L. Zhang, H. Wu, H. Qian, D. Ren, Z. Y. Li, X. Q. Sun, *Chem. Commun.* **2021**, *57*, 5782.
24) Y. S. Hsiao, F. C. Chien, J. H. Huang, C. P. Chen, C. W. Kuo, C. W. Chu, P. Chen, *J. Phys. Chem. C* **2011**, *115*, 11864.
25) Y. S. Hsiao, F. C. Chien, J. H. Huang, C. P. Chen, C. W. Kuo, C. W. Chu, P. Chen, *J. Phys. Chem. C* **2011**, *115*, 11864.
26) S. Sardar, S. K. Pal, *Nanotechnology Rev.* **2016**, *5*, 113.
27) H. Yamamoto, M. Taomoto, A. Ito, D. Kosumi, *J. Photochem. Photobiol., A: Chem.* **2020**, *401*, 112771.
28) N. Madhukar, T. Misato, A. Ito, *Bull. Chem. Soc. Jpn.* **2024**, *97*, uoae023.
29) B. Yan, H. J. Zhang, J. Z. Ni, *Mater. Sci. Eng. B* **1998**, *52*, 123.
30) C. Ye, S. X. Jun, C. W. Min, Y. Y. Ning, C. Dan, *Mater. Chem. Phys.* **2003**, *80*, 371.
31) H. J. Zhang, L. S. Fu, S. B. Wang, Q. G. Meng, K. Y. Yang, J. Z. Ni, *Mater. Lett.* **1999**, *38*, 260.

Chapter 4 Enhanced luminescence of terbium(III) ion doped in gallic acid capped CaF_2 nanoparticles for selective detection of chromate and permanganate ion

4.1. Summary

In this work, ligand-sensitized lanthanide(III)-doped CaF_2 nanocrystals (NCs) were synthesized that can selectively detect nanomolar quantities of chromate ($Cr_2O_7^{2-}$) and permagante (MnO_4^-) ions. The gallic acid (GA) capped-CaF_2:terbium(III) nanoparticles are used to achieve this. By efficiently transferring energy from surface-functionalized gallic acid molecules to terbium(III) ion via UV light activation, these NCs exhibit vivid green emission. An appropriate organic capping molecule was chosen to act as a capping ligand to regulate the growth of the nanoparticles, sensitize the luminescence of terbium(III) ion, and selectively change the luminescence when chromate and permanganate ions are present. Since the carboxylic acid group is anticipated to attach to the surface of nanoparticles during nanoparticle development, gallic acid was selected as a capping ligand. The intense UV absorption of gallic acid acts as an efficient sensitizer for the terbium(III) ion luminescence, and ultimately, these nanoparticles act as efficient sensors for the chromate and permanganate ions.

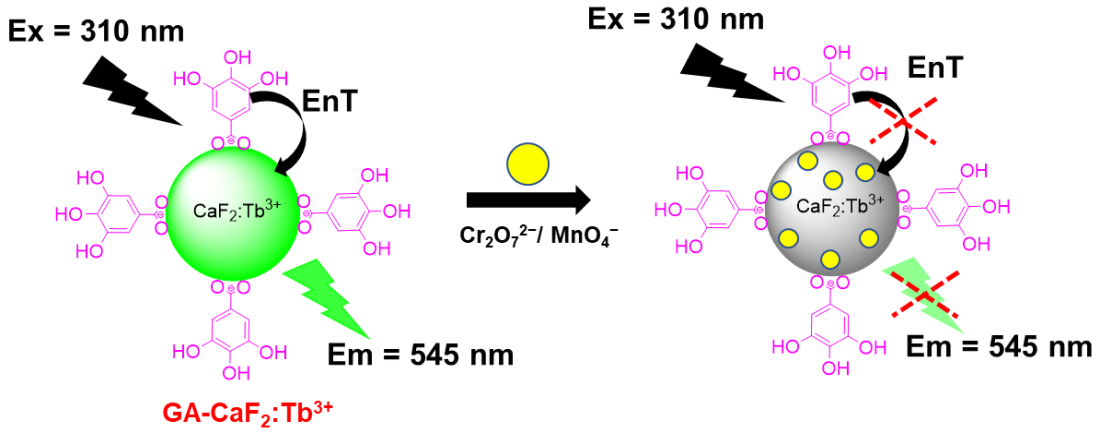

Figure 4-1. Systematic energy transfer from GA-CaF_2 to terbium(III) ion.

4.2. Introduction

Chromium ion is one of the most extensively used metal ions in industries because of its various applications like polishing, printing, tanning, etc.[1–3] However, the vast use of chromium in the industry results in the generation of huge amounts of chromium waste worldwide, which ultimately leads to environmental concerns. Due to the high water-soluble nature of chromate ions like $HCrO_4^-$, CrO_4^{2-}, or $Cr_2O_7^{2-}$, there is a high probability for the intake of chromium

ions in the human body. This leads to many diseases such as cancer, DNA damage, etc.[4–8] The Environmental Protection Act (EPA) has allowed the maximum chromium concentration to be 0.01 ppm in water to be considered safe.[9] Therefore, a systematic study for determining chromium content in water is significant. Likewise, permanganate ions are another class of toxic global pollutants caused by their ubiquitous use in different fields such as medication, dermatitis, oxidizing agents in chemistry laboratories, and more.[10–11] Excess manganate uptake can result in many health issues, such as throat swelling, kidney damage, low blood pressure, skin irritant problems, etc.[12] The permanganate ion contributes to a toxic environment for the aquatic organism as well.[13–14] The maximum concentration of $KMnO_4$ allowed in the human body is 7 mg L^{-1} according to the EPA. Thus, the detection of permanganate ions is also essential. The aforementioned points clearly suggest the need to develop a cost-effective detection strategy for dichromate and permanganate ions particularly in a water medium. Different methods, such as ion chromatography,[15] mass spectrometry (MS),[16] ion mobility spectrometry (IMS),[17] and differential pulse polarography, have been employed for the detection of dichromate anions and permanganate ion detection. Despite these methods having shown great selectivity towards the detection of permanganate and chromate ions, due to their high instrument cost, less portability, and time-consuming process prevent their use in on-field applications. Alternatively, fluorescence-based methods find immense application for detection studies due to their high response time, cost-effectiveness, and good sensitivity along with easy sample preparation for on-field applications. This method can be used both in solid and solution state. Various research papers have been published for the selective sensing of dichromate and permanganate ions using fluorescent-based materials. For instance, Zhang et al., developed a fluorescent supramolecular organic framework (HNU-35)[18] having three-dimensional structures that are very effective for the selective $Cr_2O_7^{2-}$ and MnO_4^- sensing in an aqueous solution with a limit of detection (LOD), 26.91 nM and 13.56 nM respectively. In a different work, Li et al. developed an organic network (CON-LDU2) which is a cationic fluorescent complex, and able to adsorb and detect dichromate ions in water efficiently.[19] In the majority of these investigations, cerium has frequently been used as a terbium ion sensitizer to promote energy transfer; the ensuing variations in luminescence efficiency are then examined in the presence of particular analytes.[20]

The narrow-band and intense luminescence from the terbium(III) ion was explored for the selective sensing of chromate and permanganate ions by doping them in the gallic acid-capped CaF_2 inorganic host matrix. The CaF_2 used as a host matrix that possesses low phonon energy and a non-hygroscopic nature, which is ideal for synthesizing the lanthanide-doped

nanocrystals.[21–23] The gallic acid is chosen because it possesses a COOH group, which can bind to the NCs surface, and multiple hydroxy groups, which can form strong hydrogen-boding interactions with oxygen atoms of the dichromate and permanganate analytes. The gallic acid ligand structure is shown in Scheme 4-1. Upon UV excitation, the nanocrystals display an intense green luminescence from terbium(III) ions. The intense green luminescence is due to the effective energy transfer from gallic acid molecules to terbium(III) ions inside the NCs. However, I have strategically employed organic ligand-based terbium(III) ions luminescence sensitizers in this work. This method selectively modifies the luminescence of terbium(III) ions in the presence of chromate and permanganate ions, in addition to increasing their brightness. Our choice of ligand plays a pivotal role in achieving these unique properties.

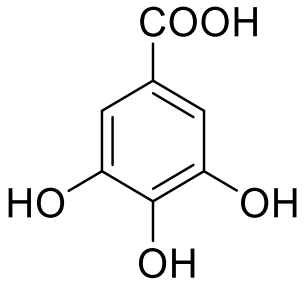

Scheme 4-1. Chemical structure of gallic acid.

4.3. Experimental

4.3.1. Materials

Tb_4O_7 (99.9%), NH_4F (99.9%), gallic acid (98.9%), $NaClO_4$(98%), Na_3PO_4 (99%), CH_3COONa (99%), Na_2SO_4 (99%), $K_2Cr_2O_7$ (99%), $Na_2WO_4{\cdot}2H_2O$ (99%), $KMnO_4$ (99%), $NaIO_3$ (99%), $NH_4VO_3{\cdot}2H_2O$ (99%), $NaAsO_2$ (99%), C_6H_5COONa (99%), Na_2SO_3 (99%), NaI (99%), NaBr (99%), Na_2S (98%), NaSCN (98%), $K_2Cr_2O_7$ (99%), and K_2CO_3(99.99%) were bought them from Sigma–Aldrich. Aqueous HNO_3 (65%), $Ca(NO_3)_2$ (98.5%), NaCl (99%), and NaF (99%) were bought from Merck. Synthesis and all the experimental measurements were done in the deionized water. All chemicals were used without further purification process.

4.3.2. Preparation of gallic acid-capped CaF_2:Tb(III) (2%) nanocrystals (NCs)

The microwave method was used for the synthesis of GA-capped CaF_2:Tb(III) (2 mol %) NCs. To make the required nitrate, the stoichiometric quantity of Tb_4O_7 was dissolved in nitric acid at 1 M concentration. NH_4F and $Ca(NO_3)_2$ were used as they were received. $Tb(NO_3)_3$ (0.02 mmol) and $Ca(NO_3)_2{\cdot}x4H_2O$ (0.98 mmol) were dispersed in 10 mL water in a 100 mL

beaker, and a 2 mmol of GA in 20 mL of H_2O was mixed with the earlier mixture and solution was vigorously stirred for 1 h. Subsequently, NH_4F (5 mL, 4 mmol) aqueous solution was added to the above solution and kept for stirring for 30 minutes. Following that, the precursor was added to a 30 mL glass vial and the vial was sealed with a teflon cap to heat at 80°C under microwave irradiation for 10 min. After the reaction was completed, the centrifugation process was performed to collect the white precipitates, rinsed 3 times with ethanol and water, and finally vacuum dried.

4.3.3. Sample preparation for $Cr_2O_7^{2-}$ and MnO_4^-

First, a dilute dispersion of the nanocrystals was prepared by taking 5 mg of sample in 25 mL DI water, and the $Cr_2O_7^{2-}$ and MnO_4^- stock solutions were prepared with 10^{-3} M aqueous solutions. The photoluminescence studies were performed by taking 1.9 mL NCs and 100 μL of $Cr_2O_7^{2-}$ and MnO_4^- salt solutions added in the 1 cm optical path length quartz cuvette. The selectivity studies for other metal ions were also performed using similar processes by taking 1.9 mL NCs dispersion and 100 μL of different metal ions stock salt solution.

4.3.4. Characterization and instruments

A Rigaku Smart Lab diffractometer was utilized to collect powder X-ray diffraction (XRD) patterns. It was fitted with a D/teX ultra-detector and a Cu-Kα source operating at 35 kV and 70 mA with a scan range from 10 to 90 º (2θ) set with 2-s count times and step size of 0.020 º. A quartz slide was used to evenly spread the powered sample. A 200-kV electron source of ultrahigh FEG-TEM (JEOL JEM2100F) was used to capture the transmission electron microscopy (TEM) images. The TEM image sample was made by taking a drop of nanocrystal aqueous dispersion on the carbon-coated 300 mesh Cu grid and drying it in the air. FT-IR measurements were done from the 4000–400 cm^{-1} range using a Perkin Elmer spectrum RX1 spectrometer by a KBr disc technique. Samples for the FT-IR measurements were prepared by using ~10 mg of nanocrystals with 200 mg of KBr and making it like a pallet. UV–visible absorption spectra of the samples in a 1 cm path length quartz cuvette at room temperature were measured using a Hitachi High-Tech U-4100 spectrometer. Luminescence spectra and decay at room temperature were measured using a Horiba Jobin Yvon Fluoromax-4 spectrofluorometer equipped with a 150-W Xe lamp and a Xe pulsed source with 25 W power, respectively.

4.3.5. Samples for luminescence measurements

All the photoluminescence experiments were carried out in aqueous media. $Cr_2O_7^{2-}$ and

MnO_4^- sensitivity studies for nanocrystals were performed by dispersing 20 mg nanocrystals in 100 mL deionized water. The excitation measurement was performed by monitoring at 545 nm, and 310 nm was selected as an excitation wavelength for photoluminescence measurements. Stock solutions of $Cr_2O_7^{2-}$ and MnO_4^- ion (10 mM) were prepared and diluted to the required concentrations according to detection experiments. The luminescence patterns of $Cr_2O_7^{2-}$ and MnO_4^- were studied using 1.9 mL nanocrystal suspensions and 100 μL of $Cr_2O_7^{2-}$ or MnO_4^- analytes. Initial pH of the nanocrystal suspension was adjusted at 7.0. The interference sensitivity studies were performed when various other ions such as VO_3^-, WO_4^{2-}, NO_3^-, AsO_2^-, AsO_4^{3-}, IO_3^-, $C_6H_5COO^-$, SO_3^{2-}, PO_4^{3-}, Cl^-, SO_4^{2-}, I^-, Br^-, F^-, S^{2-}, CH_3COO^-, SCN^-, ClO_4^- were present to ensure there is no interference from other ions while the identification of $Cr_2O_7^{2-}$ and MnO_4^-. The stock solutions of these ions were prepared in deionized water.

4.4. Phase analysis

The XRD pattern of the as-prepared materials matched the standard pattern of cubic phase CaF_2, confirming the synthesis of pure cubic phase GA-capped CaF_2:Tb(III) (2%) nanocrystals, as shown in Figure 4-2. The narrow diffraction peaks in the XRD pattern indicate good crystallinity of the synthesized nanocrystals.

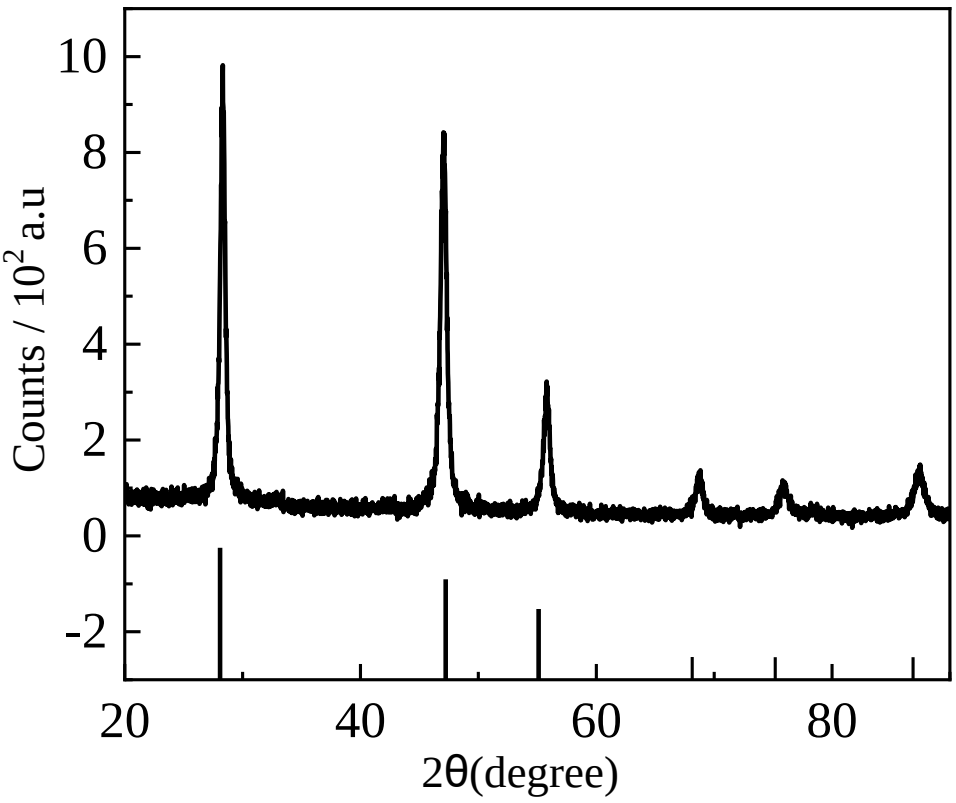

Figure 4-2. Powder XRD pattern of GA-capped CaF_2:Tb(III)/2% NCs. The vertical pattern at the bottom is the standard pattern of bulk CaF_2 (PDF card No. 00-004-0864).

4.5. Morphology and structural analysis

The morphology and size of the synthesized nanocrystals were characterized using TEM images as depicted in Figure 4-3. The images reveal that the nanocrystals possess a spherical shape with an average size of approximately 17 nm, as successfully determined by the histogram size analysis. To verify the binding of gallic acid to the surface of terbium(III)-doped CaF_2 nanocrystals, FT-IR analysis was performed (Figure 4-4). Gallic acid exhibits a intense absorption of C=O stretching of –COOH group at 1639 cm^{-1}. The signal was shifted to 1631 cm^{-1} after hybridizing with the nanocrystals suggesting ligation or binding of gallic acid (or gallate) to the nanocrystals surface. The binding of gallic acid to the surface of nanoparticles makes the surface hydrophilic, thus rendering the nanoparticles water-dispersible.

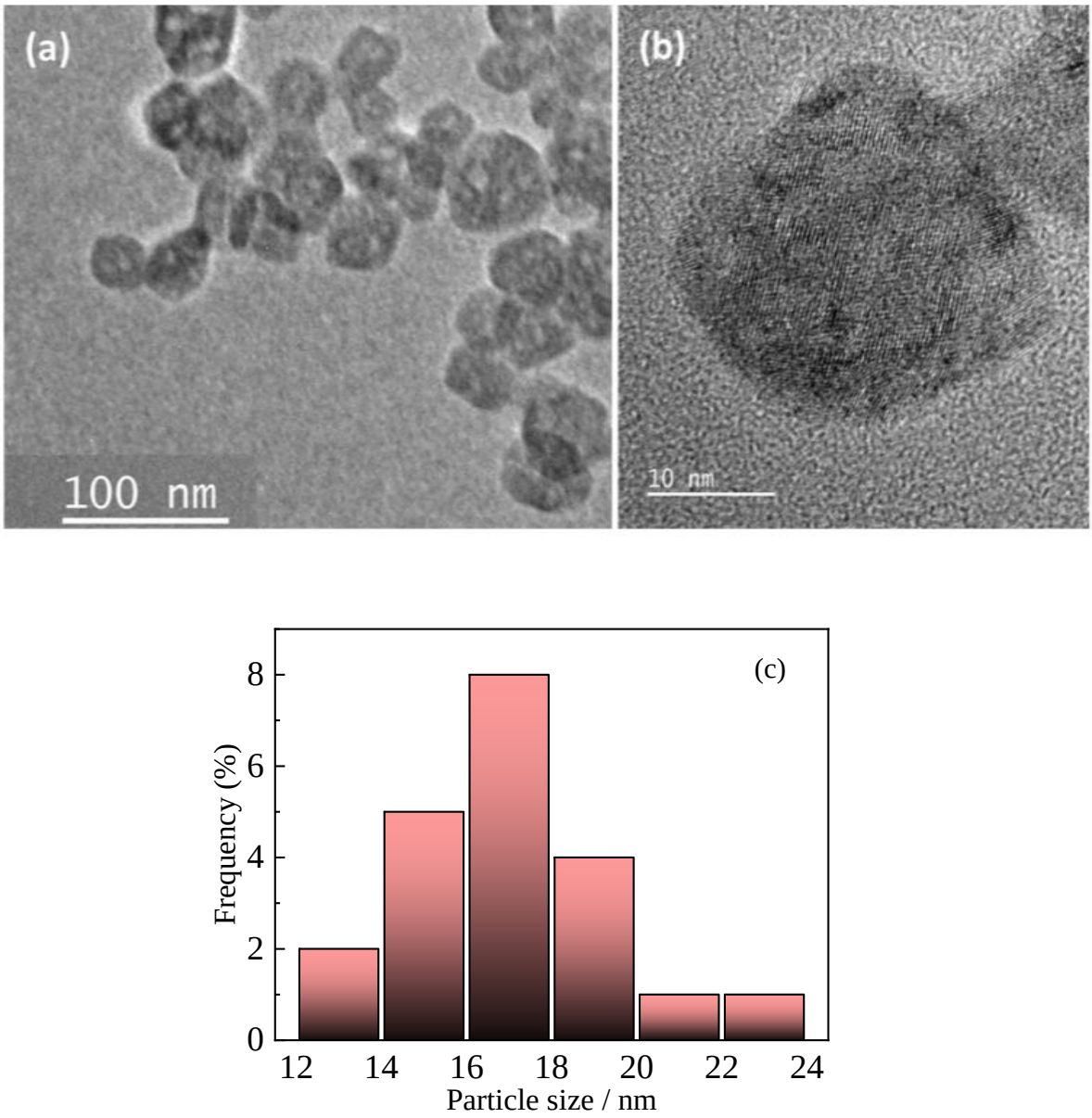

Figure 4-3. TEM image of GA-capped CaF_2:Tb(III)/2% NCs (a), high-resolution TEM image of a single nanocrystal (b). and histogram analysis showing particle size distribution (c).

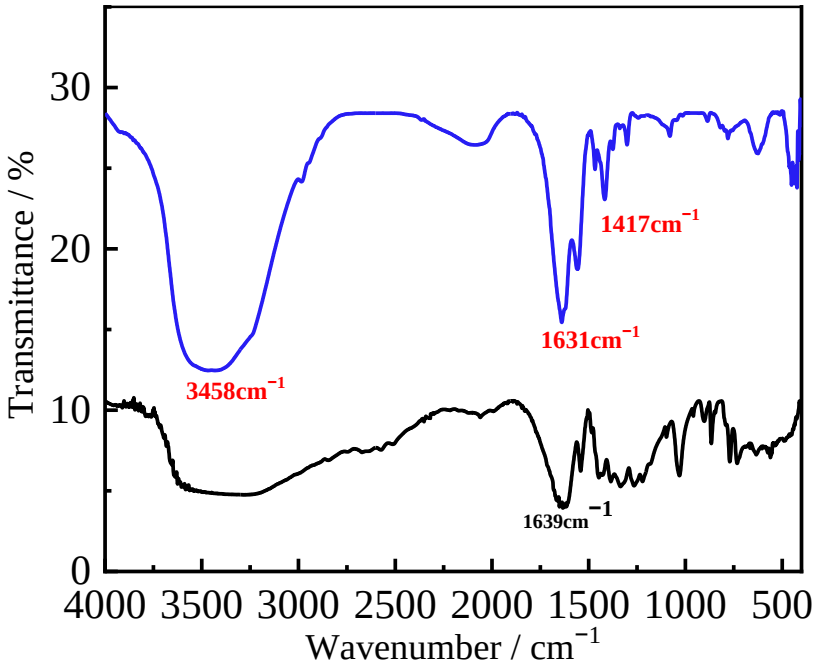

Figure 4-4. FT-IR spectra of GA-capped CaF_2:Tb(III)/2% NCs (blue) and gallic acid (black).

4.6. Spectroscopic and photophysical properties

Figure 4-5 shows absorption spectra of GA-capped CaF_2:Tb(III) and GA. GA shows two transitions, i.e., π–π* and n–π*, with maxima at around 218 nm and 268 nm, respectively. After binding of GA molecules on the surface of the CaF_2:terbium(III) NCs, the $\pi \rightarrow \pi$* and $n \rightarrow \pi$* slightly shifted to a lower wavelength and appeared at 212 nm and 262 nm. The results confirm the binding of GA to the surface of the GA-capped CaF_2:Tb(III) NCs. The photoluminescence and excitation spectra of an aqueous dispersion of GA-capped CaF_2:Tb(III) (2%) nanocrystals in water are shown in Figure 4-6. Upon excitation at 310 nm, strong emissions occur at 488 nm, 541 nm, 583 nm, and 620 nm. The emissions are ascribed to $^5D_4 \rightarrow {}^7F_J$ (J = 3–6) transitions. These transitions correspond to the characteristic of the terbium(III) ion. The luminescence from the terbium(III) ion was expected to come from the ligand excitation. This is confirmed by observing a broad peak in the excitation spectra with maxima at 310 nm (λ_{em} = 542 nm). This clearly suggests the occurrence of energy transfer from gallic acid to terbium(III) ion in gallic acid capped terbium(III)-doped CaF_2 NCs. The emission intensity of terbium(III) ion is nearly 45-times enhanced via gallic acid sensitization in CaF_2 NCs, compared to direct excitation of terbium(III) ion (see Figure 4-6). The energy transfer from gallic acid to terbium(III) in gallic acid-capped terbium(III)-doped CaF_2 nanocrystals (NCs) is further corroborated by the results of lifetime measurements. The photoluminescence (PL) decay

curves of GA-capped CaF_2:Tb(III) NCs were recorded by monitoring the emission wavelength at 545 nm, corresponding to the $^5D_4 \rightarrow {}^7F_5$ transition of terbium(III) ions. A semi-logarithmic plot of the decay curve indicates a multi-exponential decay behavior, as depicted in Figure 4-7. The calculated luminescence lifetime for this transition was approximately 1.02 ms. This relatively longer lifetime for the $^5D_4 \rightarrow {}^7F_5$ transition of terbium(III) ions strongly suggests efficient energy transfer from gallic acid to the terbium(III) ions within the nanocrystals. This observation underscores the role of gallic acid as an effective sensitizer, facilitating the energy transfer process and enhancing the luminescence of terbium(III) in the hybrid system.

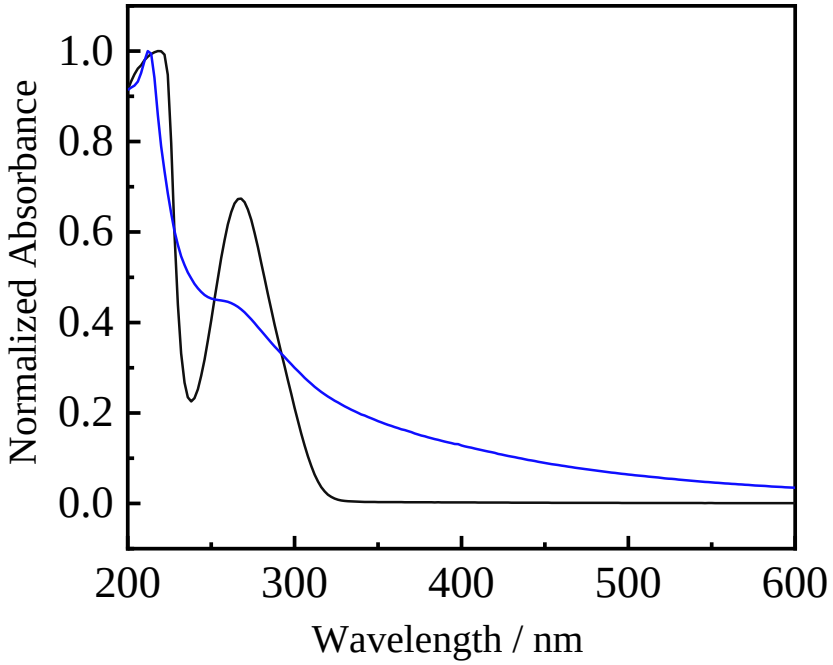

Figure 4-5. UV–visible absorption spectra of GA-capped CaF_2:Tb(III)/2% NCs (blue) and gallic acid (black) in water.

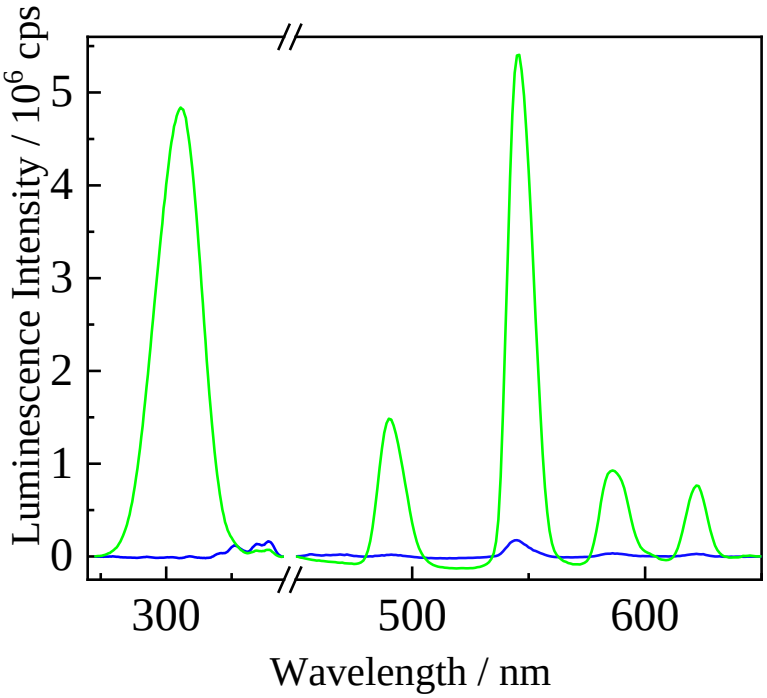

Figure 4-6. Photoluminescence and excitation spectra of GA- (green, λ_{ex} = 310 nm and λ_{em} = 545 nm) and citric-acid-capped CaF_2:Tb(III)/2% NCs (blue, λ_{ex} = 276 nm and λ_{em} = 545 nm) in water.

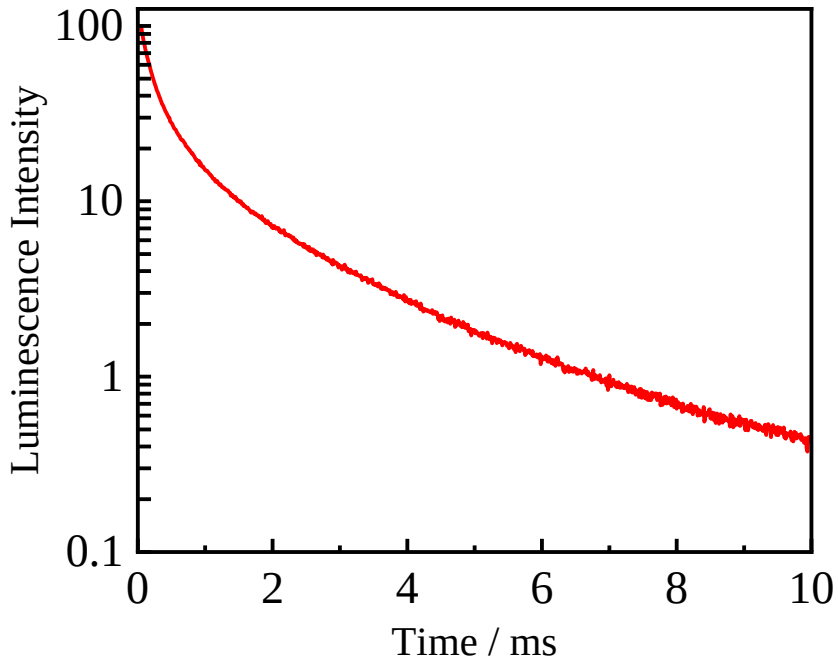

Figure 4-7. Photoluminescence decay profile of GA-capped CaF_2:Tb(III)/2% NCs (λ_{ex} = 310 nm and λ_{em} = 545 nm) in water.

The proposed energy level diagram and energy-transfer mechanism between GA and terbium(III) ions are shown in Figure 4-8. Briefly, the GA ligand is excited from the ground state the HOMO level to the excited state of the LUMO level. The energy transfer occurs from LUMO to the nearest excited energy level, presumably to the $^5D_4$ level of the terbium(III) ion, via a nonradiative pathway. From there via nonradiative relaxation, the $^5D_4$ level is further populated. Subsequently, multiple emissions occur in the visible region via radiative transitions to the ground state energy levels.

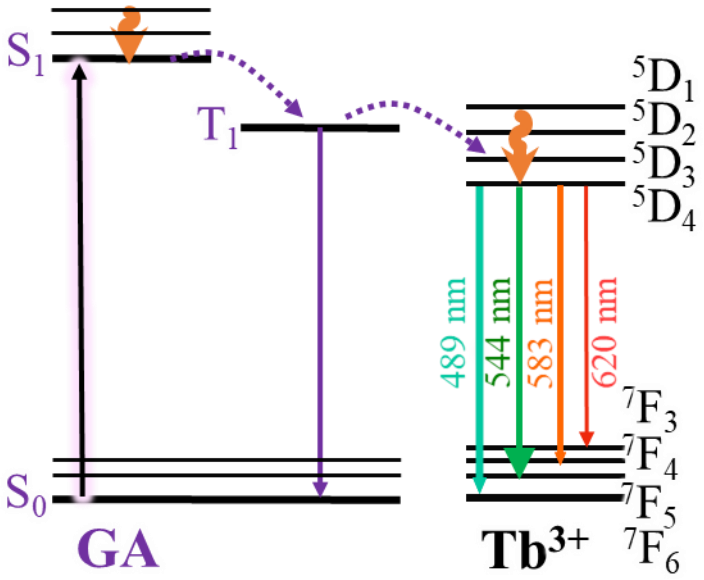

Figure 4-8. Schematic energy level diagram and energy transfer mechanism of GA-capped CaF_2:Tb(III)/2% NCs.

4.7. Detection of dichromate and permanganate

To understand the detection performance of the NCs towards the chromate and permanganate ions, the luminescence experiments of the GA-Capped CaF_2:terbium(III) NCs in the presence of chromate and permanganate ions were performed. Aqueous solutions of $Cr_2O_7^{2-}$ or MnO_4^- ions in the concentration range between 1 nM and 3000 nM (3 µM) were added to the NCs dispersion. From Figure 4-9, it is clear that the terbium(III) emission intensity gradually decreases with an increase in the concentration of the analytes. More than 90% of the luminescence intensity from the colloidal NCs is decreased after the addition of 3000 nM of $Cr_2O_7^{2-}$ or MnO_4^- ions

To verify the selectivity of the GA-capped CaF_2:terbium(III) NCs towards $Cr_2O_7^{2-}$ and MnO_4^- ions, the detection study was performed with other anions (analytes). The concentration of different analytes used is 2 times higher (6 µM) compared to $Cr_2O_7^{2-}$ and MnO_4^- (3µM) ions

for the selectivity and interference studies. The results of the analysis are represented as a bar diagram in Figure 4-10. The results suggest that about a 50% decrease in the intensity is noted for Cr^{3+}, VO_3^- and WO_4^{2-} ions whereas there is not much decrease in the terbium(III) emission intensity with the addition of other anions.

The interference study was performed by taking 100 µL of the aqueous solution of each analyte into 1.8 mL of the NCs dispersion followed by the addition of 100 µL of $Cr_2O_7^{2-}$ or MnO_4^- ions. The final concentration for each analyte ion was 6 µM, and for the $Cr_2O_7^{2-}$ or MnO_4^- ions were 3 µM, respectively. The results of the interference study are shown in Figure 4-11 for $Cr_2O_7^{2-}$ and MnO_4^- ions. The results demonstrate that the reduction in the intensity of terbium(III) ions solely occurred due to the existence of $Cr_2O_7^{2-}$ and MnO_4^- ions, and hardly any interference was observed due to the presence of other analytes. These results further suggest that the GA-Capped CaF_2:terbium(III) NCs are selective towards $Cr_2O_7^{2-}$ and MnO_4^- ions. Please note that the concentrations of the interfering analytes are two times higher than the $Cr_2O_7^{2-}$ and MnO_4^- ions.

The quenching of terbium(III) luminescent emission intensity with $Cr_2O_7^{2-}$ and MnO_4^- ions was analyzed using the Stern-Volmer equation to determine the gallic acid capped CaF_2:terbium(III) NCs sensitivity towards $Cr_2O_7^{2-}$ and MnO_4^- ions. The Stern-Volmer equation: $I_0/I = 1+K_{SV}[C]$, where I_0 and I are the luminescent intensity of NCs with and without $Cr_2O_7^{2-}$ or MnO_4^- ions, [C] is the concentration of $Cr_2O_7^{2-}$ or MnO_4^- ions, and K_{SV} is the quenching constant. Figure 4-12 represents a plot of luminescence intensity ratio Vs concentration of analytes for the GA-capped CaF_2:terbium(III) NCs. The graphs show the superior linearity ($R2 = 0.98$), with concentrations ranging from 1 nM to 3000 nM for $Cr_2O_7^{2-}$ and MnO_4^- ions. To calculate the limit of detection (LOD), the equation $3\sigma/K$ was used where σ is the standard deviation of the NCs blank emission, and K is the slope of the linear calibration plot. The evaluated LOD values for $Cr_2O_7^{2-}$ and MnO_4^- are ~ 77 nM and 55 nM, respectively.

UV–visible absorption analysis was performed to determine the reason behind the reduction in the luminescence intensity of CaF_2:terbium(III) NCs in the presence of $Cr_2O_7^{2-}$ and MnO_4^- ions, as shown in Figure 4-13. The UV-Vis absorption spectra reveal that the $K_2Cr_2O_7$ has broad absorption around 230 to 310 nm, 310 to 414 nm, and 414 to 520 nm. The $KMnO_4$ absorbs from 270 nm to 410 nm and 430 nm to 590 nm. The excitation and emission spectra of gallic acid largely overlap with the absorption spectra of $Cr_2O_7^{2-}$ and as well as with MnO_4^- ions. From the above results, the luminescence quenching of the terbium(III) ions in GA-capped CaF_2:terbium(III) NCs could be mainly due to competing absorption or inner filter effect of the analyte molecules with the excitation spectra of the NCs.

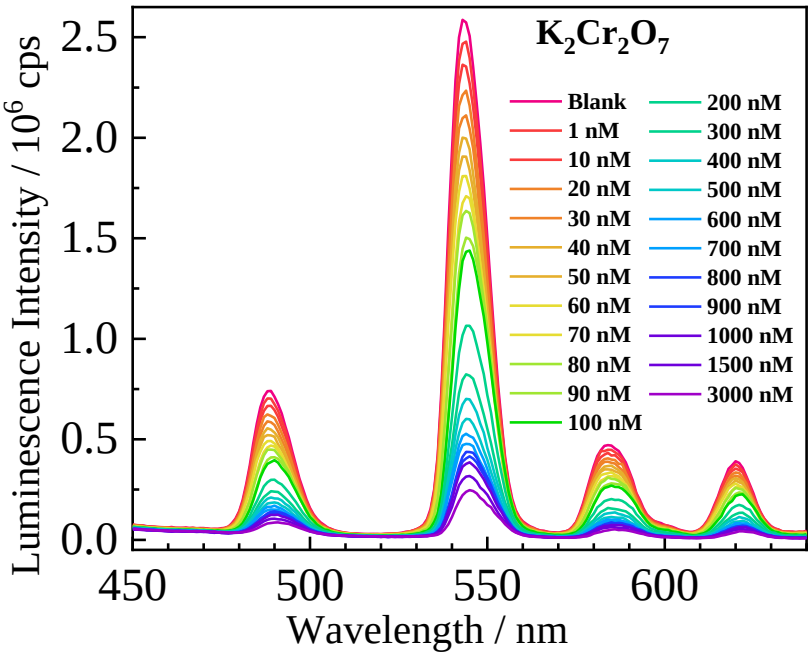

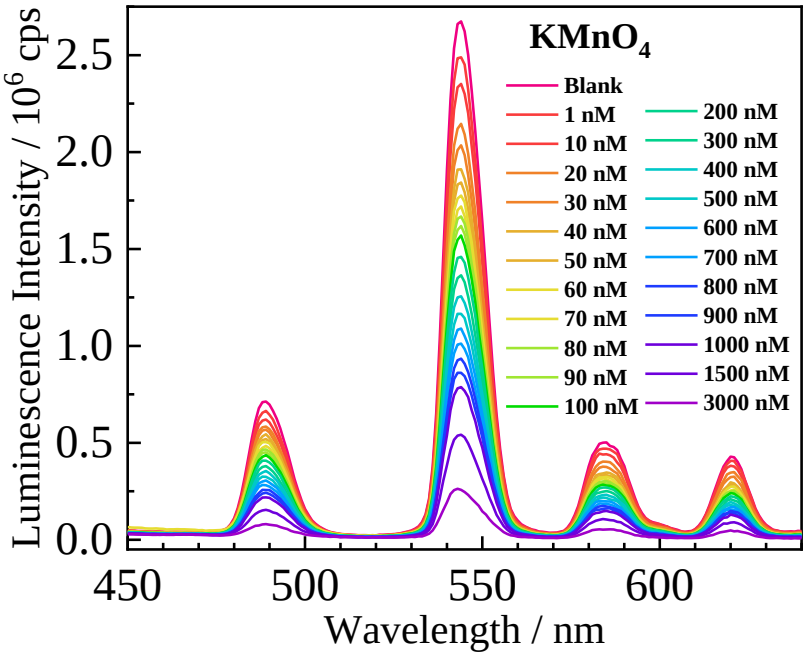

Figure 4-9. Photoluminescence spectra of GA-capped CaF_2:Tb(III)/2% NCs upon addition of $Cr_2O_7^{2-}$ (upper panel) and MnO_4^- ions (lower panel).

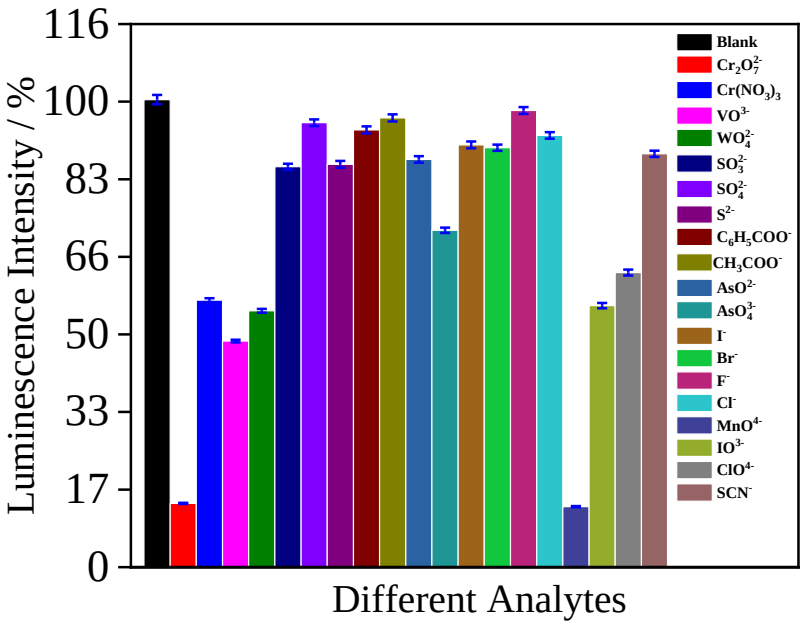

Figure 4-10. terbium(III)-ion luminescence quenching of GA-capped CaF_2:Tb(III)/2% NCs by an addition of $Cr_2O_7^{2-}$ (3 μM), MnO_4^- (3 μM), and other analytes (6 μM).

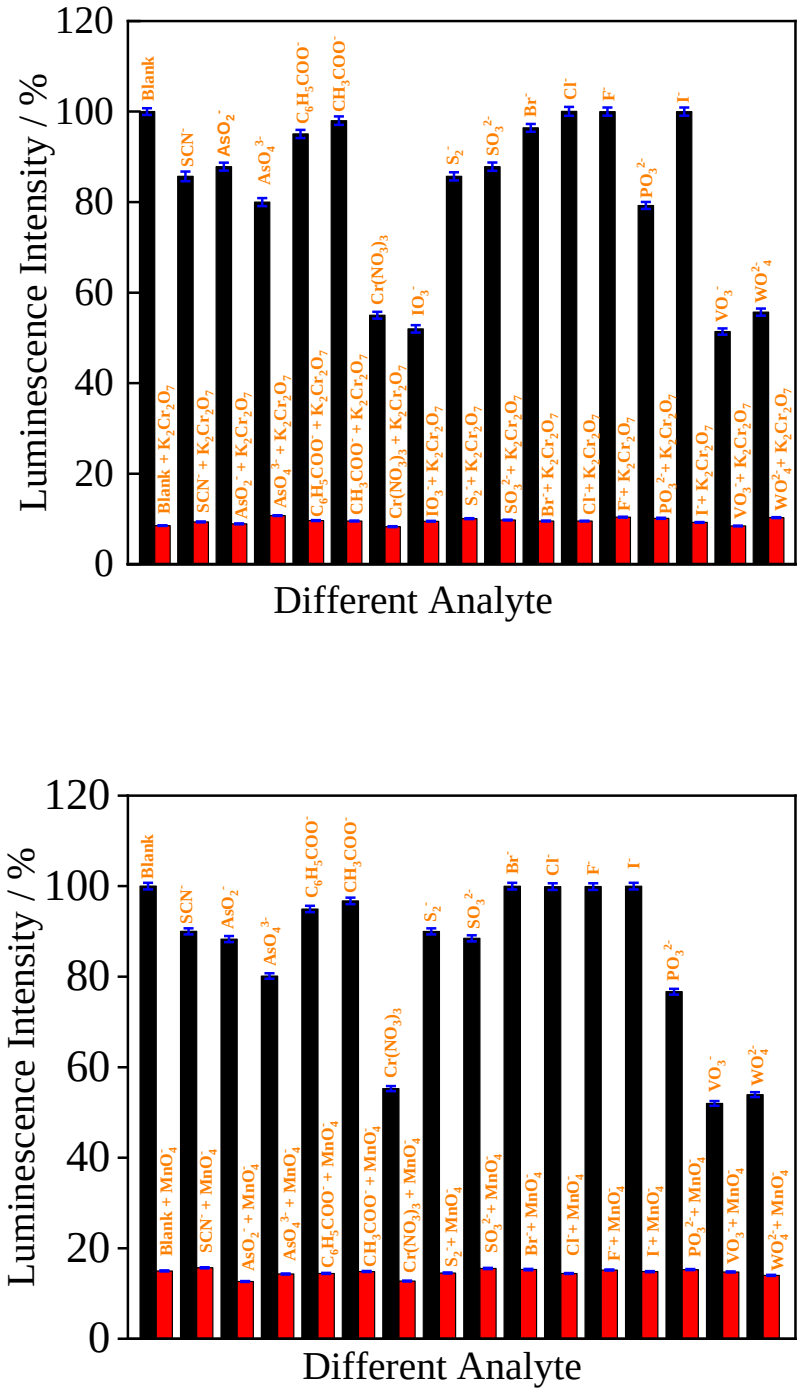

Figure 4-11. Interference study for the GA-capped CaF_2:Tb(III)/2% NCs for a variety of anions (6 µM) with (3 µM) $Cr_2O_7^{2-}$ (upper panel) and (3 µM) MnO_4^- (lower panel).

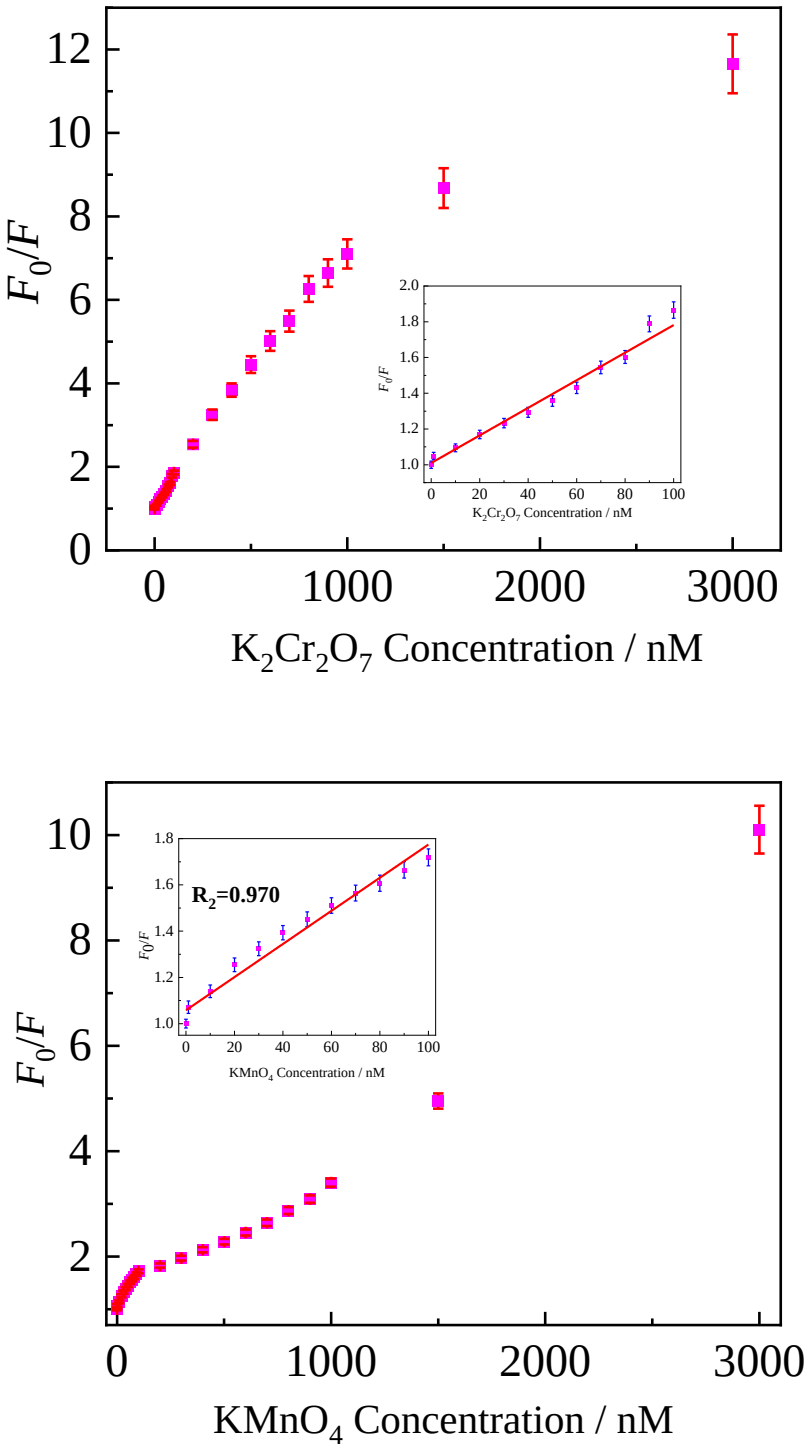

Figure 4-12. Stern–Volmer plots of GA-capped CaF_2:Tb(III)/2% NCs with the addition of $Cr_2O_7^{2-}$ (upper panel) and MnO_4^- (lower panel) in water.

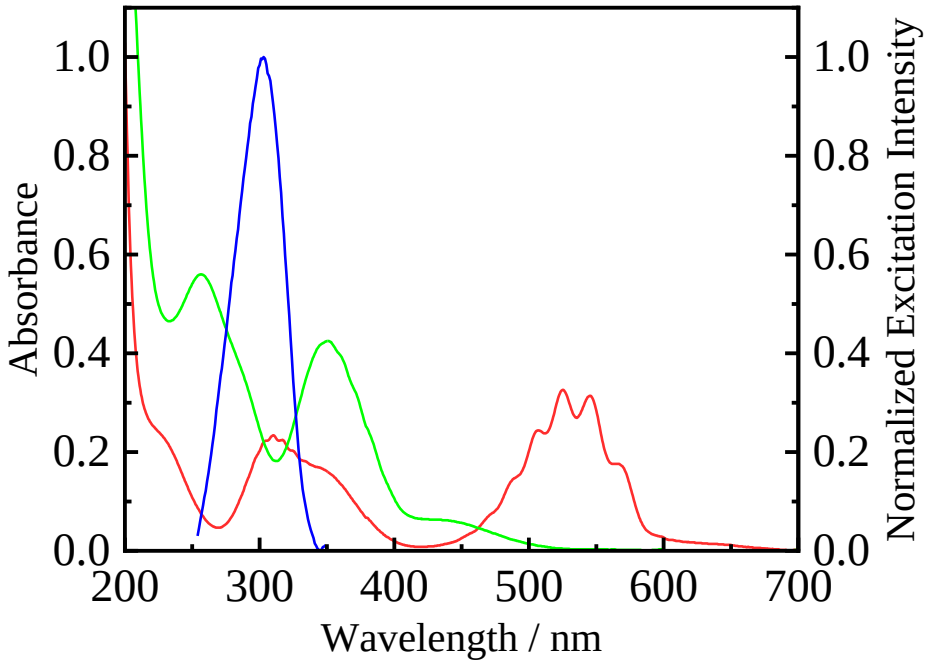

Figure 4-13. Excitation spectrum of GA-capped CaF_2:TbIII) NCs (blue) with absorption spectra of $K_2Cr_2O_7$ (green) and $KMnO_4$ (red).

4.8. Conclusion

In conclusion, gallic acid (GA)-capped CaF_2:terbium(III) NCs with a mean size of 17 nm were prepared by the microwave method. Gallic acid serves as both a capping agent and sensitizer to control the size/shape of nanocrystals and to boost the emission efficiency of terbium(III) ions via energy transfer. The NCs displayed strong green emission on UV light excitation. Photophysical studies confirm the energy transfer from GA molecules to terbium(III) ions. The gallic acid (GA)-capped CaF_2:terbium(III) NCs showed high selectivity towards detecting analytes like chromate or permanganate ions. An effective quenching in the luminescence of terbium(III) ions was observed upon binding these analytes to the nanocrystals. Interestingly, very minimal changes occurred in the luminescence intensity in the terbium(III) ions when the other analytes were present. The calculated LOD from the experimental results (for the 3σ/slope criterion) were 77 nM and 55 nM for $K_2Cr_2O_7$ and $KMnO_4$, respectively. Detection of $K_2Cr_2O_7$ and $KMnO_4$ ions is essential as both chromium and manganese are present in a high valence state.

4.9. References

1) E. Carneiro, J. D. Castro, S. M. Marques, A. Cavaleiro, S. Carvalho, *Surf. Coat. Technol.* **2021**, *418*, 127271.
2) X. Xia, S. Wu, Z. Zhou, G. Wang, *J. Hazard. Mater.* **2021**, *401*, 123685.
3) M. Zeiner, I. Rezić, D. Ujević, I. Steffan, *Coll. Antropol.* **2011**, *35*, 89.
4) J. J. Coetzee, N. Bansal, E. M. N. Chirwa, *Expo Health* **2020**, *12*, 51.
5) R. Kumar, S. J. Kim, K. H. Kim, S. Hun Lee, H. S. Park, B. H. Jeon, *Appl. Geochem.* **2018**, *88*, 113.
6) S. Guo, C. Xiao, N. Zhou, R. Chi, *Environ. Chem. Lett.* **2021**, *19*, 1413.
7) J. B. Vincent, *Curr. Opin. Clin. Nutr. Metab. Care* **2019**, *22*, 483.
8) T. H. Lim, T. Sargent, N. Kusubov, *Am. J. Physiol. Regul. Integr. Comp. Physiol.* **1983**, *244*, R445.
9) G. Huang, J. Xie, T. Li, P. Zhang, *Int. Arch. Occup. Environ. Health* **2021**, *94*, 1581.
10) J. L. Adcock, N. W. Barnett, C. J. Barrow, P. S. Francis, *Anal. Chim. Acta* **2014**, *807*, 9.
11) P. C. Spricigo, M. M. Foschini, C. Ribeiro, D. S. Corrêa, M. D. Ferreira, *Food Bioproc. Tech.* **2017**, *10*, 1622.
12) A. Shaabani, P. Mirzaei, S. Naderi, D. G. Lee, *Tetrahedron* **2004**, *60*, 11415.
13) J. G. França, M. J. T. R. Paiva, S. Carvalho, L. Miashiro, J. V. Lombardi, *Aquaculture* **2011**, *322*, 249.
14) K. L. Ong, T. H. Tan, W. L. Cheung, *Emerg. Med. J.* **1997**, *14*, 43.
15) H.Hagendorfer, W.Goessler, *Talanta*. **2008**, *76*, 656.
16) M. Labra, E. Gianazza, R. Waitt, I. Eberini, A. Sozzi, S. Regondi, F. Grassi, E. Agradi, *Chemosphere* **2006**, *62*, 1234.
17) J. Puton, J. Namieśnik, *TrAC, Trends Anal. Chem.* **2016**, *85*, 10.
18) X. Zhang, G. Ren, Z. He, W. Yang, H. Li, Y. Wang, Q. Pan, X. Shi, *Cryst. Growth Des.* **2020**, *20*, 6888.
19) Z. J. Li, H. D. Xue, Y. X. Ma, Q. Zhang, Y. C. Li, M. Xie, H. L. Qi, X. D. Zheng, *ACS Appl. Mater. Interfaces* **2019**, *11*, 46197.
20) N. Lian, H. Zhao, C. Sun, S. Chen, Y. Lu, L. Jin *Microchem. J* **2003** *74* 223.
21) A. Kar, A. Patra, *J. Nanosci. Nanotechnol.* **2018**, *18*, 8047.
22) X. Cantarelli, M. Pedroni, F. Piccinelli, P. Marzola, F. Boschi, G. Conti, A. Sbarbati, P. Bernardi, E. Mosconi, L. Perbellini, L. Marongiu, M. Donini, S. Dusi, L. Sorace, C. Innocenti, E. Fantechi, C. Sangregorio, A. Speghini, *Biomater. Sci.* **2014**, *2*, 1158.

23) N. N. Dong, M. Pedroni, F. Piccinelli, G. Conti, A. Sbarbati, J. E. Ramírez-Hernández, L. M. Maestro, M. C. Iglesias-De La Cruz, F. Sanz-Rodriguez, A. Juarranz, F. Chen, F. Vetrone, J. A. Capobianco, J. G. Solé, M. Bettinelli, D. Jaque, A. Speghini, *ACS Nano* **2011**, *5*, 8665.

Chapter 5 Conclusion

The work presented in this thesis has significantly advanced the understanding of the development of highly luminescent lanthanide(III)-ions-doped materials. By focusing primarily on the enhancement of luminescence in terbium(III) and europium(III) ions, various approaches were explored to sensitize their luminescence and address critical challenges in photochemistry and material science. The primary objective was to achieve high-efficiency luminescence while maintaining material stability, low cost, and simplicity in the synthetic procedures. The findings presented in this dissertation demonstrate the potential of these materials for diverse applications such as sensing, bioimaging, and optical technologies.

To accomplish the objectives of this research, a comprehensive investigation was carried out, covering theoretical analysis, experimental studies, and data analysis. Chapter 1 describes the background of the study of lanthanide(III) ions luminescence research, discusses the existing literature, and identifies the gap, leading to the formulation of the research purpose for this dissertation. Chapters 2, 3, and 4 systematically describe the study of sensitized luminescence of lanthanide(III) ions across various hybrid materials. These chapters provide detailed insights into the design, synthesis, and characterization of the materials, as well as a discussion of our findings highlighting the innovations and breakthroughs achieved during the research. The summary of this dissertation is discussed as follows:

Chapter 2 focuses on the sensitized luminescence of terbium(III) ion hybridized with a novel sensitizer, the ionic nanosphere. In this study, the luminescence sensitization of terbium ions was achieved using a straightforward ion exchange process, which is both simple and efficient. The ionic nanosphere served multiple crucial roles for terbium(III) ion: it acted as a host matrix, provided a hydrophobic environment to minimize non-radiative quenching, and functioned as a sensitizer to enhance the luminescence efficiency of terbium(III) ion. This innovative method holds a significant advantage over conventional techniques explored by other researchers, as the hybridization of terbium(III) ion and the photosensitizer was accomplished through a simple mixing process. This approach is not only novel but also time-saving and highly efficient. The results of this study demonstrate the immense potential of these terbium(III)-ion-based hybrid materials for practical applications in bioimaging, sensing, and optoelectronic devices. The scalability and practicality of the method offer a promising pathway for the development of advanced luminescent systems. By addressing key challenges in the synthesis and functionalization of lanthanide-based materials, this work significantly contributes to the field of photochemistry and material science.

Chapter 3 explores the sensitization of lanthanide(III) ions using ionic nanospheres copolymerized with a 5-(4-vinylphenyl)-1,10-phenanthroline ligating moiety. This hybrid system was designed to enhance light harvesting and sensitize terbium(III) and europium(III) ions. Unlike the conventional ionic nanospheres in Chapter 2, which only utilized light below 280 nm and failed to sensitize europium(III) ions, the copolymerized nanosphere overcame these limitations. The phenanthroline ligand effectively coordinated with the lanthanide(III) ions, enabling efficient energy transfer to both terbium(III) and europium(III) ions. This novel light-harvesting system demonstrated improved luminescence sensitization and broadened the application potential of ionic nanospheres. It offers promising applications in sensing, bioimaging, and biomedical technologies, advancing the field of luminescent materials.

Chapter 4 investigates the sensitization of terbium(III) ion by incorporating them into the inorganic host material. The process is achieved by choosing CaF_2 inorganic material as a host for the terbium(III) ion and a capping agent called gallic acid, which acts as a sensitizer for the terbium(III) ion. This is supported by the successful synthesis of small (~ 17 nm) nanocrystals of GA-capped terbium(III)(2%)-doped CaF_2 nanocrystals, which exhibit strong luminescence from terbium(III) ions through energy transfer from GA molecules. In addition, the GA-capped terbium(III) (2%)-doped CaF_2 nanocrystals were quite selective towards detecting toxic chromate and permanganate ions. A huge reduction in the luminescence intensity of terbium(III) ions was observed in the presence of dichromate and permanganate ions. Therefore, these materials offer significant potential in detecting toxic ions or molecules which are hazardous to the environment.

Conference presentations and awards

Presentations at international conferences

1. The 8th International Symposium on Frontier Technology. (2024/07/27-28, Kochi University of Technology, Kami, Japan (Oral presentation)
   Title: Ionic Nanosphere as A Novel Sensitizer for Luminescence from Terbium(III) Ion Hybridized by Facile Ion-Exchange Process
   Authors: Nikita Madhukar, Taizo Misato and Akitaka Ito

2. The 27th International SPACC Symposium (Online, 2022/12/10–11) (Poster presentation)
   Title: Sensitized Luminescence from Terbium(III) Ion Doped in Ionic Nanosphere
   Authors: Nikita Madhukar, Taizo Misato and Akitaka Ito

Presentations at domestic conferences/symposiums

1. The 104th CSJ Annual Meeting (2024) (Nihon University, College of Science and Technology, Funabashi Campus, March 18-21, 2024) (Oral presentation)
   Title: Effects of Monomer in Ionic Nanospheres on Sensitized Luminescence from Terbium(III) Ion
   Authors: Nikita Madhukar, Taizo Misato and Akitaka Ito

2. The 35th Symposium on Photochemistry and Photophysics of Coordination Compounds (United Nations University/Aoyama Gakuin University Aoyama Campus, 2024/08/11–13) (Poster presentation)
   Title: Sensitized Europium(III)-Ion Luminescence by Using Ionic Nanosphere with A Ligating Moiety
   Authors: Nikita Madhukar, Taizo Misato and Akitaka Ito

3. The 103rd CSJ Annual Meeting (2023) (Tokyo University of Science, Noda Campus, 2023/03/22–25) (Oral presentation)
   Title: Luminescence from Terbium(III) Species upon Sensitization using Ionic Nanosphere
   Authors: Nikita Madhukar, Taizo Misato and Akitaka Ito

4. The 33rd Symposium on Photochemistry and Photophysics of Coordination Compounds (Online, 2022/08/05–07) (Poster presentation)
   Title: Sensitization of Terbium(III)-Ion Luminescence by Ionic Nanosphere
   Authors: Nikita Madhukar, Taizo Misato and Akitaka Ito

Awards

Poster presentation award

The 27th International SPACC Symposium (Online, 2022/12/10–11)

List of papers

1. **Ionic nanosphere as a novel sensitizer for luminescence from terbium(III) ion hybridized by facile ion-exchange process**
   Madhukar, Nikita, Taizo Misato and Akitaka Ito
   Bulletin of the Chemical Society of Japan, **2024**, *97*, uoae023.

2. **Selective Detection of Chromate and Permanganate Ions Using Gallic Acid Capped CaF2:Eu Nanocrystals**
   Madhukar, Nikita, Venkata NKB Adusumalli, Heramba VSRM Koppisetti, Ayan Mondal, Akitaka Ito, Yong II Park and Venkataramanan Mahalingam
   Chemistry–An Asian Journal, **2024**, *19*, e202400597 .

3. **Development of a Strongly Fluorescent Light-Harvesting system: From Ionic Nanopshere to Ligating Moiety for the sensitization of Europium(III) and Terbium(III) Ion.**
   Madhukar, Nikita, Taizo Misato and Akitaka Ito
   Inorganic Chemistry (by March 2025)